Hadronic Structure Measurements of the Photon by DELPHI at LEP II

Thesis submitted for the degree of
Doctor of Philosophy in Physics

by

Andreas Nygren

Department of Physics
Lund University, 2001

LUND UNIVERSITY

.

Hadronic Structure Measurements of the Photon by DELPHI at LEP II

Thesis submitted for the degree of
Doctor of Philosophy in Physics

by

Andreas Nygren
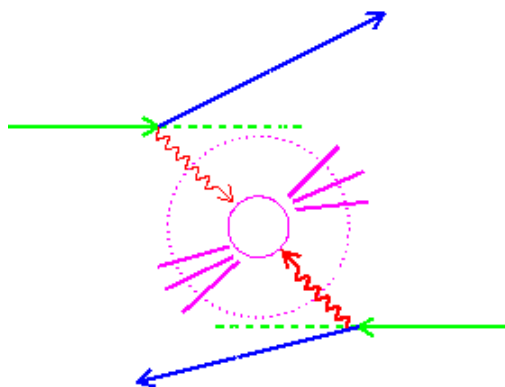
Department of Physics
Lund University, 2001

LUND
UNIVERSITY

Abstract:

This thesis is mainly an analysis of data taken by the VSAT detector in the DELPHI experiment at the LEP II collider at CERN. The analysis spans from 1998 to 2000, with a center of mass energy ranging from 189 to 206 GeV. The VSAT calorimeter was constructed to be a luminosity and background monitor for the DELPHI experiment, and a full description of the luminosity and background analysis for the LEP II conditions is presented.

The VSAT detector is located in the very forward direction and covers angles between three and eight milliradians since 1998. This also makes the detector an excellent tool for studying two photon physics, as the outgoing electrons from a two-photon collision mainly are located at small angles. A full study of the VSAT double tag data between 1998 and 2000 is presented. Gamma-gamma collisions with an invariant mass reaching up to 100 GeV could be explored in a Q^2 range of 0.2-0.8 GeV. With help of data from the STIC detector, which is located at larger polar angles, two photon collisions could also be probed with a Q^2 between 20 and 100 GeV.

DOKUMENTDATABLAD enl SIS 61 41 21

Distribution by (name and address): Andreas Nygren,
Lund University, Department of Physics, Box 118, 221 00 Lund, Sweden

Signature: Date: 30th August, 2001

Hadronic Structure Measurements of the Photon

by DELPHI at LEP II

By due permission of the faculty of mathematics and natural science at the University of Lund, to be publicly discussed at the lecture hall B of the Department of Physics, Sep 28, 2001, at 13.15, for the degree of Doctor of Philosophy

by

Andreas Nygren

Department of Physics
Lund University
Professorsgatan 1
Box 118
SE-221 00 Lund
Sweden

This thesis is based on following papers, included as Appendices A to H:

A. **Exact position of VSAT modules and LEP beam parameters measurements in 1998-2000.** *DELPHI Note 2001-005 CAL 145*

B. **Proceedings from QFTHEP 2000 in Tver, Russia.**
DELPHI Note 2001-002 Talk 021

C. $\gamma\gamma$ **-Physics background in VSAT.**
DELPHI Note 2000-173 Phys 884.

D. **LEP machine background and noise in the DELPHI calorimeters.**
DELPHI Note 99-157 LEDI 87.

E. **VSAT Background and Luminosity 1999.**
DELPHI Note 2000-054 Phys 857.

F. **VSAT trigger and energy response for LEP II.**
DELPHI Note 99-163 CAL 143 .

G. **Forthcoming results in two-photon collisions.**
DELPHI Note 98-175 Phys 814 .

H. **1998 Running review workshop, the VSAT project**
DELPHI 99-49 LEDI 11

Abstract

This thesis is mainly an analysis of data taken by the VSAT detector in the DELPHI experiment at the LEP II collider at CERN. The analysis spans from 1998 to 2000, with a center of mass energy ranging from 189 to 206 GeV. The VSAT calorimeter was constructed to be a luminosity and background monitor for the DELPHI experiment, and a full description of the luminosity and background analysis for the LEP II conditions is presented.

The VSAT detector is located in the very forward direction and covers angles between three and eight milliradians since 1998. This also makes the detector to an excellent tool for studying two photon physics, as the outgoing electrons from a two-photon collision mainly are located at small angles. A full study of the VSAT double tag data between 1998 and 2000 is presented. Gamma-gamma collisions with an invariant mass reaching up to 100 GeV could be explored in a Q^2 range of 0.2-0.8 GeV. With help of data from the STIC detector,which is located at larger polar angles, two photon collisions could also be probed with a Q^2 between 20 and 100 GeV.

Contents

Chapter 1

Introduction

The world around us is perceived by the human by our five senses, and our reality is built up from how our brain is interpreting the signals from our sensor organs. Presumably our vision, formed by the light detected in our eyes, is the most fundamental way to describe the world we live in. Light is however not only confined to the light we can see, light (or more general electromagnetic radiation) is also the origin of a numerous phenomena in every day life. Among these are for instance, the earth magnetic field, heat radiation and all types of radio communication, and it is clear that life would quickly perish without any source of light.

The interest for light has always been in focus of the curiosity of mankind. Already in the most ancient religions man was worshipping the sun god, but it was not until the 20th century that we started to grasp what light really is. For a long time light was thought to be a wave propagating in the so called ether, which was thought to be a medium that filled all space (including vacuum). The ether theory poses the problem that it results in a fixed reference system, in which the ether is at rest. The Michelson-Morley experiment in 1887 more or less put an end to the ether theory as it showed that there is no preferred system of motion for the light.

Light was showing properties of being quantized in particles (from Planck's explanation of the blackbody radiation in 1905), which however seemed to be in total disagreement with light diffraction experiments (Fig. 1.1). The solution to this was presented by Einstein in his work about the photo electric effect, when he showed that light can be described both as a wave or as a particle. In 1924 Louis de Broglie suggested that particles can be described as waves, to make the wave-particle duality complete. In an experiment similar to the one in Fig. 1.1, electron diffraction was observed independently by Davisson and Germer in 1927 and by G. P. Thomson in 1928.

Quantum mechanics tells us that we cannot determine an object's position exactly, we can only measure a probability to see an object at a certain place. For large (bigger than atoms) and slow (non relativistic) moving objects there is no wave function to speak about and things are actually where we see them. The photon (which is point-like and relativistic) is however much more elusive and cannot be fixed in position and momentum at the same time. It therefore behaves like a wave, with an amplitude determined by the probability to be in that location. It has been shown that if the position of the photon is determined, the wave-function property of the photon instantly breaks down.
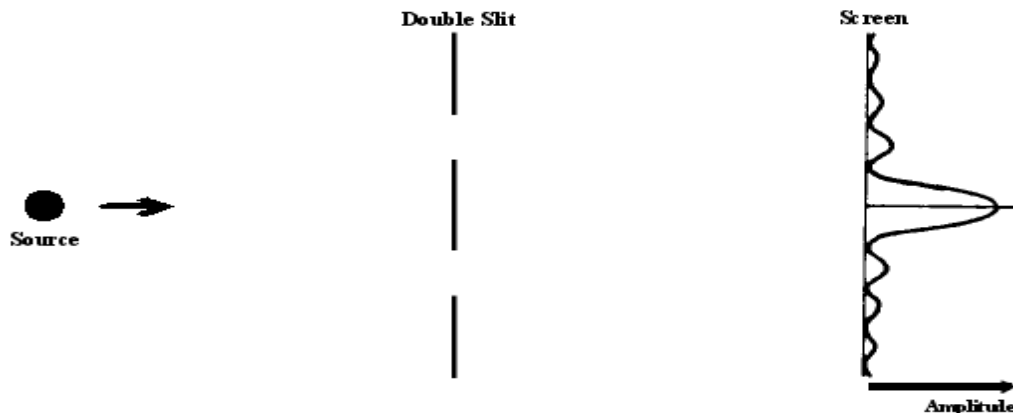
Figure 1.1: Diffraction of light through a two slit wall. In the classical approach light behaves like a soundwave in air or as a wave on a water surface, and interference of the waves from the two slits makes an amplitude pattern on the rear screen. If the intensity of light is brought down so that only one photon passes through the slit and there is no interference to speak about, the amplitude pattern is however still seen on the screen. This is explained by quantum mechanics telling us that the photon only has a certain probability to either go through the upper or lower slit. Any attempt to determine which path the photon took, will automatically destroy the wave pattern. The experiment (on a different scale though) has the same outcome if electrons instead of photons are used.

The photon is the mediator of the electromagnetic force and as charged particles (like the electron and the proton) couples to this they exchange photons when they interact with each other. The photon itself has no charge and photons do not interact among themselves (nothing will thus happen when you cross two laser beams). The photon does not have any restmass, but as shown by Einstein energy and mass are distinctly connected with his famous formula $E = mc^2$.

As shown to the world for the first time at large scale over Hiroshima and Nagasaki in August 1945, mass can be converted into energy. The opposite is however also possible and if the energy of a photon is high enough it can fluctuate into a particle and anti-particle pair. All particles have their corresponding anti-particles with same mass, but opposite quantum numbers (like the charge). In order for any particle transition to be possible all the quantum numbers must be conserved.

By the help of quantum mechanics, the photon can thus be described as a superposition of a number of possible particle pairs. A photon is thus not only a bare photon, it can fluctuate into different virtual states. These states are described by something that is called the photon structure functions, which will be described later (section 6.3). This mechanism makes collisions between photons possible, as they sometimes are something else than photons.

Electrons are surrounded by a cloud of virtual photons, they are called virtual because they only live on the existence of energy borrowed from the electron. Quantum mechanics allows energy to be created out of nothing during a very short period of time as long as it is payed back at the next instant. A cloud of photons is therefore constantly created and eliminated around any charged particle. The higher energy the electron has, the more energy is available to be borrowed and the virtual cloud grows.

If two electrons are close to each other and the energy is large enough, there is thus a distinct probability that two of these virtual photons will collide (if the virtual photon has fluctuated into a charged particle pair). As a photon normally is symbolized by the Greek letter gamma ($=\gamma$) this is referred to as a two photon- or a $\gamma\gamma$-collision (Fig. 1.2). By studying such collisions it is possible to probe the structure function of the photon and thereby give us a better understanding of both Quantum Electro Dynamics (QED) and Quantum Chromo Dynamics (QCD).
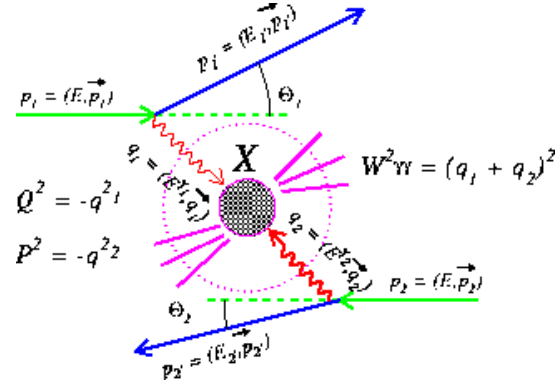
Figure 1.2: The collision of two virtual photons radiated from the electron and positron in the LEP beam. The invariant mass of the $\gamma\gamma$-system ($W_{\gamma\gamma}$) can be extracted from measurments on the outgoing leptons.

The LEP accelerator at CERN has accelerated electrons to the highest energy achieved yet, and this paper is based on $\gamma\gamma$ collisions detected with help of the VSAT detector in the DELPHI experiment. The VSAT (Very Small Angle Tagger) detector is, as the name suggest, located at very low angles and can measure both of the leptons coming out from a $\gamma\gamma$-collision. A measurement of the full kinematics of the $\gamma\gamma$-system can then be obtained. VSAT will, due to the small angles, provide data with a very low Q^2 (the momentum transfer to the photons), which is a very interesting region to study [1].

Chapter 2

VSAT in DELPHI at LEP

2.1 The LEP collider at CERN

In the proximity of Geneva in Switzerland there is an international laboratory called CERN, which is probably the most well known research complex for particle physics in the world. CERN houses a large variety of experiments and is a collaboration between 20 European member states. It has a yearly funding of a middle size European University and explores most fields of both experimental and theoretical particle physics.

The largest part of the CERN research community is focused on high energy physics. This is the science that is trying to probe the inner most structures of matter and to analyze the most fundamental forces in the universe we live in. In order to do this, particles are accelerated to high energies in huge accelerator complexes (Fig. 2.1) and then smashed together in what one could call a small BIG BANG (=the theory of the creation of the universe). The research in accelerator technology at CERN has resulted in numerous applications for the medical community, which has for instance improved the treatment of cancer.
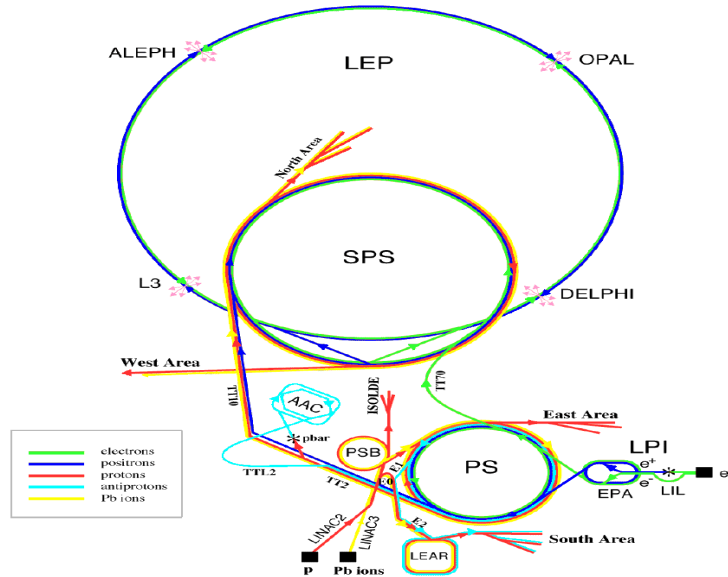
Figure 2.1: The LEP accelerator with the pre-accelerator complex.

Once the raw data from a experiment has been stored, the most essential tool for data analysis are computers. As a result of this, CERN has built up a large computer network to facilitate data analysis and communication. The most famous offspring of this is probably the World Wide Web, which was created at CERN to allow better communications between home institutes and CERN. But maybe the most important advantages for a complex like CERN is how it connects different people and cultures together to push through new ideas and let young people come forward to explore the newest aspects and theories of modern science.

The flagship of CERN during the last 10 years has been the Large Electron Positron collider (LEP). It is a 27 kilometer long accelerator ring (see Fig. 2.1) located on average 100 meters under ground on the border between Switzerland and France. Electrons and positrons (the antiparticle of the electron) are circulated in opposite direction of the ring, being held in orbit by hundreds of magnets. Recently the particles have been accelerated to over 100 GeV (200 000 times the normal electron mass of 0.5 MeV), making a center of mass energy of the collision up to 208 GeV.

2.2   DELPHI at LEP

There are four regions on the LEP ring where the beams are brought together to collide with each other. Around these interaction points experiments are built to detect and measure the properties of the particles coming out from the e^+e^- collision. The DELPHI (DEtector with Lepton, Photon and Hadron Identification) experiment (fig 2.2) was built to put special emphasis on powerful particle identification. To accomplish this, it is equipped with the largest super conducting magnet in the world, with a diameter of 5.2 meters and a length of 7.2 meters. DELPHI itself is about ten meters long and has a weight of about 3500 tons. The experiment is built up of 20 sub-detectors that can be subdivided into four categories.
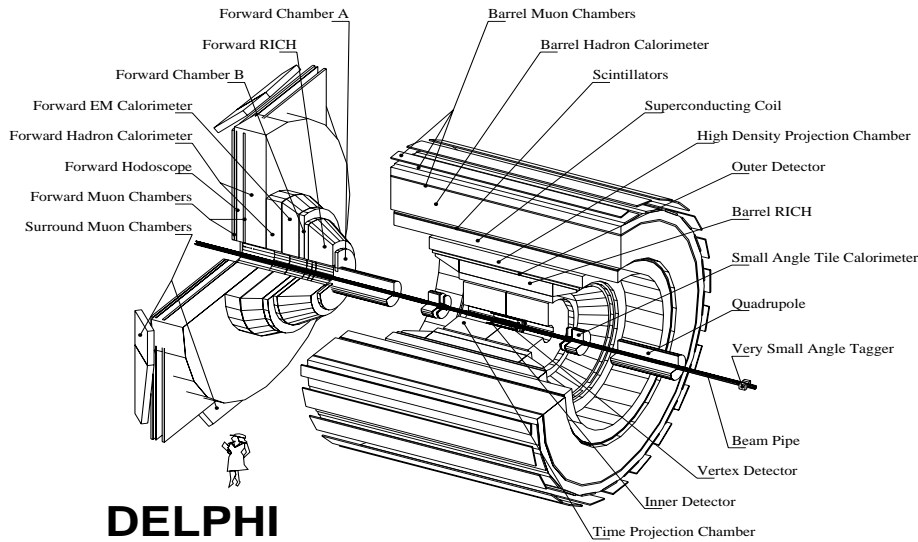

Figure 2.2: The DELPHI experiment with its subdetectors.

2.2.1 Tracking and particle identification detectors

Closest to the interaction point are the transparent tracking detectors, that make non-destructive measurements of the particle trajectories through the detector. At the very center of DELPHI is the vertex detector (VD) [2], which measure the vertex of the interaction point very precisely (a $R\phi$ resolution of 8 μm and a z resolution of 18 μm). The vertex detector is surrounded by the Inner Detector (ID) [3], which covers tracks between 15° and 165° in θ. The detector is a drift chamber giving 24 $R\phi$ points per track with a resolution of 60μm in R and 1.5 mrad in ϕ.

The main tracking detector of DELPHI is called TPC (Time Projection Chamber) [4]. It consists of two 1.5 meters long cylindrical chambers covering a radius between 40 and 120 cm on each side of the interaction point. The TPC makes a three dimensional track reconstruction with 16 spacial points with a resolution of 230 μm in $R\phi$ and 0.9 mm in z. Charged particle identification is achieved with dE/dx in the TPC and the radiation of light emitted by particles faster than light in the Ring Imaging Counter. The Outer Detector (OD) [5], Forward Chamber A and B (FCA and FCB) [6] are the outer most tracking devices and improve the momentum determination and give fast trigger information.

2.2.2 Electromagnetic calorimeters

In order to measure the energy of the outgoing electrons and photons, a number of calorimeters are positioned around the tracking detectors. The particles collide with the massive detectors to generate particle showers that are contained in the detector and the energy sum is measured. In the barrel region the High density Projection Chamber (HPC) [7] is positioned between 208 and 260 cm. The detector has a resolution of about 1° in ϕ and about 4 mm in z, and the energy can be determined to a precision of about $25\%/\sqrt{E}+7\%$. To close the barrel region of the HPC, two diskshaped calorimeters are placed in the forward region. This is the FEMC (Forward Electromagnetic Calorimeter) [8] that is 5 meters in diameter and has and angular precision about 1° and a energy resolution of about 4% at 45 GeV.

2.2.3 Hadronic calorimeters and Muon Chambers

The HAC (Hadronic Calorimeter) [9] is positioned both in the barrel region and on the end caps and is enclosing the electromagnetic calorimeters. It provides energy measurement of charged and neutral hadrons and covers the full theta angle between 11° and 169°. Muons are the only charged particles that can transverse iron and lead without any strong interaction. Because of this they mainly leave the calorimeters almost unaffected, allowing for μ/π separation. Muons are instead detected as tracks in the muon chambers, which are the outer most layer of detectors in the DELPHI experiment.

2.2.4   Small Angle Detectors

In order to measure particles leaving the collision point at very small angles, DELPHI has two small angle detectors. The main purpose of these are to record Bhabha events and thereby accurately determine the luminosity recorded by the experiment. The main detector for luminosity measurements is called STIC (Small angle TIle Calorimeter) [10] and covers an angular region between 29 and 185 mrad in θ. The resolution varies from 0.25-1.2 mm in different parts of the detector and the energy precision is in the order of 2.7% at 45 GeV. Primarily built as a luminosity monitor the Very Small Angle Tagger (VSAT) [11] was constructed to register electrons between 5 and 8 mrad. This is the main detector used for this analysis and its performance will be described in detail below.

2.3   VSAT in DELPHI

The VSAT detector consists of four identical modules placed symmetrically in two pairs on each side of the beam pipe $\pm$ 7.7 meters from the interaction point (Fig. 2.3). This placement is optimal for studying Bhabha events, as the two outgoing electrons from Bhabhas head off back to back and should give a signal in both modules in any of the two diagonals in the detector. In 1998 the LEP beampipe radius at VSAT was decreased from 60 to about 55 mm in size and the VSAT modules are since then placed around 5.8 cm from the beamline. To squeeze down the transverse beamsize at the DELPHI interaction point, there are two focusing quadrupoles in front of the VSAT modules. Outgoing particles will defocuse in x making the VSAT angular coverage to be 3-8 mrad instead of 7.7-10.4 mrad (without the quadrupole the beampipe would in fact shadow the particle trajectory).

Figure 2.3: The position of the VSAT modules.

Figure 2.4: The FAD and strip plane layout of a VSAT module

Each of the modules consists of eleven 5x5 cm^2 Full Area Silicon Detectors (FADs), interspaced with tungsten layers (Fig. 2.4). When an electron hits the detector it cascades into a particle shower that travels along the detector and is absorbed by the tungsten plates. The FADs are used for energy measurements and VSAT has an energy resolution of about 4% at 45 GeV. Since the detector was optimized for 45 GeV, the gain of the electronics was adjusted [12] so it could continue to make high precision measurements (4-5% resolution) of the energies above 100 GeV (Fig. 2.5).

Three strip plane layers with 1 mm pitch have been interspaced between the tungsten layers at shower maximum for x- and y-position measurements (precision is about 170 μm at 45 GeV). The primary purpose of this is to make detector leakage corrections. When the particle shower travels through the detector some part of it will leak out through the sides, and the closer to the edge the shower is, the more energy will be lost. Energy leakage correction is made by correcting the data with exponential curves both in y and x (Fig. 2.6).
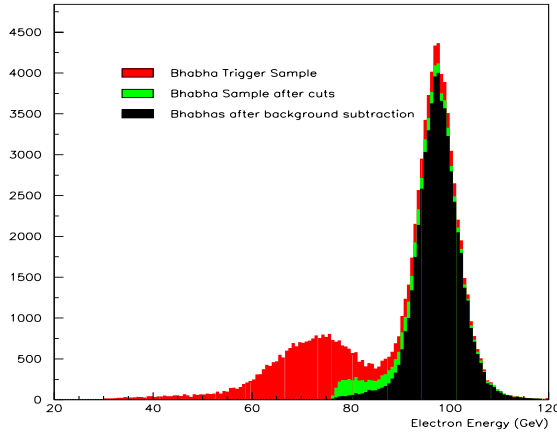

Figure 2.5: The energy distribution of Bhabha events before and after the cuts in energy and in x- and y-position. Some background still remains in the Bhabha sample, which has to be subtracted afterwards.
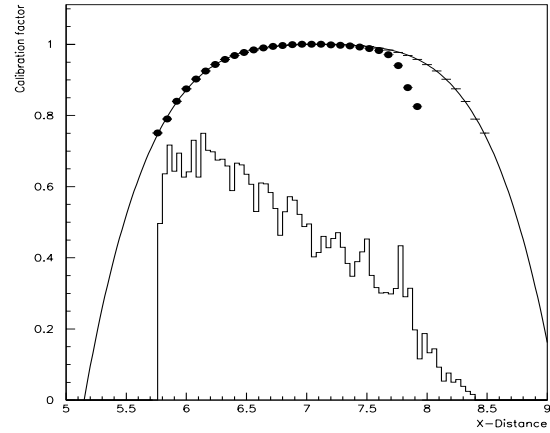
Figure 2.6: The leakage correction curve (solid line) as a function of x-position (shown as a histogram). The drop of the raw energy (dots) at the far edge is due to interaction with a flange in front of the VSAT modules.

The x- and y-position measurements are necessary in order to isolate the Bhabha peak (Fig. 2.5) from the off-energy electron background and to remove both of them from the $\gamma\gamma$-collision signal. The VSAT detector is also used as a fast luminosity and background monitor for the DELPHI experiment and the LEP central operation. It therefore has a local trigger system in order to monitor more events. The VSAT can since 1999 store 25 events in a local buffer before it is read out by a DELPHI trigger [13]. In the unlikely event that the buffer becomes full, VSAT will trigger the whole DELPHI experiment. For LEP II running, there are three different types of events that can trigger the VSAT detector:

- Every time there is a DELPHI trigger, VSAT will be read out as well, no matter what is recorded in the VSAT modules. In the raw data this represents around 25-30% of all the readout triggers. In the primary stage of offline processing, events with no signal in any of the VSAT modules are removed, reducing the DELPHI+VSAT events to about 5% of the total VSAT data.

- If there are simultaneous signals in two of the diagonal VSAT modules the Bhabha trigger is activated and the event is read out. This is the main VSAT trigger and represents about 80% of the data.

- Every time there is a signal in any of the VSAT modules the T1 trigger is activated. This is however heavily downscaled, due to the high rate of off-energy background that hits the detector, so only a small fraction of this is read out. The single electron signal is important for background studies and occupies around 15% of the data sample.

Both the beampipe upgrade in 1998 and the increase of LEP energy from 45 GeV to above 100 GeV put new requirements of the VSAT electronics and trigger system [14]. The problems encountered were however solved [15] and VSAT continued to give high quality data till the end of LEP data taking and dismantling in November year 2000.

Chapter 3

Off-Energy Background

The LEP ring has one of the best vacuum pressures in the world, and can achieve a pressure of about 10^{-10} Pa. This is about 10 million times lower pressure than in open space in the universe or 10^{15} times lower than the atmospheric pressure at sea level. The LEP beampipe has a total volume of 270 000 liters and to achieve the vacuum pressure needed, a number of different pumping methods has to be applied.

First the LEP ring is heated up to about 150-300° C, this is called the bake-out and removes all the water vapor. An initial vacuum of about 10^{-7} Pa is then created by 60 mobile pumping stations. About 2200 stationary ion pumps then take the pressure down to 10^{-8}, and finally 20 km of getter ribbon and titanium sublimation pumps push the pressure down to 10^{-10} Pa.

When the electrons and positrons are injected to the LEP ring, the vacuum pressure can unfortunately not be contained at the initial level. When the beam is started a radiation pressure is created as synchrotron radiation from the beam hit the beampipe walls, which will then heat up and emit particles. This so called dynamic pressure increases with the radiated power from the beam (Fig. 3.1). Other sources such as small leaks and astray beam particles will contribute to the static pressure build up from beam-gas particles that reside in the vacuum tube.
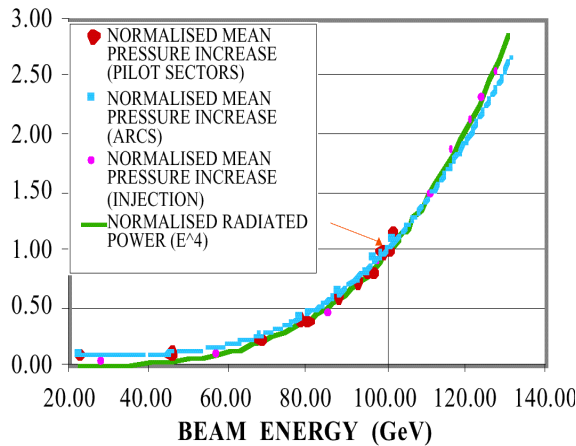

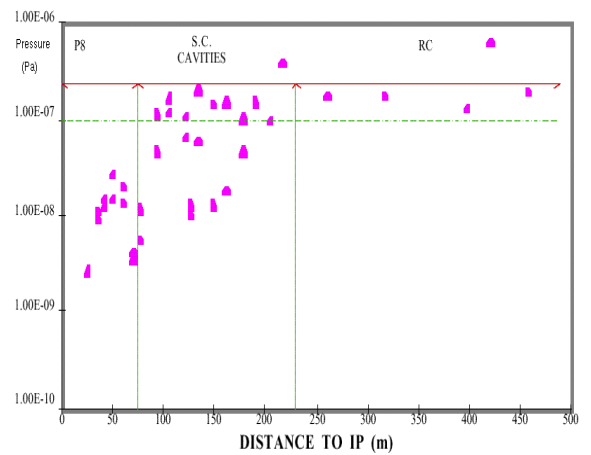Figure 3.1: The dynamic pressure as a function of energy.

Figure 3.2: The vacuum pressure in the interaction point region.

During operation with a four mA beam LEP II therefore has an average pressure of
about 10^{-7} Pa. In the proximity of the interaction point the LEP ring is straight and the
beampipe is pumped harder, reducing the pressure with about a factor ten (Fig. 3.2).
Beam particles that interact with the rest gas in the beampipe vacuum will loose part of
their energy. Particles that are off the beam energy will experience directional changes in
the bending magnets and will create a beam halo and some beam loss. This is called the
off-energy background.

3.1   Trigger Rate

As the VSAT is positioned directly on the beampipe it is flooded by off-energy electrons
that were bent off from the beamline. There are mainly two types of background electrons
that hit the detector. If the interaction between a beam- and residual gas- particle results
in a small energy loss, the deflection from the beam will also be small. This background
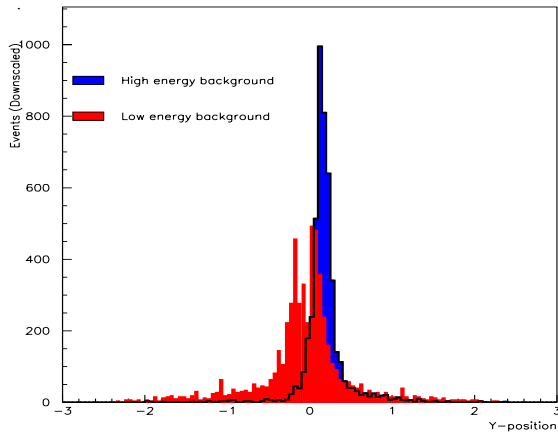thus comes from far away, has high energy and is focused in the vertical plane of the beam
(Fig. 3.3).

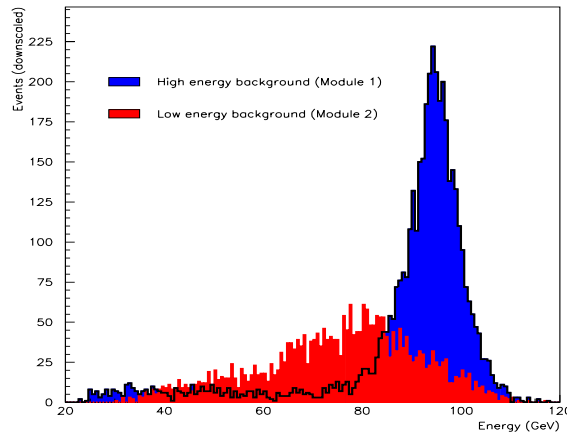Figure 3.3: The Y-position of the low and   Figure 3.4: The energy of the low and high
high energy background.   energy background.

If the energy loss with the beam-gas interference is large, the resulting background
will be more deflected and have lower energy. This background comes from a region close
to DELPHI as it can not travel very far before it hits the beampipe walls. The low
energy background is spread over all of the four VSAT modules, whereas the high energy
background is concentrated in the outer modules (Fig. 3.4).

The vacuum is better in the region close to the interaction point (Fig. 3.2), resulting
in a much lower background rate from the low-energy background. The VSAT detector
therefore has about a factor five lower background in the inner modules than in the outer
(Fig. 3.5). It is also clear that the background at Z0 running is much lower, only reaching
a total trigger rate of about 300-400 hz (compared to about 1200-1400 for high energy
running). This amount of data would require a lot of storage space and dead time if it
was recorded. The background trigger is therefore downscaled, and only a small fraction
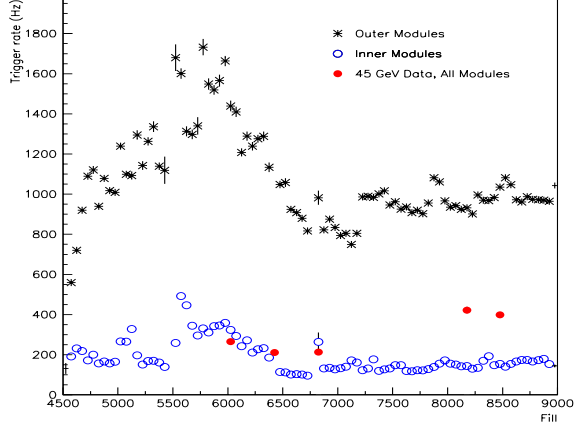of the events are read out.

Figure 3.5: The online trigger rates for the inner and outer modules. These are downscaled individually to get a balanced rate below 1 Hz in the recorded data (blocked in terms of fills=one filling of the LEP ring).
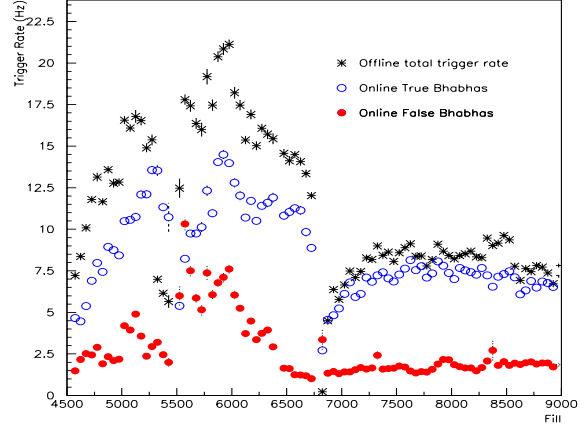
Figure 3.6: The Bhabha trigger rate. The online total Bhabha trigger rate is the sum of the true and false Bhabhas. Some events are removed in the offline processing reducing the offline trigger rate somewhat.

3.2 Background coincidences

The off-energy electron background disturbs the VSAT data in many ways, as will be discussed in section 4.1 the coincidence of two off-energy electrons can trigger a Bhabha event. This "false Bhabha" rate normally stays below 30% of the number of Bhabha triggers, but can at times go above 50% (Fig. 3.6). Most of the false Bhabhas can be removed with narrow cuts due to the well confined properties of a true Bhabha event. The remaining background can be quantized by a linear combination of four different measurements [16]:

$$ E_{cut}/(\frac{S_1 \cdot S_2}{SE_1 SE_2} - 1) \qquad \frac{SE_1 \cdot SE_2}{\Delta T} \qquad B_{soft} - B_{hard} \qquad FB_{scal} $$

Here E_{cut} is the number of events cut away by the Bhabha energy cut, S and SE the number of downscaled off-energy electron triggers with and without the energy cut. The duration of the measured data is given by ΔT and $B_{soft} - B_{hard}$ is the difference between the normal Bhabha sample and one with especially hard background cuts. Finally the FB_{scal} is the online delayed Bhabha scaler (taken as the coincidence of two opposite hits separated by four bunch crossings), which only is usable in cases of bad statistics.

A $\gamma\gamma$-event is triggered by cuts on the hadronic system in the DELPHI detector (section 5.1). If an off-energy electron coincides with the hadronic trigger, it can result in any of the following VSAT $\gamma\gamma$-event:

- If the off-energy electron is just in coincidence with a no-tag $\gamma\gamma$-event, it will be visible as a single tag.

- If the off-energy electron is in coincidence with a single tag $\gamma\gamma$-event, it can result in a double tag trigger.

- The coincidence of two off-energy electrons can also be triggered as a double tag $\gamma\gamma$-event.

The most troublesome background for this analysis is the second , as the confinement of the off-energy background is mixed up with the spread of true $\gamma\gamma$-events. The other two background triggers could in principle be completely removed by strong cuts, without too much loss of the signal. This is not possible for second type and the size of the background has to be estimated in order to make an efficiency calculation.

3.3   Probabilities

The most straight forward way to calculate the expected size of the off-energy background is to measure the probability to have an off-energy electron in any of the modules. The expected number of background events is then the probability multiplied with the number of hadronic triggers. The easiest way to measure the off-energy electron probability is to measure the coincidence rate with a Bhabha event.

For this purpose both the coincidence of a STIC or a VSAT Bhabha with an off-energy electron was measured [17]. The STIC Bhabha trigger will only use DELPHI events, whereas the VSAT Bhabha trigger covers separate VSAT events. The two individual measurements will provide a double crosscheck and assure a good result. Unfortunately the background conditions vary strongly and rapidly over the year. When the final data is selected the average probability obtained by the STIC and VSAT Bhabha measurement therefore might not be totally accurate.

The off-energy electron probability is therefore also estimated with a number of other methods (section 5.2). Table 3.1 shows off-energy electron probabilities that were found to best fit all measurements for the energy intervals used for LEP II. The probability to have two off-energy electrons in the VSAT is simply constructed as the joint probability of the two modules. The coincidence with a single tag $\gamma\gamma$-event is also calculated in a similar fashion.

	Module 1		*Module 2*		*Module 3*		*Module 4*	
Energy	Prob.	Events	Prob.	Events	Prob.	Events	Prob.	Events
189	0.935	3497	0.141	530	0.880	3309	0.320	865
192	1.340	742	0.400	222	1.465	812	0.415	230
196	1.398	2306	0.320	528	1.350	2227	0.310	511
200	1.065	1819	0.180	307	1.080	1844	0.165	282
202	0.890	725	0.075	61	0.800	651	0.105	85
206	0.850	2775	0.165	539	0.915	2987	0.070	228

Table 3.1: The probability (in %) and the expected number of events of the off-energy background.

3.4 γγ Cut-maps

In order to achieve as good purity as possible in the final γγ sample, it is necessary to impose hard cuts on the data. As mentioned before all background cannot be removed, but any physical analysis of the final sample needs a signal purity of at least 70%. This requires background rejection in the order of 90%, and at the same time it is desirable not to loose more than 50% of the signal.

The off-energy background spreads out over the whole horizontal plane of the detector and can not be confined in x. The high energy background (mainly in the outer modules) is however very well confined in the y-plane of the beam (Fig. 3.3). Unfortunately the y-position experiences rapid changes during LEP-running (Fig. 3.7).
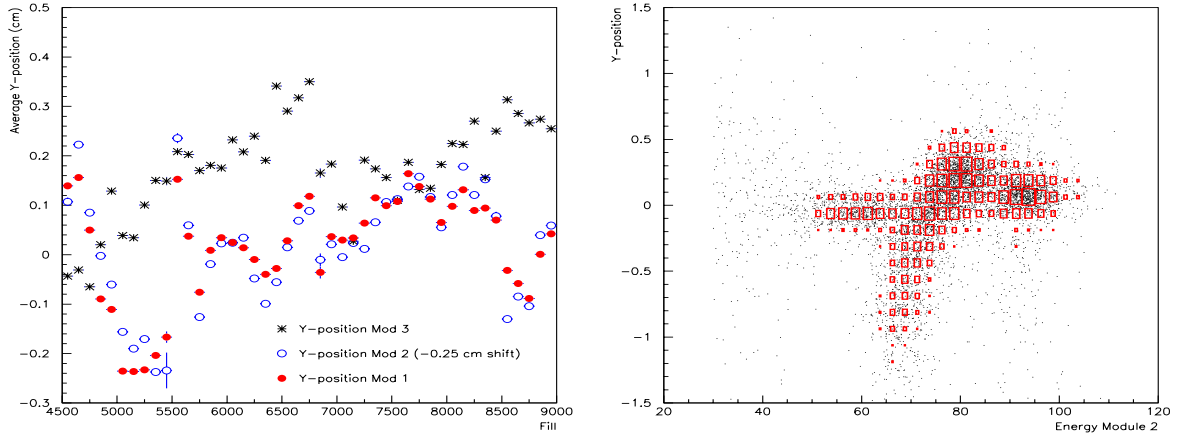

Figure 3.7: The y-position changes (equal for modules on the same side of the detector) of the off-energy background.

Figure 3.8: The energy and y-position of the off-energy background tagged in VSAT. The boxed area represent the cut-map used.

The low energy background is less confined in y, but as seen from Fig. 3.7 it follows the same changes in the beam position as the high energy background. Both the energy and y-position of the background are used for confinement. From Fig. 3.8 it is clear that no trivial mathematical expression can be used to define the rejection region for the off-energy background. Instead the imposed cut was defined with a grid map, as a function of the VSAT energy and y-position measurement [18]:

$$Y_{map} = (y_{pos} - \overline{y_{off}} + 1.6) * 25 + 1, \qquad X_{map} = E_{beam} - E + 11$$

To improve and narrow down the distribution, the y-position changes of the background ($\overline{y_{off}}$) shown in Fig. 3.7 was implemented on a run by run basis (blocks of about 20 minutes data taking in DELPHI). The grid size of the maps were set to 80, which is the origin of the constant numbers in the expressions. A map is created by filling it with off-energy electron events from the single electron trigger (Fig. 3.9). A map was defined for each module and energy interval of LEP, resulting in total of 24 different maps.
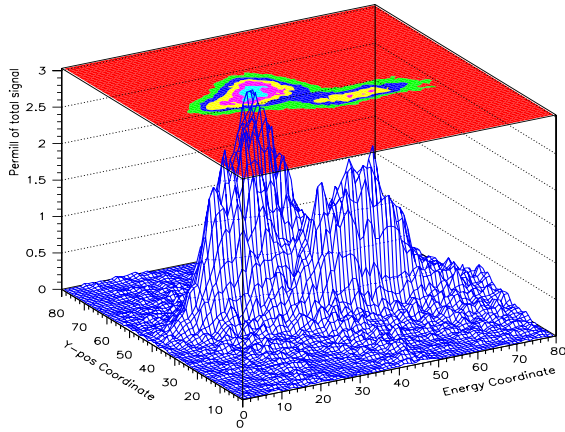
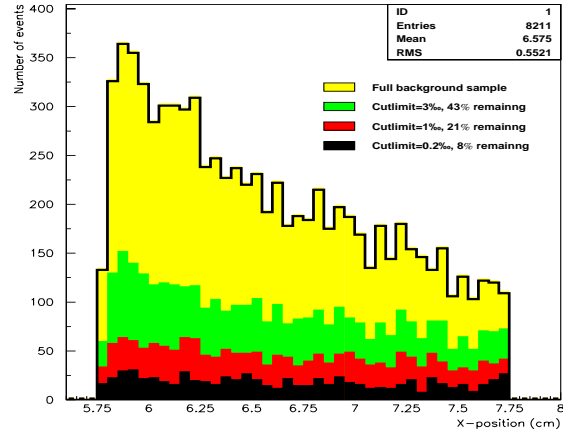Figure 3.9: The distribution of events in a cut map, a cut is imposed by specifying a level on the Z-axis.

Figure 3.10: The amount of remaining background after imposing cuts at different cut limits.

The height of each bin in the maps is defined as the relative probability (in permill) for an off-energy electron to hit that bin. The total sum of all the bins is thus equal to one (or 1000 permill). The cut is then easily imposed by specifying a horizontal cut limit in the map, removing all events that are in bins that have a height above that limit.

As the outer modules have a more confined background than the inner modules, the cut limits has to be set separately. The impact of adjusting the cut limit is shown in Fig. 3.10, where cut limit of about 0.2 permill is needed for a background rejection over 90% in the outer modules. The background rate in the inner modules is smaller and less background need to be cut away (a cut limit at around 0.4-0.6 is normally enough for the inner modules).

Chapter 4

Luminosity

All processes in elementary particle physics are based on probabilities, as it is impossible to tell in advance what is going to happen in a specific e^-e^+ collision. The probability for a specific process to happen is called its cross section, as it has the unit of m^2 (for practical reasons 1 barn$=10^{-28}m^2$ is used instead). This can be schematically viewed as the electron and positron cover certain areas in space, and the total cross section for a collision is then the sum of these areas.

The probability for a collision is then the cross section area of the two particles (σ) divided by the total area of the beams ($2\pi \cdot \sigma_x \cdot \sigma_y$). Normally there is more than one particle in the beam, so this should be multiplied with the number of electrons(N^-) and positrons(N^+) in the beam. The probability $\mathcal{P}$ for an event to happen and the collision rate per unit time $\mathcal{N}$ in a e^+e^- collider is then:

$$\mathcal{P} = \frac{N^+N^-\sigma}{2\pi \cdot \sigma_x \cdot \sigma_y} \qquad \mathcal{N} = \frac{fN^+N^-\sigma}{2N_b \cdot 2\pi\sigma_x\sigma_y} = \mathcal{L} \cdot \sigma$$

In the second expression, f is the revolution frequency and N_b is the number of bunches in the beam. The definition of the luminosity ($\mathcal{L}$) appears at the end, and is thus defined as the interaction rate per unit cross section. An accelerator is mainly defined by two parameters, the energy of the beams and its ability to achieve high luminosity. As seen from the expression above, it is clear that it is important to keep the beam-width as small as possible and at the same time to pack as many electrons and positrons in each bunch as possible. Normally the luminosity is integrated over time and the natural unit for the integrated luminosity then becomes $barn^{-1}$.

In order to compare different experiments with each other it is essential to have a good luminosity measurement, so that the cross section for different processes is comparable. The beam parameters mentioned above are hard to measure with high enough accuracy, so instead the number of events in a process with a well defined cross section are counted. For this purpose elastic electron-positron scattering (Bhabhas) normally is used. This process has a well determined cross section (eq. 4.1) as well as a distinctly defined energy and momentum distribution.

$$\frac{d\sigma_0}{d\Omega} = \frac{a^2}{16s}\frac{(3+cos^2\theta)^2}{sin^4\theta/2} \tag{4.1}$$

4.1   VSAT Bhabha Selection

From Eq. 4.1 it is clear that the cross section for Bhabha events increases rapidly at small angles, which makes the VSAT position at 3-8 mrad ideal for Bhabha measurements. Unfortunately the off-energy background also increases at small angles, and the VSAT is flooded by background hits. There is a certain probability that two off-energy electrons will hit two of the VSAT diagonal modules at the same time, and this will thus be triggered as a Bhabha event.

This so-called false Bhabha rate can be quite high (Fig. 3.6) and disturbs the VSAT Bhabha measurement. As the Bhabha process is elastic, both of the scattered outgoing electrons have the same energy and an opposite momentum. A Bhabha event can therefore be quite well contained in a circular area (due to the detector resolution) around beam energy (Fig. 4.1). The positions of the electron and positron in both x and y are strongly related as they are back to back. To isolate the Bhabha sample further an elliptical cut in $\Delta x (= x_{e^-} + x_{e^+})$ and $\Delta y (= y_{e^-} + y_{e^+})$ is made, shown in Fig. 4.2.
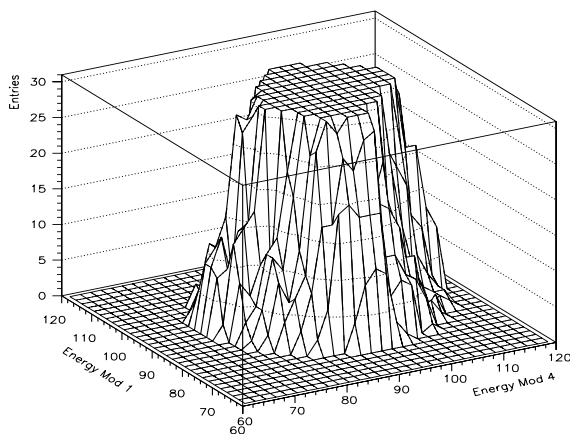

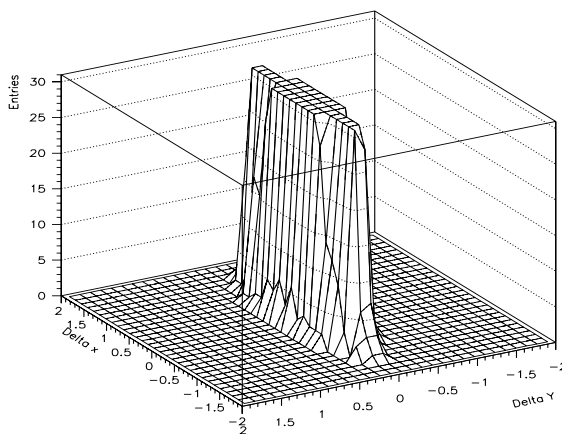Figure 4.1: The joint energy distribution of the Bhabha electron and positron.

Figure 4.2: The joint ΔX and ΔY distribution of the Bhabha sample.

The quadrupole that is placed in front of the VSAT focus the scattered electrons in the vertical plane and have a defocusing effect in the horizontal. This is the reason for that the distribution in Fig. 4.2 is more narrow in Δy. The two cuts removes about 80% of the false Bhabha background, resulting in a Bhabha purity above 90%.

4.2   STIC Normalization

The geometry of the VSAT detector and the quadrupole can not be determined to a high precision, as there is no line of sight through DELPHI. The precise shape of the flange in front of the VSAT is not known as well as one would like. The exact amount of remaining background in the Bhabha sample also suffers from some uncertainty. The accepted Bhabha cross section for the VSAT also depends on some beam-parameters that varies during data taking.

All this makes accurate absolute luminosity measurements by the VSAT difficult, which means that the VSAT absolute luminosity has to be calibrated to an accurate and well known luminosity measurement [19]. The relative luminosity measured by the VSAT is on the other hand quite accurate. Fortunately DELPHI has a second detector closer to the interaction point and at larger polar angle to measure the integrated luminosity. This is the STIC detector and it has much lower systematical error than VSAT and provides a fixed absolute luminosity measurement. The STIC has however much higher statistical error than VSAT as it collects much less data, about a factor of 15 for LEP II.

The average VSAT Bhabha cross section cannot simply be extracted by dividing the number of recorded Bhabhas with the STIC luminosity. As mentioned in the previous section, there is still some background left in the VSAT Bhabha sample, which needs to be subtracted before the average cross section can be obtained.

As shown in section 3.2 four different methods are used to extract the expected false Bhabha background rate in the Bhabha peak. These are linearly combined and are fitted simultaneously with the VSAT Bhabha cross section against the VSAT-STIC luminosity difference (Fig. 4.3). As there are two free parameters (the Bhabha cross section and the background rate) this cannot be done in one fit, so a number of fits are done converging to a minimal VSAT-STIC luminosity difference.
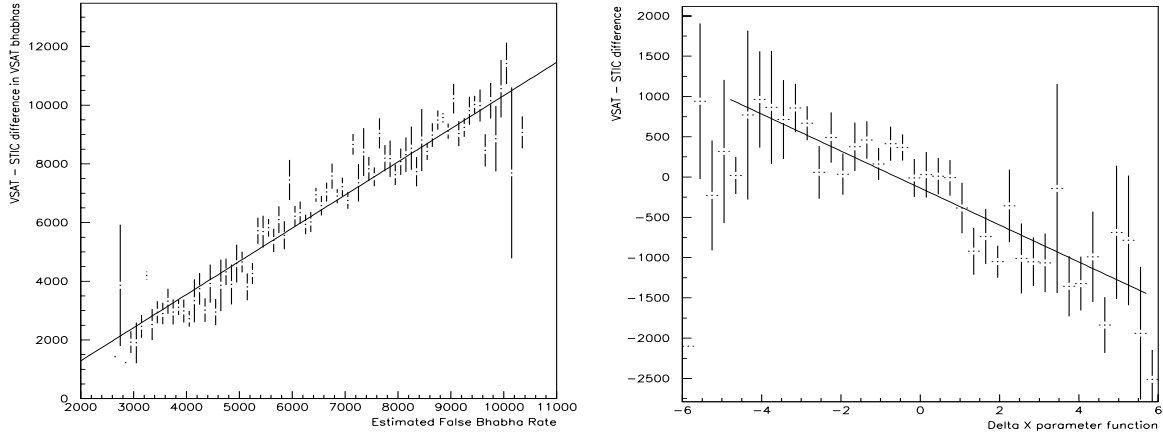

Figure 4.3: Fitting the remaining off-energy background rate to the STIC-VSAT difference.

Figure 4.4: Fitting the Δx parameter to the corrected STIC-VSAT difference.

To improve the VSAT luminosity measurement further the variations of the accepted Bhabha cross section (σ_{acc}) have to be taken into account [20]. It has been found that the cross section varies with the beam acollinearity (=angle between the beams) in both x and y. The average tilt and the width of the beams in x also changes the VSAT Bhabha cross section. Fortunately all these parameters can be estimated and parameterized by quantities measured by the VSAT detector [21]. The Bhabha diagonals are treated separately and the corrected VSAT cross section can be expressed as:

$$\sigma_{acc} = \sigma_0(1 + A(\Delta x - \overline{\Delta x})^2 + B(\Delta x - \overline{\Delta x}) + C(\sigma \Delta x + \overline{\sigma \Delta x}) - D(\Delta y - \overline{\Delta y}) + E(A_S - \overline{A_S}))$$

The Δx and Δy are the same as before, $\sigma \Delta x$ is the width of the Δx distribution and A_S is the counting asymmetry between the Bhabha diagonals. The constants A,B,C,D and E have to be determined by a fit to STIC data. This is a quite wide parameter space, so each parameter is first fitted individually (Fig. 4.4) and then a number of Monte Carlo (random selection of numbers, normally within some allowed ranges) generations are performed from that. They converge to a set of numbers that gives the smallest VSAT-STIC luminosity difference.

In all of the fits used for luminosity normalization it is important to only use half of the available data. The second half is needed to verify that the normalizations indeed improved the VSAT luminosity and not only some statistical difference between VSAT and STIC. The amount of data in each of the data-points cannot be too small, as the STIC statistical error then would be too big. To get a good and reliable result, a number of different set of data points were tried in blocks ranging from 500 to 1200 STIC Bhabhas. The fitted parameters should not depend on the block size of the data, which is a second verification that they have been correctly extracted.

4.3   LEP II Data selection

When the decision was made to upgrade the LEP I accelerator to LEP II, there were mainly two goals to achieve. The energy should be upgraded from 45 GeV to reach an energy above 100 GeV and the luminosity should be increased by introduction of so-called minibunches. This means that each bunch in the accelerator was to be split up to 4 minibunches in order to pack more electrons into the ring.

The minibunch scheme was tried out with some success for 45 GeV data in 1995, but when the energy was increased in 1996 big problems occurred. This can be seen in Fig. 4.5, where the long flat line for 1996 corresponds to about 60 days without any stable beams. Finally the minibunch scheme was abandoned for high energy data, but kept for the calibration runs with Z0 data. Clearly the luminosity improved in 1997, and was outstanding for the years 1998 to 2000.
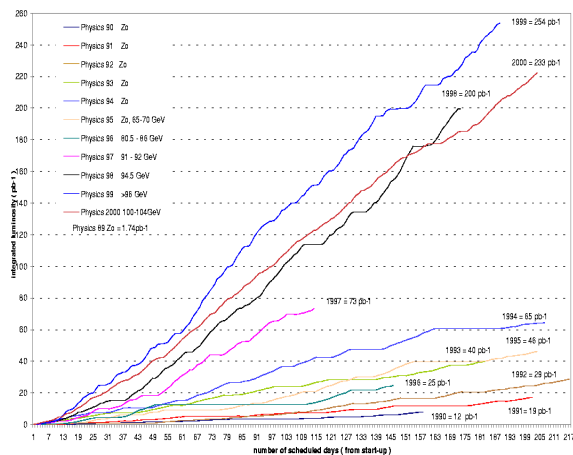

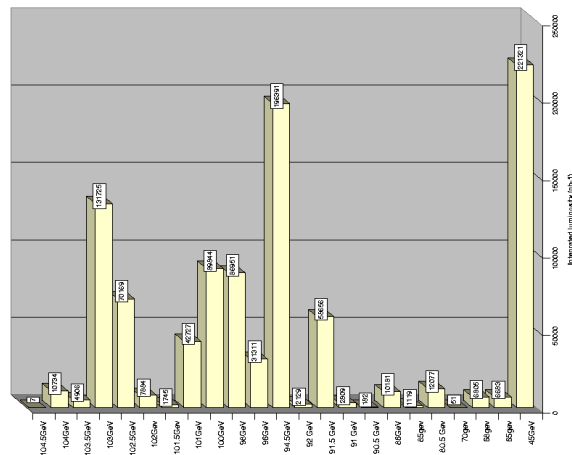Figure 4.5: The integrated luminosity over year 1990-2000.

Figure 4.6: The integrated luminosity per energy interval.

The minibunch scheme was quite difficult for the VSAT, as the minibunch spacing was shorter than the rise time of the calorimeter signal. Some new electronics were developed [22], but this never really worked as intended and suffered from big problems. So for the VSAT point of view it was good luck that the minibunch scheme was abandoned.

In 1996 the VSAT detector was experiencing some saturations in its fad and strip planes [15], which was fix in the shutdown 1996-1997. In the beginning of 1998 year data taking, it was clear that there should be no more minibunch running at high energy. The rise time problem could then be cured by delaying the VSAT trigger, and since then the energy reconstruction works without any problems. Although a method has been developed to reconstruct the energy for 1996 and 1997 [14], these years are kept out of this analysis. There are three reasons for this:

- In order to recover the correct energy the data needs to be reprocessed in the central DELPHI processing farm, which has not been done.

- The luminosity for 1996 is totally negligible and the 1997 running would add less than 10% to the data, which is not worthwhile with the extra work needed.

- VSAT was moved closer to the beampipe in 1998, and a coherent analysis can not be made with data before that.

The data from 1998 to 2000 can be grouped into six different energy intervals. The whole of 1998 was taken on 94.5 GeV and in 1999 the energy was fixed on four energy levels (96, 98, 100 and 101 GeV). In year 2000 the LEP accelerator was pushed to extreme limits and there was no fixed ($\pm 1.5 GeV$) energy within the LEP fills, and an average of 103 GeV was obtained over the whole year. The integrated luminosity delivered to the experiments can be seen in Fig. 4.6. From the VSAT point of view, the luminosity from 1998 should be multiplied with about a factor of 1.8. This is the cross section increase the VSAT gets for $\gamma\gamma$ physics due to the movement of the VSAT modules, and it is clear that data before 1998 (or a beam energy less than 94.5 GeV) is almost of no significance.

Chapter 5

$\gamma\gamma$-Collision Data

Before any two photon physics analysis can be performed on the VSAT data, it is necessary to both purify the data from background as well as calculating the size of the total $\gamma\gamma$ sample. Good purity is needed to extract physical properties of the two-photons events. The determination of the expected number of $\gamma\gamma$ events seen in the VSAT is needed to compare data with Monte Carlo and to estimate the remaining background.

5.1 $\gamma\gamma$-Trigger

The primary $\gamma\gamma$-trigger is made on the DELPHI particle system, which is referred to as a no-tag event if there are no signals in the VSAT detector. In this analysis leptonic $\gamma\gamma$-events are of no interest, so the following cuts were imposed on the DELPHI particle system:

- At least three charged tracks should be recorded in the DELPHI detector in order to have a hadronic event. A charged track is required to have a P_T of at least 0.4 GeV and to be in a theta range between 10-90 degrees.

- The invariant mass of the hadronic system should be larger than 3 GeV.

- The total energy and transverse momentum of all particles in the hadronic system should be less than 24.0 and 5.0 GeV respectively. The maximum number of allowed tracks (charged and neutral) should be less than 17. Similar cuts are also made on charged and neutral particles separately, in order to contain the hadronic system as much as possible.

- No other particle with an energy greater than 30 GeV should be seen in the DELPHI detector unless it is in STIC (which is then a STIC+VSAT double tag). This is normally called an anti-tag, and assures that the second electron ends up in the beampipe with a Q^2 around zero.

Decays from tau pairs created in $\gamma\gamma$ collisions can produce more than two charged tracks and give some background. This is however very small in the VSAT Q^2 region and can be neglected. If there is a single or double hit in the VSAT in coincidence with the DELPHI hadronic system, we get a so called single or double tagged $\gamma\gamma$ event. The tagged electron must be well reconstructed in the VSAT so there are some restrictions on the recorded hits:

- An electron is not allowed to hit any of the edges of the detector, as an accurate energy reconstruction then is impossible.

- If an electron is further out than 8 cm, it is likely to interact with the flange of the beampipe in front of VSAT and loose energy. All such triggers are thus removed due to uncertainty in the energy measurement.

- The energy of the measured electron should be greater than 30 GeV, due to the high background rates and low energy resolution at lower energies.

- The joint energy of the hadronic and VSAT system should not be larger than the double beam-energy plus the VSAT energy resolution.

If both of the electrons is tagged the full kinematics of the $\gamma\gamma$-system can be obtained. The interesting quantities to measure is the momentum transfer in the lepton-photon vertex (Q_i^2) and the invariant mass of the $\gamma\gamma$-system $(W_{\gamma\gamma})$. In the VSAT region, where the θ-angles of the scattered leptons are small, the expression for these quantities can be simplified [23]:

$$Q_i^2 \approx 4E_{beam}E_i sin^2\frac{\theta_i}{2} \qquad W_{\gamma\gamma}^2 \approx 4E_1^\gamma E_2^\gamma$$

Here $E_i^\gamma = E_{beam} - E_i$ is the energy of the radiated photon. With the VSAT detector it is possible to achieve and accuracy of 5 GeV in $W_{\gamma\gamma}$ and 0.02 GeV^2/c^2 in Q^2 [19].

5.2 Expected number of $\gamma\gamma$-Events

The expected $\gamma\gamma$-signal is extracted as the total number of events seen minus the expected background. There are two different ways to classify the total number of single and double tags. Either a trigger is accepted if there is nothing else in the other modules, or an event is tagged regardless of what is seen in the other VSAT modules.

The first method should be used if the physics in single tag events should be studied, as the second electron then is assumed to go in the beampipe with $Q^2 \approx 0$. In this analysis the single tag events are mainly used to extract the expected size of the $\gamma\gamma$-signal, therefore the second method is to prefer.

The expected background can easily be extracted as the off-energy background probability times the number of notag events, as explained in section 3.3. This gives the correct value within 5-10%, due to systematical errors and off-energy background fluctuations over the data taking period. Therefore other methods of measuring the off-energy background also had to be adopted in order to get the best possible background estimation. In this analysis the background also was adjusted to the following measurements:

- The ratio of the number of $\gamma\gamma$ events between the modules fluctuates with the beamspot position, but should be quite stable for a whole data taking period.

- The relative number of recorded events should correspond to the relative luminosity.

- By adjusting the size of the cut maps and compare the impact on data, background and $\gamma\gamma$-Monte Carlo, it is possible to extract the expected background [18].

- The energy distribution of the data should be comparable to that of the Monte Carlo, or at least the same for all modules. The off-energy background and γγ energy distribution look quite different, so a change in the size of the subtracted background will directly reflect in the final energy distribution.

Taking these measurements into account, the off-energy background probability obtained from STIC and VSAT Bhabha measurements could be fine tuned. Once the expected number of background events (Table 3.1) have been obtained, the γγ-signal is extracted as the remaining part of the data. This is presented in table 5.1 along with the probability to have a single tag event, when the hadronic system is triggered.

Energy	Module 1		Module 2		Module 3		Module 4	
	Events	Prob.	Events	Prob.	Events	Prob.	Events	Prob.
189	2571	0.81	2234	0.71	2177	0.69	2290	0.72
192	415	0.73	360	0.64	347	0.61	369	0.65
196	1405	0.81	1216	0.71	1179	0.68	1252	0.73
200	1447	0.78	1250	0.67	1199	0.64	1277	0.69
202	678	0.74	584	0.64	569	0.62	599	0.65
206	2558	0.73	2288	0.65	2187	0.62	2348	0.67
TOT	9073	0.77	7932	0.67	7659	0.65	8135	0.68

Table 5.1: The expected number and probability(in %) of single tag γγ-events.

If the two photons in a γγ collision were totally independent, the probability for a double tag would just be the joint combination of two single tags. The cuts on the particle system do however relate the two electrons and thereby increases the double tag probability. The expected number of double tags is therefore extracted by partly looking on the double tag data when the expected background has been subtracted and partly on the probability of a single tag [18]. This is presented in table 5.2 along with the Monte Carlo expectations.

Energy	1+4	2+3	1+3	2+4	Tot	MC
189	27	22	26	22	97	92
192	4	3	4	3	14	16
196	15	12	14	12	53	48
200	14	11	14	12	51	52
202	6	5	6	5	23	25
206	24	20	23	21	89	93
Tot	90	74	87	75	326	327

Table 5.2: The expected number of double tag γγ-events for different module combinations and the total sum compared with Monte Carlo

5.3 Cut-map Efficiency

The cut-maps described in section 3.4 works very well on single tag data, and a purity over 85% in the data can be achieved after the cuts. The double tag case is harder to deal with as the main background is a single tag $\gamma\gamma$ plus an off-energy electron. This background is not as confined as the pure off-energy electron background, and the cut-maps will be less effective. Applying the cut-maps on both of the electrons in a double tag event is however the best approach to reject the most of this background.

A purity over 75% in the final sample is desirable in order to get good quality of the data. The cut limit for the outer and inner modules were set to 0.15 and 0.5 respectively (removing all events that hit the cutmap in bins with more than 0.15/0.5 permill of the background signal). An average purity of 75% was then obtained, with only a 36% loss of the $\gamma\gamma$ signal (Table 5.3).

Energy	Events	Exp. Gam	Purity	$\gamma\gamma$-loss	Full	Prob.
189	78	56	0.72	0.43	101	97
192	12	8	0.63	0.35	13	14
196	47	34	0.72	0.32	49	53
200	43	35	0.81	0.31	51	51
202	9	6	0.66	0.35	9	23
206	74	58	0.79	0.37	93	89
Tot	263	197	0.75	0.36	317	326

Table 5.3: The remaining $\gamma\gamma$-signal, its purity, data loss, expected full signal and signal expected from probability calculations

The cuts used on data also have to be used on the Monte Carlo in order to get comparable results. As mention in section 3.4, the cut-maps are run-dependent as the y-position of the off-energy background changes. Monte Carlo has a fixed beam position over the whole year, and therefore an average fixed Y-value had to be used.

5.4 VSAT+STIC Double Tags

From the VSAT data it is also possible to study the coincidence of a single tag electron in VSAT and a high energy electron in the STIC detector. If the VSAT background is cut away efficiently enough, this will result in a new set of double tag data in the Q^2 region of 20-100 GeV. As a result of this, the cuts on the maximum number of tracks and energies in the hadronic system must be removed, so that no important events are cut away.

To achieve good purity in the data sample, only STIC events with an angle greater than three degrees and an energy above 40 GeV were accepted. The normal cut-maps were applied to the VSAT data, resulting in a purity above 85%. In total 223 STIC+VSAT double tag events were found after the imposed cuts, with an expected background of about 33 events. This shall be compared with the 218 events seen in Monte Carlo, which is slightly higher but within the expected errors.

Chapter 6

Two Photon Physics

As already mentioned in the introduction, the photon can be described as a superposition of a number of virtual states. Each state represents the probability to fluctuate into a quark-antiquark or lepton-antilepton pair and can be represented by a wave-function. Due to theoretical difficulties the quark-antiquark pair is subdivided into high and low virtuality fluctuations, with a cutoff-limit (p_T) in the transverse momenta of the quarks. The high virtuality part can be calculated by perturbative QCD, whereas the low-virtuality part is described in a non-perturbative phenomenological model involving the summation over vector meson states. In mathematical form the photon therefore is described as the bare photon plus three summation terms [24]:

$$|\gamma> = c_{bare}|\gamma_{bare}> + \sum_{V=\rho^0,\omega,\phi,J/\psi} v_V|V> + \sum_{q=u,d,s,c,b,t} c_q|q\overline{q}> + \sum_{l=e,\mu,\tau} c_l|l^+l^-> \qquad (6.1)$$

The last term describes the fluctuation into a lepton-antilepton pair and is calculable to high precision by QED and is in this scenario of less interest and will be discarded from the analysis. The two other terms describe the hadronic part of the photon wave-function and photon-photon collision studies will help to improve our understanding of QCD.

6.1 $\gamma\gamma$ Interactions

A hadronic $\gamma\gamma$ collision can be described by any of the hadronic terms in equation 6.1, which gives rise to a wide range of possible interactions. Previously these processes could be reduced into two main classifications, a vector dominance process for soft hadronic interaction (Fig 6.1) and a direct coupling to pointlike quarks (Fig 6.2) [25].

In the late 80's experiments started to produce results that could not be explained by these two processes [26]. As the photon can fluctuate into a $q\overline{q}$ state, which can fluctuate into more complex partonic states, it is convenient to define Parton Density Functions (PDF's) for the photon in a similar way that is done for the hadron. This means that the photon is described as an object with smaller partonic constituencies of quarks, antiquarks and gluons. One of the photons may react directly with one of the partons of the other photon (Fig. 6.3), or partons from both of the photons can react with each other (Fig. 6.4) [25].
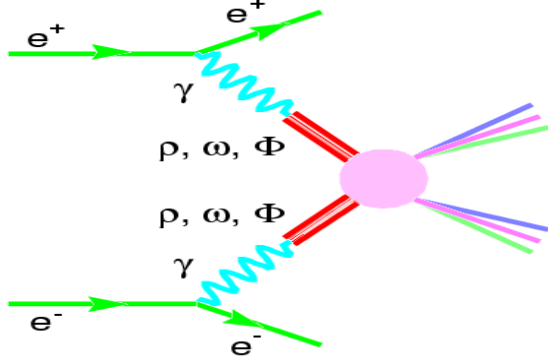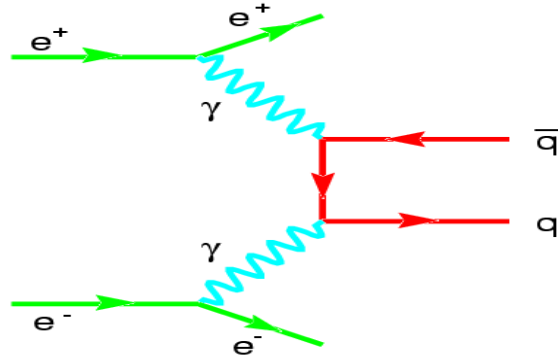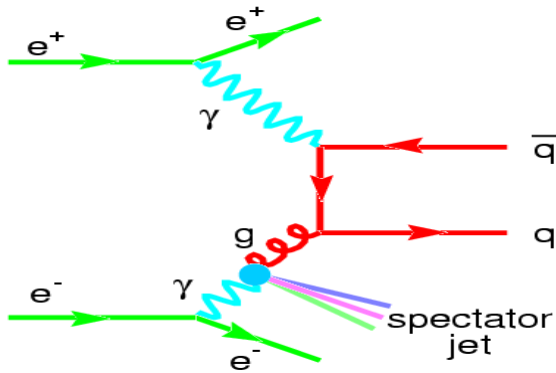
Figure 6.1: The VDM process

Figure 6.2: The QPM process
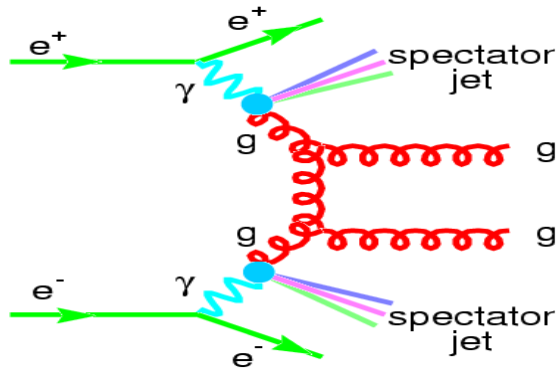

Figure 6.3: The single resolved process

Figure 6.4: The double resolved process

6.2   Monte Carlo models

The different processes above have to be simulated using theoretical assumptions, where the physical properties of the reaction is translated into a mathematical form in a Monte Carlo model (see chapter 7). The process in Fig. 6.1 is simulated by a non-perturbative phemenological model called the Vector Dominance Model (VDM). This was developed about 25 years ago in order to relate $\gamma\gamma$-collisions with hadron-hadron physics.

The VDM model assumes that the virtual fluctuation of a photon into a quark-antiquark pair has a lifetime long enough to form a bound vector meson state. This is possible when the transverse momenta (p_T) of the branching $(\gamma \rightarrow q\bar{q})$ is small, and the model is thus describing the low p_T part of a $\gamma\gamma$-collision.

At higher p_T the photons can give a $q\bar{q}$-pair, which is described by the QPM model. The direct and pointlike coupling of photons to quarks is described by perturbative calculations and is treated in similar way as the QED reaction $e^+e^- \rightarrow e^+e^-\mu^+\mu^-$. The QPM model is only applicable at large Q^2, high p_T or large quark masses. The contribution to the total cross section of the relatively low Q^2 of most two-photon events is therefore quite small, but grows to become more important with increasing Q^2.

The $q\bar{q}$ pair from a photon can fluctuate further into more complicated states, as shown in Fig. 6.3 and 6.4. The photon can therefore be described by a set of Parton Density Functions (PDF's). These functions give, for each parton, the parton density for a given x and Q^2 value. Here x is the fraction of the total longitudinal momentum of the photon carried by the parton.

The PDF's are used in the QCD Resolved Photon Contribution model (QCD-RPC), which is needed in order to describe data at low Q^2. The QCD-RPC model considers hadronic scattering subprocesses to be perturbative and has therefore a p_T^{min} cut on all PDF's, setting the lower transverse momentum limit on the outgoing partons. This cut separates the model from contributions from the non-perturbative region at low p_T. There are several different parameterizations available to describe the parton density of the photon. The difference in their behavior is mainly seen at low values of x [27].

6.3 Photon Structure Functions

A hadron can be described by its parton contents, and as photons fluctuate into partonic states a similar description can also be adopted for the photon. The partonic content of a photon is described by the photon structure functions, which is closely related to the PDF's described previously. If one of the photons in a $\gamma\gamma$-collision is almost on-shell with a $Q^2 \approx 0$, the whole process can be viewed as deep inelastic scattering of the tagged electron off the quasi-real target photon. The cross section can then be expressed as:

$$\frac{d\theta_{e\gamma \to eX}}{dxdQ^2} = \frac{2\pi\alpha^2}{xQ^4}[(1 + (1-y)^2 F_2^\gamma(x,Q^2) - y^2 F_L^\gamma(x,Q^2)]$$

, where

$$x = \frac{Q^2}{2q_2 \cdot q_1} \approx \frac{Q^2}{Q^2 + W^2} \qquad , \qquad y = \frac{q_2 \cdot q_1}{kq_2} \approx 1 - \frac{E_{tag}}{E_{beam}} cos^2(\frac{\theta_{tag}}{2}).$$

y is normally very small in the region studied, so it is only possible to measure F_2^γ. In the simple parton model F_2^γ is taken as a sum over the quark and antiquark density functions. The Q^2 evolution of these PDF's are described by the Altarelli-Parisi equations. In case of the photon, there is an extra term corresponding to a gamma going into a $q\bar{q}$ pair. This renders the equations inhomogeneous and a linear rise of F_2^γ with $\ln(Q^2)$ is expected. This was seen by the LEP experiments, and is presented in Fig. 6.5.

One of the more important results from HERA was the observed rise of the proton structure function (F_2^p) at low x-values. A similar rise is also expected for the F_2^γ structure function at very low x. Evidence for this is piling up from the latest results (Fig. 6.6) of the LEP experiments [27].
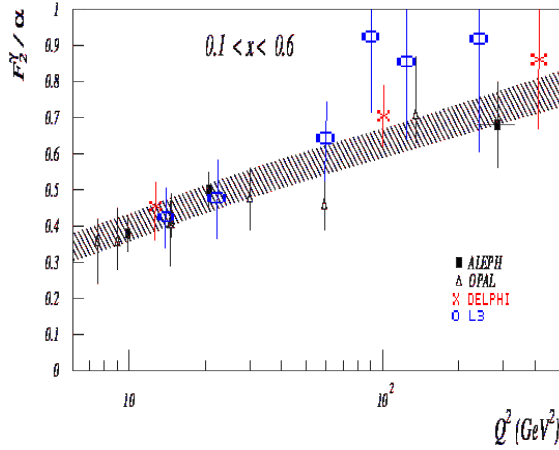
Figure 6.5: F_2^γ as a function of log Q^2.
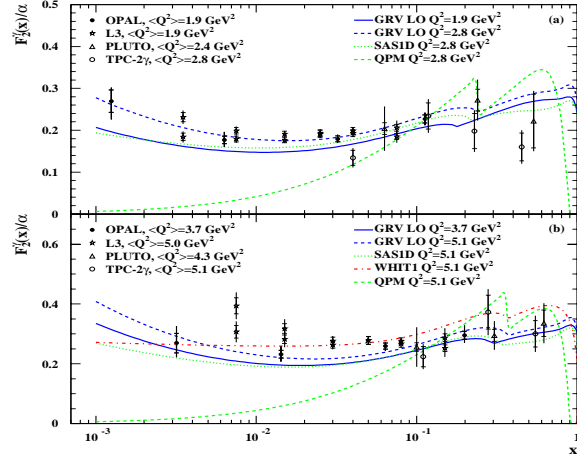
Figure 6.6: The low-x behavior of F_2^γ.

6.4   Total Cross section

The $\gamma\gamma$-collision processes have for LEP II energies typically cross sections that are two to three orders of magnitude larger than e^+e^- annihilation processes [28]. The cross section for the process $\gamma\gamma \rightarrow hadrons$ is extracted from the measurement of $e^+e^- \rightarrow e^+e^- + hadrons$ [29]:

$$\frac{d\sigma_{ee}}{dW_{\gamma\gamma}^2/s} = \int \frac{dQ_1^2}{Q_1^2}\frac{dQ_1^2}{Q_1^2} \sum_{a,b=T,S} \mathcal{L}_{ab}\sigma_{ab}^{\gamma\gamma}(W_{\gamma\gamma}^2,Q_1^2,Q_2^2)$$

Here $d\sigma_{ee}$ is the measured cross section for the $e^+e^- \rightarrow e^+e^- + hadrons$ reaction for a certain dW interval. The center of mass energy is given by $\sqrt{s}$ and $\mathcal{L}_{ab}$ is the two photon luminosity function, which describes the photon flux. Q_i^2 are the virtualities (momentum transfer in the eγ vertice) of the radiated photons. The hadronic cross sections σ_{ab} correspond to specific helicity states (T=transverse and S=Scalar) of the interacting photons. If $W^2 >> Q_i^2$ it is possible, to a very good approximation, assume factorization of the Q and W dependencies of σ_{ab} [30]:

$$\sigma_{ab}(W_{\gamma\gamma}^2,Q_1^2,Q_2^2) = h_a(Q_1^2)h_b(Q_2^2)\sigma_{\gamma\gamma}(W_{\gamma\gamma}^2)$$

The functions $h_{a,b}$ are model dependent and describe the Q^2 behavior of the hadronic cross section. If this is known it is possible to extrapolate the $\sigma_{ab}(W_{\gamma\gamma}^2,Q_1^2,Q_2^2)$ to $Q_i^2 = 0$ without any loss of the W dependence. It is clear that the extrapolation to $Q^2 = 0$ is better for small values of Q_i, which favor notag data. At low Q^2 most of the hadronic system is however lost in the beampipe and the W measurement of notag data needs to be unfolded with different MC simulations.

Double tag data do on the other hand provide an excellent W measurement from the tagged electrons, and no model dependent unfolding is needed. The extrapolated to $Q^2 = 0$ is however strongly model dependent for large Q^2 values and this can result in large uncertainties in the $\sigma_{\gamma\gamma}(W^2)$ measurement. The VSAT detector therefore has a unique advantage, as is it can measure double tag events at low Q^2 values.

Chapter 7

Monte Carlo

Physics today consists of models trying to describe properties of the reality in the most simple and logical way. In order to test the validity of any theoretical model of a physical process, it must be compared with real measurements by a experiment. The theoretical assumptions and model descriptions are implemented into a Monte Carlo (MC) computer program that randomly generate events according to some preset rules. The generated events are then run through a simulation program that should describe the detector response, which then can be compared with real data.

7.1 MC Generators

There are a number of different MC models on the market to describe two-gamma physics. Some earlier models could recently be rejected, as the quality of the data now is good enough to discard them. There are mainly four different MC generators used in the $\gamma\gamma$-physics analysis today [28]:

- **HERWIG 5.9** [31] is a general-purpose QCD generator to simulate Hadron Emission Reactions With Interfering Gluons. The old version of HERWIG 5.9 has been replaced with HERWIG 5.9+k_t (dyn) for $\gamma\gamma$ studies. In the new version the quarks inside the photon have a modified transverse momentum distributions (k_t).

- **PHOJET 1.05** [32] is a minimum bias event generator for pp, γp and $\gamma\gamma$ interactions, described with the Dual Parton Model (DPM) in terms of Reggeon and Pomeron exchanges combined with the QCD-improved parton model. PHOJET has in particular a detailed modelling for diffractive and soft interactions.

- **TWOGAM** [34] is a pure $\gamma\gamma$ event generator where all $\gamma\gamma$-interactions are stripped down to three different processes: The Quark Parton Model (QPM), the Vector Dominance Model (VDM) and also the Resolved Photon Contribution (RPC).

- **PYTHIA** [33] is a general-purpose event generator for high energy physics, which recently also is used to simulate $\gamma\gamma$ physics. The model uses, similar to TWOGAM, three components to describe the photon. In $\gamma\gamma$ interactions there should then be 3x3 event classes, but the 'off-diagonal' combinations appear pairwise. The program therefore uses six event classes to describe two-photon collisions.

7.2   Twogam

TWOGAM is the MC generator that is most commonly used in DELPHI and was therefore
used in this analysis. The TWOGAM generator has the advantage of generate the different
model constituencies separately, which allows to easily qualify the importance of a model
in a certain Q^2 region. For this analysis five data sets were generated by the TWOGAM
generator, presented in Table 7.1.

Name	Luminosity	Center of mass energy	Radiative Corrections
98	300	189	No
98 R	450	189	Yes
99	450	200	No
00	450	206	No
00 R	450	206	Yes

Table 7.1: The generated MC samples.

The generated MC events are then processed through two simulators, DELSIM [35]
and FASTSIM [36], in order to generate the detector response for the DELPHI and VSAT
detectors respectively. It is vital that the coordinate systems of DELPHI and VSAT are
the same as the one of the generated MC. The DELPHI coordinate system is fixed with
help of the vertex detector, that can measure the location of the interaction point very
accurate. The VSAT position is fixed by using the symmetries of Bhabha events [37].

As mentioned in section 6.2 the QPM model describes data at high Q^2, and is of less
importance in the VSAT region (which has a Q^2 between 0.02 and 0.6). The size of the
QCD-RPC model depends on the value chosen for the p_T^{min} cut-off limit for the Parton
Density Functions. As seen from Fig 7.1 even a small change in the p_T^{min} value will make
a clear change in the size of the QCD-RPC contribution. The weights of each of the
contributions for a p_T^{min} of 2.05 are shown in Fig. 7.2.
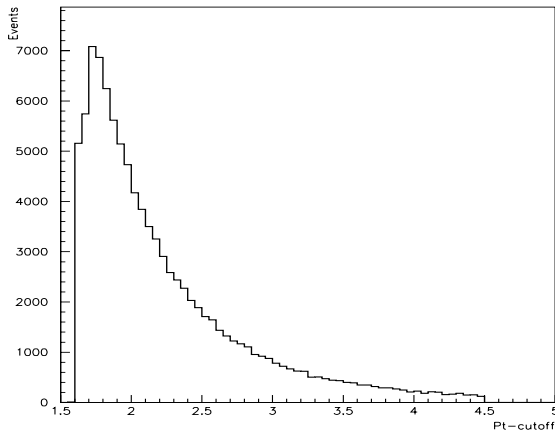
Figure 7.1: The p_T^{min} distribution for the QCD-RPC model.
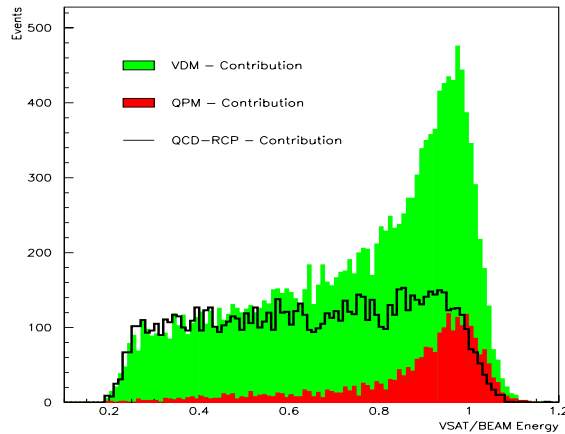
Figure 7.2: The size of the different MC models in the VSAT Q^2 region.

7.3 The p_T cut-off

If the exact normalization of the MC was known it would be easy to find p_T^{min}, as the number of events in data and total MC would be equal. There is however a rather large (10-20%) uncertainty in the total cross section of the MC, so it would not be correct just to normalize the size of the data and MC with help of the p_T^{min} factor. Instead distributions of physical quantities sensitive to the QCD-RPC model have to be compared with data for the best fit of p_T^{min}. From Fig. 7.2 it is clear that the total energy distribution of the tagged electron will change with the p_T^{min} cut-off limit. This has been compared with data in Fig. 7.3 for three different values of p_T^{min} (There is in principle no QCD-RCP contribution for p_T^{min} greater than five).
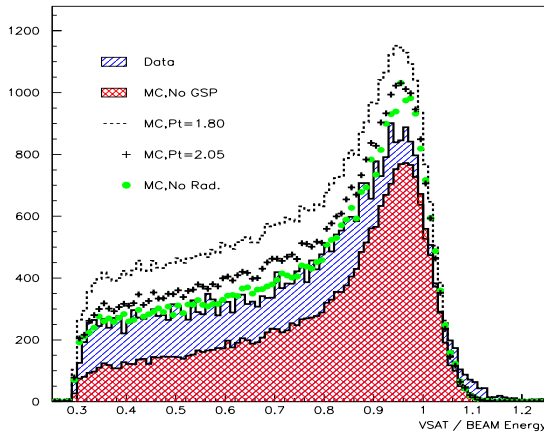
Figure 7.3: The total energy distribution of MC with different values of p_T^{min}.
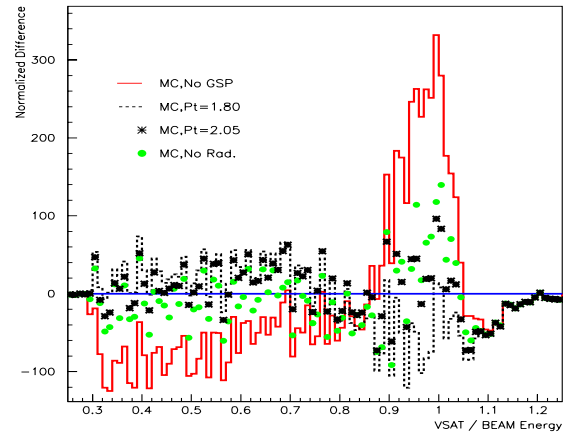
Figure 7.4: The normalized energy distribution for different values of p_T^{min}

It is clear that MC with p_T^{min} equal to 1.8 gives too many events and MC with no QCD-RCP contribution results in too few events. This could however be due to a bad normalization of the MC, so instead the normalized difference between data and MC was calculated in Fig. 7.4. Clearly the QCD-RCP contribution is needed in the MC, but the exact limit of p_T^{min} is hard to extract from this quantity.

The invariant mass reconstructed from the hadronic system also differs for the three MC models (Fig. 7.5). The invariant mass can thus also be used to find the p_T^{min} cutoff limit. The ratio between the invariant mass distribution for data and MC is plotted in Fig. 7.6 for the same values of p_T^{min} as before.

The main bulk of events in Fig. 7.5 and 7.6 is between 3 and 10 GeV, so it is clear that p_T^{min} equal to 1.8 results in an excess of events and with no QCD-RPC contribution there are again too few events. The slope of the ratio is however more interesting to look at, as it should be more or less flat when a good agreement with data is found. A p_T^{min} cut at 2.05 seems to agree quite well with the data, and it is clear that the other two p_T^{min} limits can be excluded.
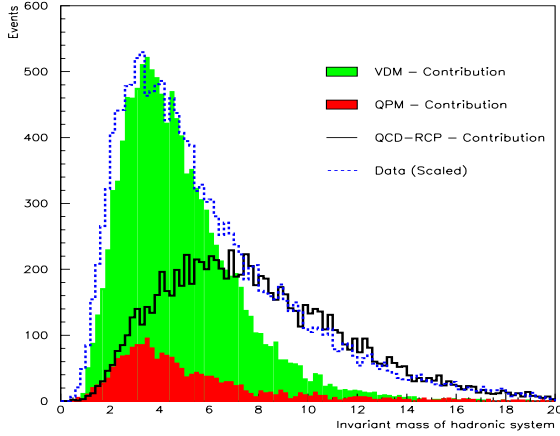
Figure 7.5: The invariant mass distribution for the different MC contributions. The distribution for data is also shown as a comparison.
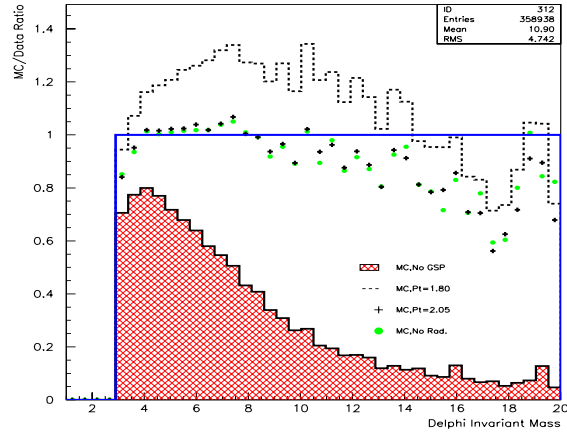
Figure 7.6: The ratio of the invariant mass distribution for data and MC samples with different values of p_T^{min} (5.0, 2.05 and 1.8).

It is quite hard to distinguish the MC with or without radiative corrections, but it is clear that a p_T^{min} around 2.05 should be used. These results came from single tag data, which has small statistical error. The double tag data suffers from much larger statistical errors, but should also be checked for cross-reference. The number of accepted double tag events for different p_T^{min} limits can be found in table 7.2.

Energy	Data	MC(p_T=1.8)	MC(p_T=5.0)	MC(p_T=2.05)	MC(2.05, NORAD)
189	97	110	57	93	79
200	140	174	72	141	127
206	89	118	49	93	88
TOT	326	402	178	327	294

Table 7.2: The number of double tag events seen in data and in MC for different values of p_T^{min}.

The MC with p_T^{min} equal to 1.8 and 5.0 is as before too big and too small respectively. The MC with radiative corrections still agree very well with the data with a p_T^{min} equal to 2.05. The MC without radiative corrections is now however too small, with about 11% loss of events. As shown in section 7.2 there is no 200 GeV MC with radiative correction generated, so this was constructed by just up-scaling the 200 GeV MC without radiative correction with 11%.

7.4 Comparison with data

All observables should be measured for both data and MC, to make sure that MC can describe the data in a satisfactory way at all instances. Data and MC were compared for the whole LEP II period to increase the statistics, the individual data set did however also show excellent agreement. Comparisons were made for p_T^{min} equal to 1.8, 2.05 and 6.0 for normal MC (200 GeV MC extracted as before) and for p_T^{min} at 2.05 for MC without radiative corrections. In the following plots the data and MC has been cut with the cut-maps and the expected remaining background distributions have been subtracted. The remaining number of events is shown on the y-axis and the following data was examined:

- Observables from the hadronic system for single tag VSAT data is shown in Fig. 7.7. Excellent agreement is seen with p_T^{min}=2.05, except for very low values of invariant mass and total energy of the hadronic system. There is no visible difference between MC with and without radiative corrections.

- Fig. 7.8 show quantities reconstructed from the tagged electrons in the VSAT double tag data. There is good (within statistical errors) agreement between data and MC with radiative corrections and p_T^{min}=2.05 is found in all plots.

- Quantities reconstructed the DELPHI hadronic system is shown both from VSAT+VSAT and VSAT+STIC double tag data. This is shown in Fig. 7.9 and 7.10. Once again MC with radiative corrections and p_T^{min}=2.05 give the best agreement with data.

- Finally the tagged electrons from the STIC+VSAT double tag data were used to extract the invariant mass. This is shown in Fig. 7.11 together with Q^2 for the tagged electrons and the total energy of the hadronic and electron system.
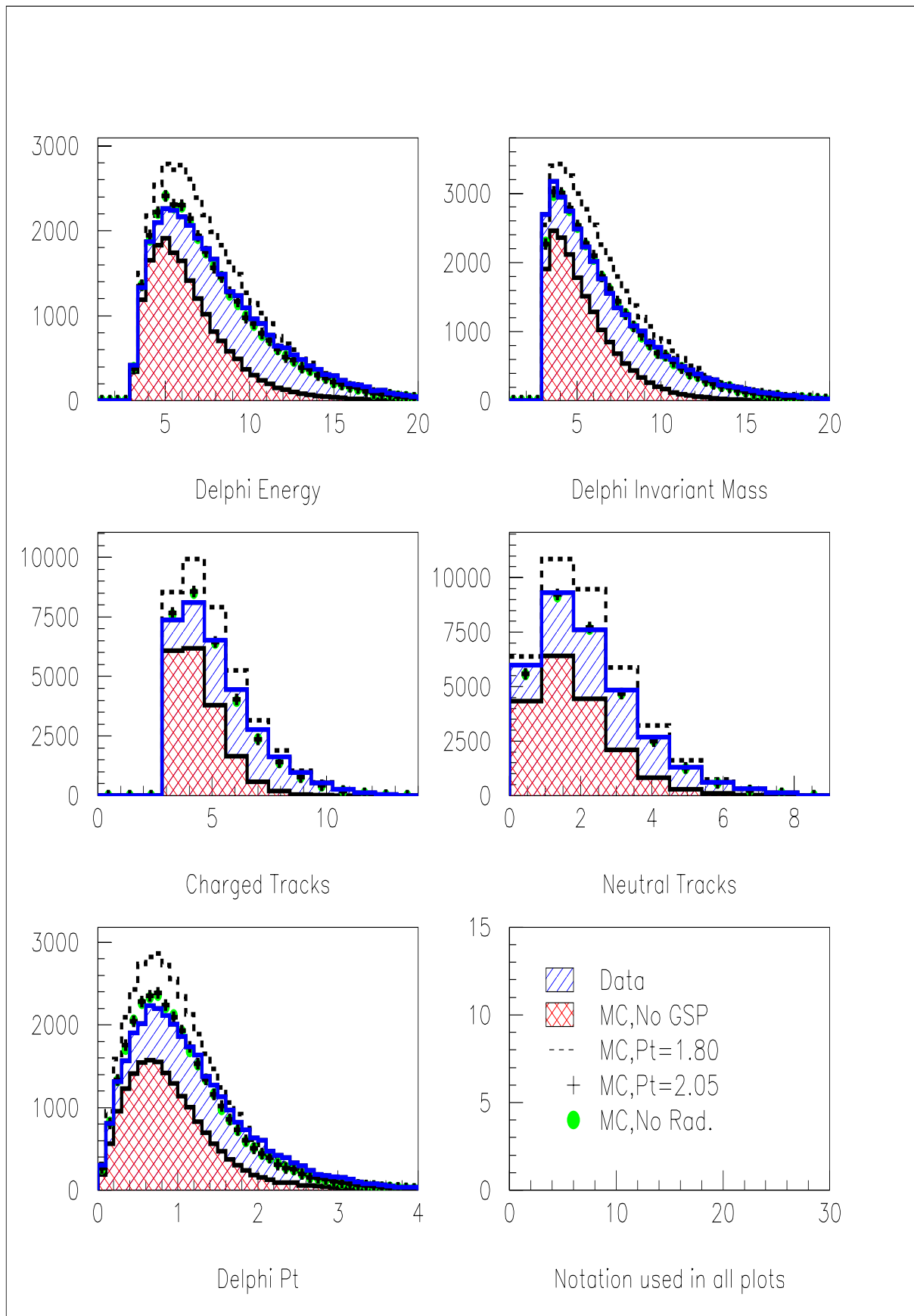
Figure 7.7: VSAT single tag data.
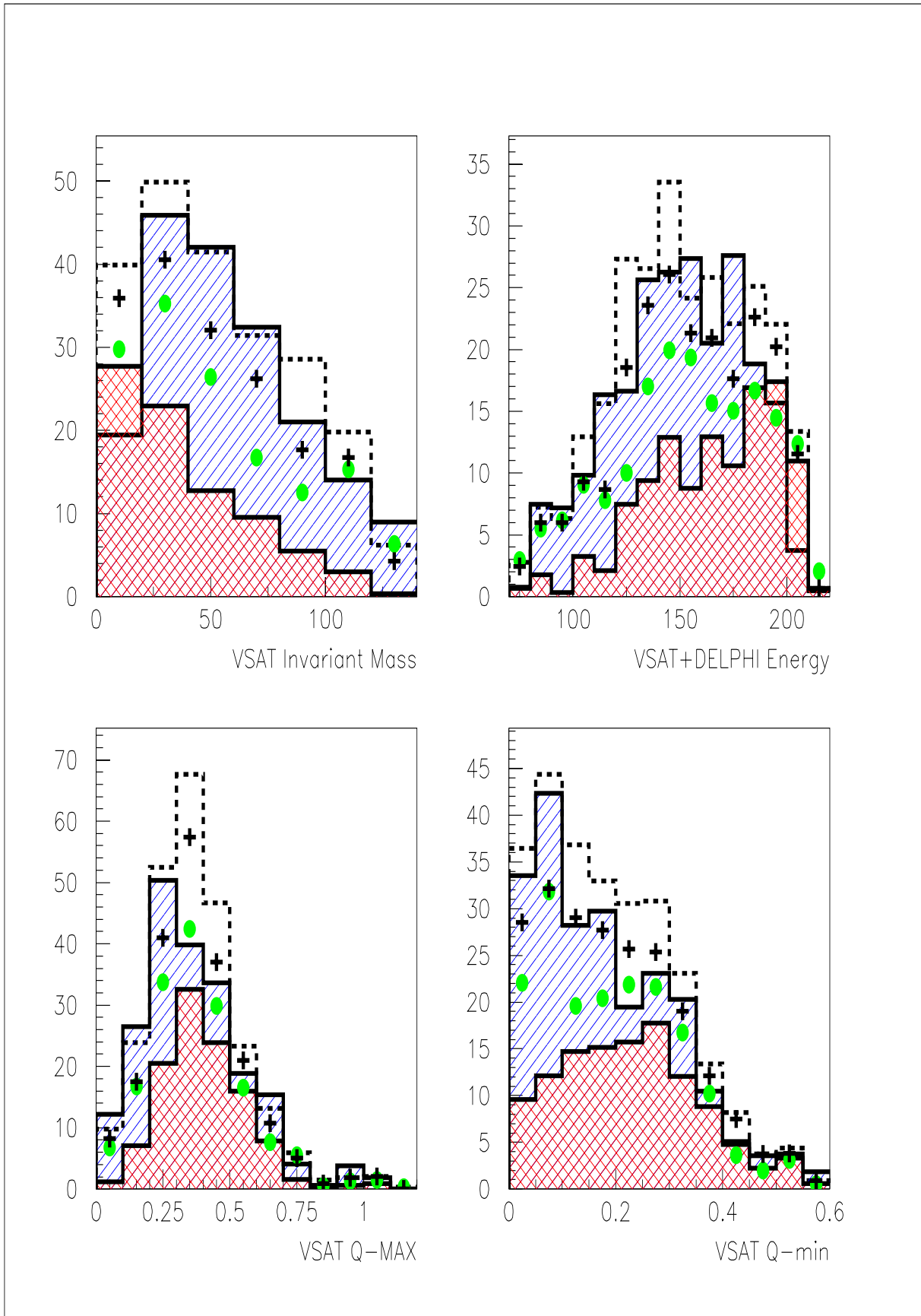
Figure 7.8: VSAT double tag data, observables taken from the e^+e^- system.
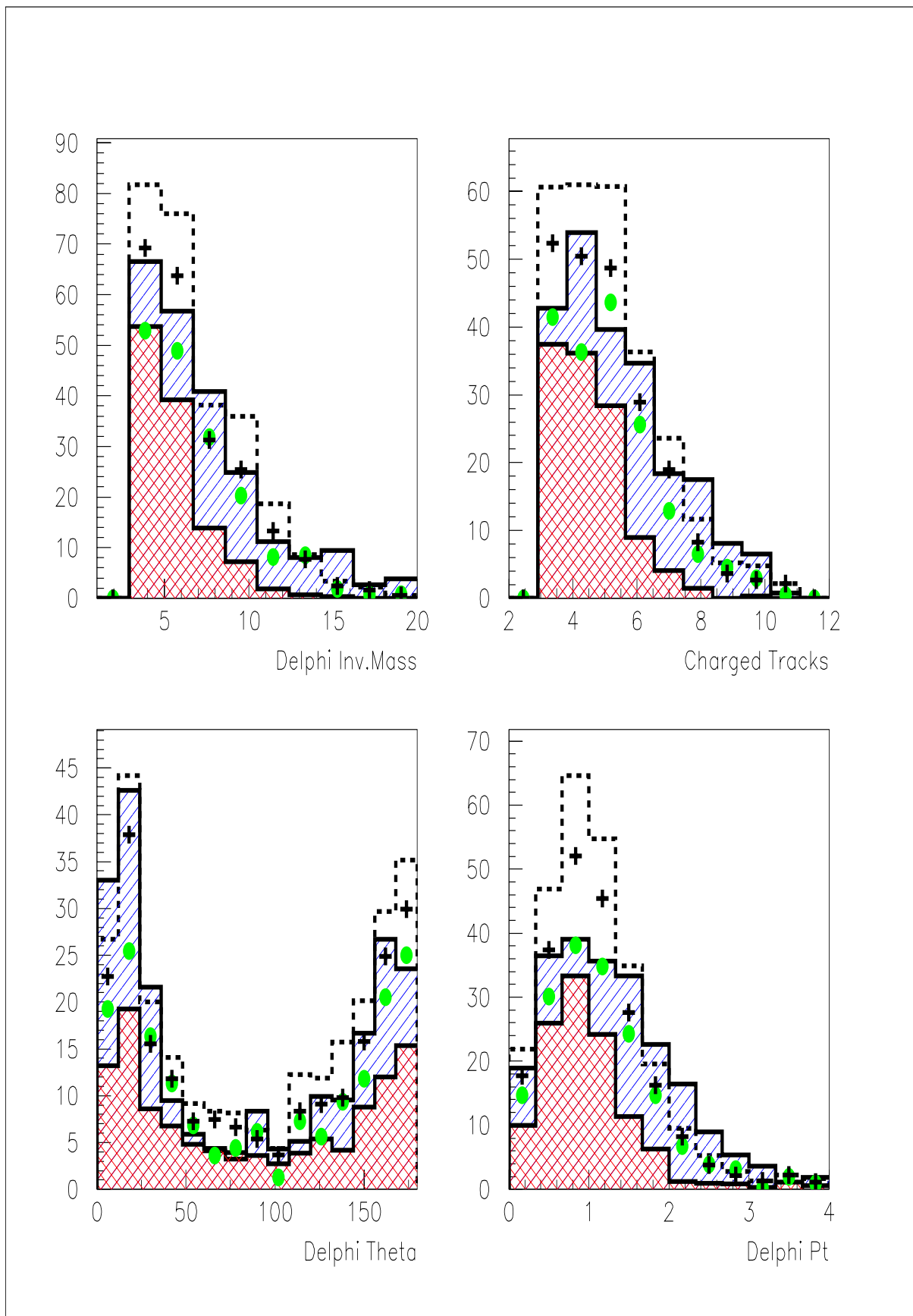
Figure 7.9: Quantities from the hadronic system in VSAT double tag data, notation as Fig. 7.7.
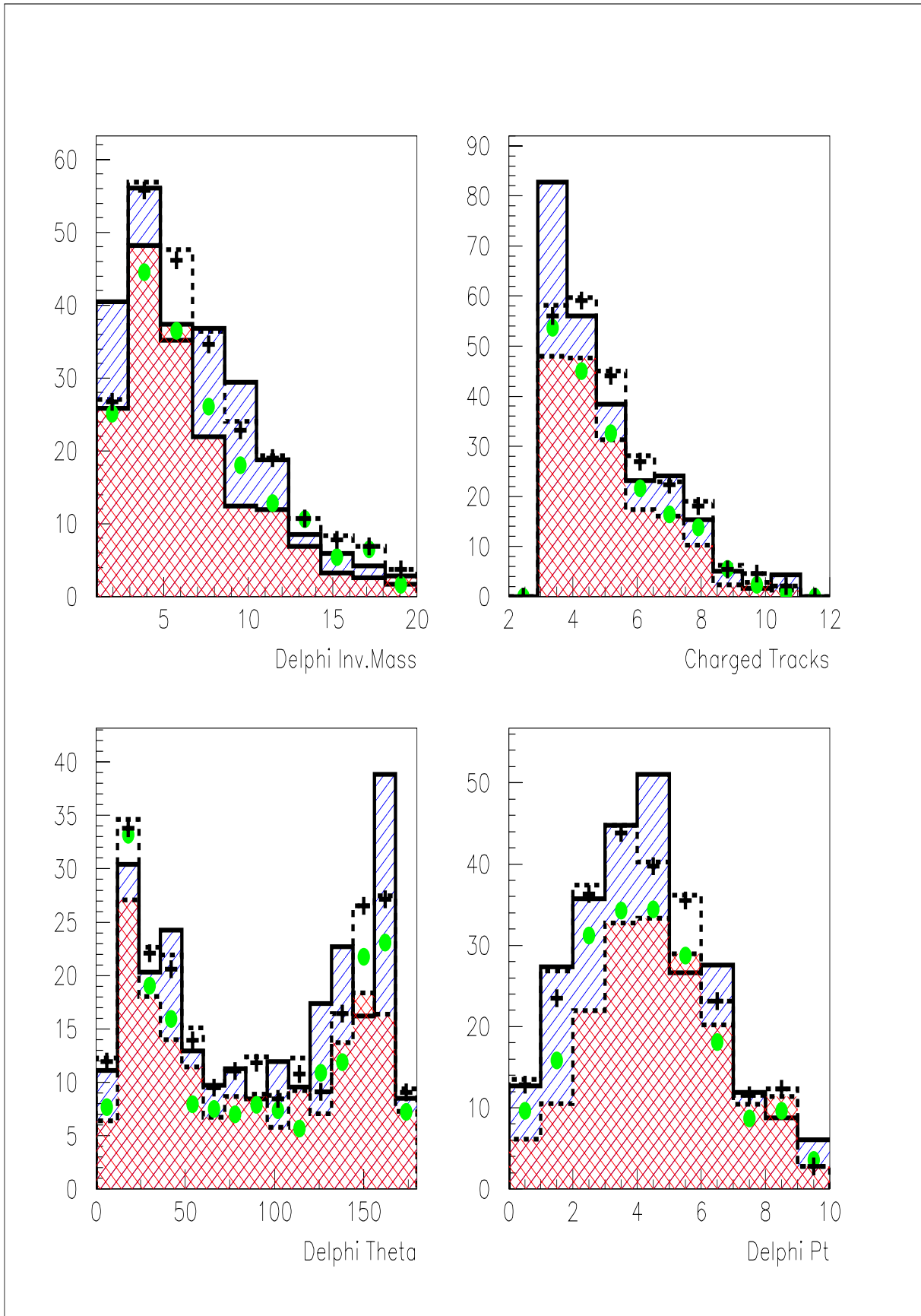
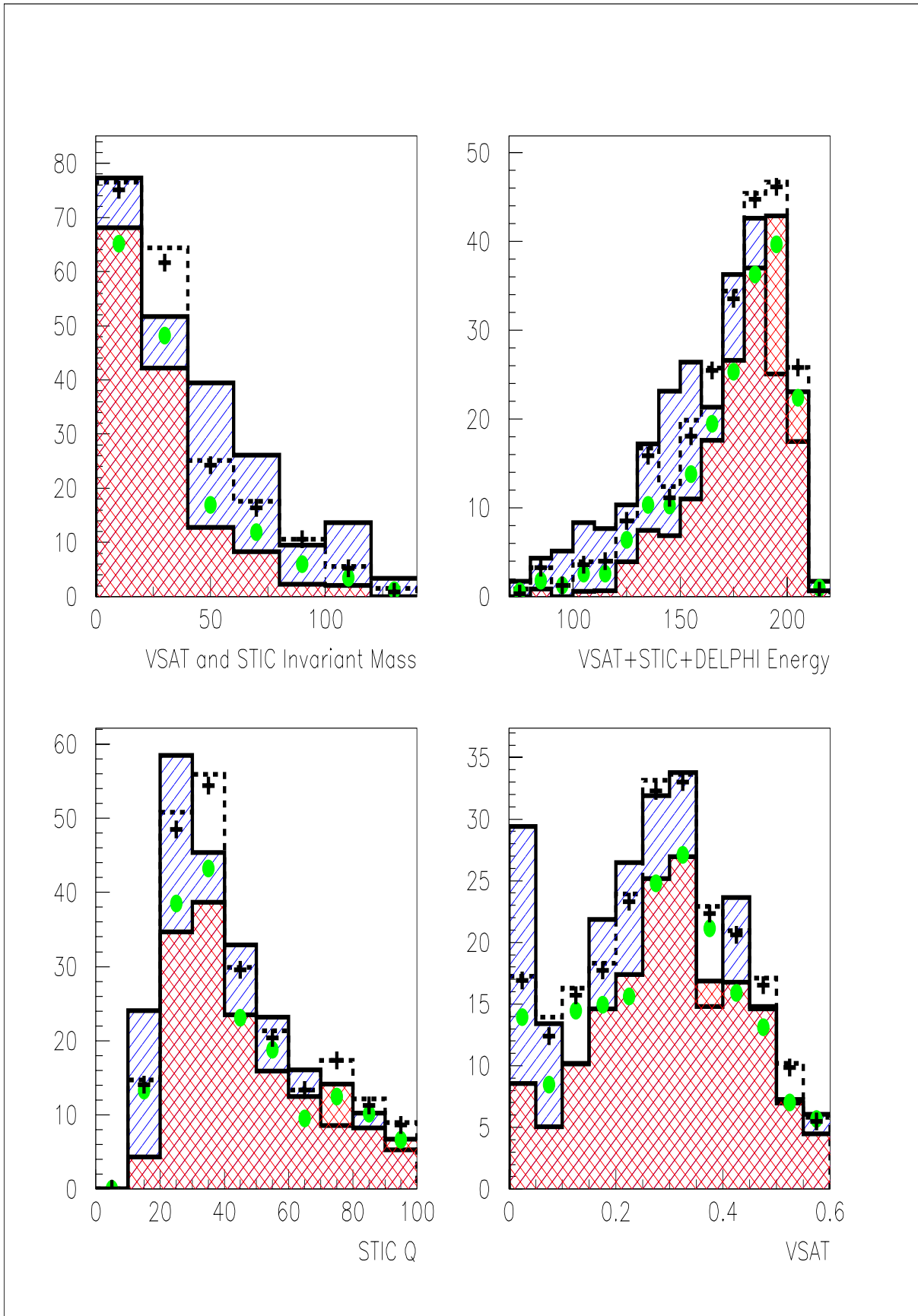Figure 7.10: STIC+VSAT double tag data, quantities from the hadronic system.

Figure 7.11: STIC+VSAT double tag data, measurements from the the e^+e^- system.

Chapter 8

Results

8.1 Luminosity

At the end of each year VSAT has provided a luminosity file to the STIC group to be used as a stability check on the STIC luminosity. The VSAT files were also used to cross-check the STIC data for any bad luminosity entries. Comparing the STIC and VSAT data has shown that a joint systematical error of the STIC and VSAT luminosity could be achieved below 1% (Fig. 8.1). The off-energy background heavily disturbs the VSAT Bhabha sample, but with optimized cuts and a good estimation of the remaining background this is fully under control. A good luminosity measurement could therefore still be obtained (Fig. 8.2), even during the worst background conditions in the beginning of 1999 (around fill 5800 in Fig. 3.5).
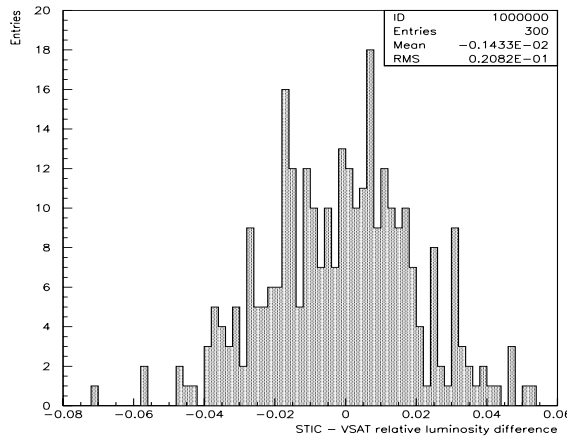
Figure 8.1: The relative difference between STIC and VSAT luminosity. The statistical error is here about 1.80-1.95%, so the joint systematical error is about 0.7-1.0%
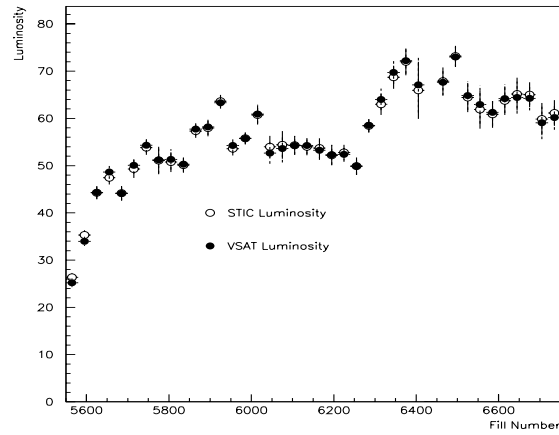
Figure 8.2: The STIC and VSAT luminosity for 1999, the severe background storms in the beginning of 1999 does not seem to disturb the luminosity measurement.

8.2   Data and MC

It has been shown that the QCD-RPC component of the Monte Carlo is needed to describe the data. Further more the p_T^{min} cut-off limit for the parton density functions in this model was adjusted to 2.05. From double tag data it is also clear that the radiative corrections are needed to better describe data. Excellent agreement of all important observables in data and Monte Carlo could then be obtained for both VSAT single tag and double tag data.

The VSAT+STIC double tag data has also been probed for the first time with very promising results. In all about 220 VSAT+STIC events were found, which shall be compared with the 260 VSAT double tag events that could be obtained after background cuts. The remaining background is slightly higher in the VSAT double tag sample, so the expected $\gamma\gamma$-signal is nearly the same for both samples (around 200).

As data and Monte Carlo agree very well, the TWOGAM generator could be used to study physics within the statistical limits of the data. The TWOGAM generator has the advantage of producing separate MC samples for each model. The Q^2 and invariant mass dependence of the QPM, VDM and QCD-RPC contributions can be seen in Fig. 8.3 and 8.4.
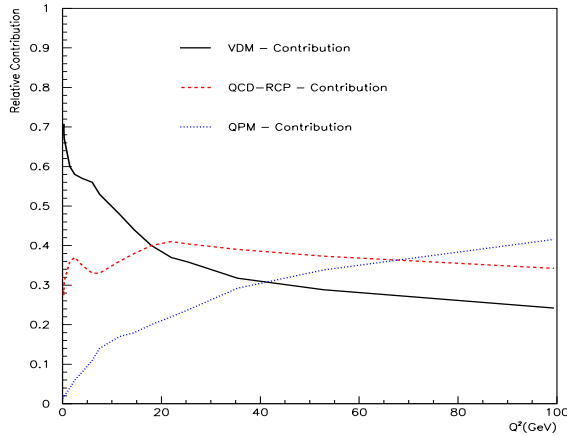
Figure 8.3: The Q^2 dependence of the three model contributions in the TWOGAM generator, taken in the W interval 15-60 GeV.
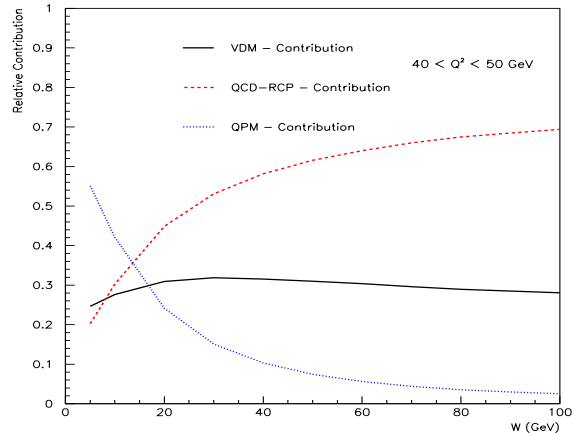
Figure 8.4:   The W dependence of the VDM,QPM and QCD-RPC models, taken in the Q^2 interval 40-50 GeV.

The curves has been obtained by running the TWOGAM generator for different Q^2 and W intervals. The value of p_T^{min} will change the size of the QCD-RPC distribution, and as seen from Fig. 8.4 this is especially important at large invariant masses. From the analysis is it clear that the value of p_T^{min} should be between 2.0 and 2.15, resulting in an uncertainty of the QCD-RPC cross section in Fig. 8.3 and 8.4 of about -15% to +8%.

8.3   Total Cross section

As mentioned in section 6.4 the total cross section for $\gamma\gamma \to hadrons$ can be extrapolated to $Q^2 = 0$ if $W^2 >> Q_i^2$. This is very useful when results from different experiments shall be compared. There are a number of different models to choose from, in this analysis the generalized vector meson dominance model (GVMD) was used. As seen from Fig. 8.5 this describe VSAT data well, but in the STIC Q^2 region it seems to be a bit low.
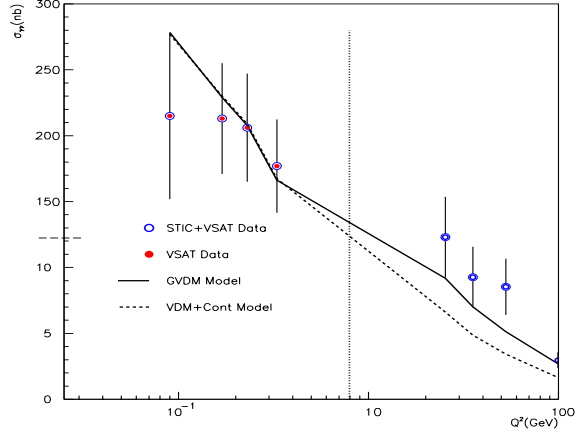

Figure 8.5: The Q^2 dependence of the total $\gamma\gamma$ cross section. The graph has been split in order to visualize the STIC data points.
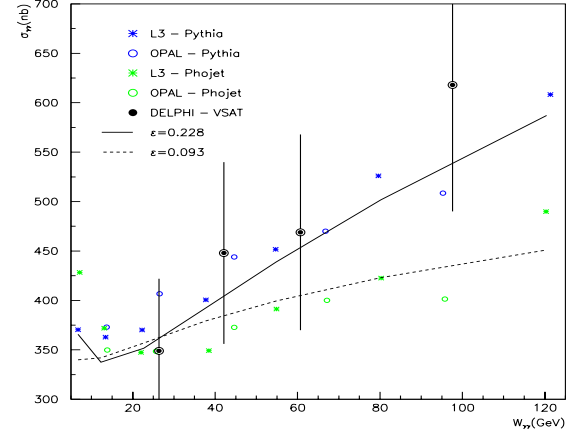
Figure 8.6: $\sigma_{\gamma\gamma}(W^2)$ for L3, OPAL and DELPHI VSAT experiments along with two values of the Regge parameterization.

The data points in Fig. 8.5 were obtained in the W interval from 15 to 60 GeV and clearly there is a logarithmic fall of $\sigma_{\gamma*\gamma*}(W_{\gamma\gamma}^2, Q_1^2, Q_2^2)$. The first VSAT datapoint at a Q^2 of 0.09 is somewhat low, this can probably be explained by some efficiency loss in the inner edge of the detector. From the VSAT region ($Q^2 < 1$ GeV) it is possible to factorize $\sigma_{\gamma*\gamma*}$ and obtain $\sigma_{\gamma\gamma}(W^2)$ at $Q^2 = 0$. This was done for four different W intervals with equal statistics and is presented in Fig. 8.6.

Q_{max}^2	$\sigma_{tot}^{\gamma\gamma}$	Q_{max}^2	$\sigma_{tot}^{\gamma\gamma}$	$W_{\gamma\gamma}$	$\sigma_{tot}^{\gamma\gamma}(Q^2 = 0)$
0.09	215±53	25.4	12.3±2.5	26.4	349±70
0.17	213±43	35.4	9.3±1.9	42.1	448±90
0.23	206±41	52.8	8.5±1.7	60.6	469±94
0.33	177±35	99.4	2.9±0.5	97.5	618±124

Table 8.1: The total $\gamma\gamma$ cross section.

In each bin about 35 events were collected, limiting the statistical errors to about 17%. There are some systematic errors coming from the luminosity function calculation and the extrapolation of the data to $Q^2 = 0$. The uncertainty in the remaining background and some errors in Q^2 and W also add up to the systematical error. These are all less than 5% and are small in comparison to the statistical error. All this result in an total (systematical and statistical) error of about 20%.

The data points from OPAL [38] and L3 [39] in Fig. 8.6 were obtained by unfolding notag data with either PYTHIA or PHOJET. It is clear that VSAT data clearly favor the results obtained by PYTHIA. The two curves in Fig. 8.6 are two Regge parameterizations with different value of ϵ. In the Regge theory [40] the total cross section of any hadronic process can be parameterized as:

$$\sigma_{tot} = As^{\epsilon} + Bs^{-\eta}$$

The coefficients A and B are process and Q^2 dependent, whereas the values of ϵ and η are assumed to be universal (0.093 and 0.358 respectively) [41]. If photons predominantly behave like hadrons the Regge parameterization also may be valid for the total hadronic $\gamma\gamma$ cross section. In Fig. 8.6 η was fixed to 0.358 for both curves, whereas ϵ was both fitted to PYTHIA data and fixed to 0.093. In an analysis performed by the L3 collaboration a value of ϵ=0.21 gives the best fit to data (for both unfolding with PHOJET and PYTHIA) and the universal value of ϵ=0.093 do not describe the W dependence correctly.

8.4   Conclusion and Outlook

It has been shown that the VSAT data can, after a serious analysis of the off-energy background, be used to explore QCD physics in the low Q^2 region. The final VSAT data and Monte Carlo from LEP II just got ready and this thesis only scraped on the surface of the potential measurements. Clearly the VSAT single tag data would be interesting to use both for measurements of the F_2^{γ} structure function at low x as well as the total $\gamma\gamma$ cross section.

It is clear that the STIC+VSAT double tag data is a very interesting data sample, with statistics comparable to that of the VSAT double tag data (after background rejection). This analysis show that TWOGAM reproduce the STIC+VSAT data very well, and further measurements should be performed.

Acknowledgements

Bibliography

[1] S. Almehed *et al.*, DELPHI 98-175 PHYS 814 (1998).

[2] N.Bingefors *et al.*, Nucl.Inst. and Meth. **A328**(1993) 447.
V. Chabaud *et al.*, Nucl.Inst. and Meth. **A368**(1996) 314.

[3] F. Hartjes *et al.*, Nucl.Inst. and Meth. **A256**(1987) 55.

[4] C.Brand *et al.*, Nucl.Inst. and Meth. **A283**(1989) 567.
C.Brand *et al.*, Nucl.Inst. and Meth. **A252**(1986) 413.
G.Darbo and B.W.Heck, Nucl.Inst. and Meth. **A257**(1987) 567.

[5] A.Amery *et al.*, Nucl.Inst. and Meth. **A283**(1989) 502.

[6] W.Bartl, Nucl.Inst. and Meth. **A337**(1994) 295.

[7] M.Berggren *et al.*, Nucl.Inst. and Meth. **A225**(1984) 447.
H.G. Fischer *et al.*,Nucl.Inst. and Meth. **A265**(1988) 218.

[8] P.Checcia *et al.*,Nucl.Inst. and Meth. **A248**(1986).
G.Barichello *et al.*,Nucl.Inst. and Meth. **A254**(1987).
P.Checcia *et al.*,Nucl.Inst. and Meth. **A275**(1989).

[9] I.Ajinenko *et al.*,IEEE Trans. on Nucl. Science NS-431996 No.3

[10] T.Camporesi *et al.* CERN-PPE/92-212 (1992).
T.Camporesi *et al.*, DELPHI 97-8 PHYS 667 (1997).
E.Falk *et al.* DELPHI 97-60 CAL 137 (1997).

[11] S.Almehed *et al.*, Nucl.Inst. and Meth. **A305**(1991) 320.

[12] G. Jarlskog *et al.* DELPHI 99-49 LEDI 11 (1999).

[13] U. Mjörnmark and A.Nygren, DELPHI 99-163 CAL 143 (1999).

[14] S. Almehed *et al.*, DELPHI 98-13 CAL 138 (1998).

[15] A. Nygren, *Mental and Digital Treatment of VSAT High Energy Data*,
Lic. Thesis, Lund Univ., ISBN 91-630-8218-7.

[16] A. Nygren, DELPHI 2000-054 PHYS 857 (2000).

[17] S. Ask *et al.*, DELPHI 99-157 LEDI 12 (1999).

[18] S.Almehed, A. Nygren and N. Zimin, DELPHI 2000-173 PHYS 884 (2000).

[19] P. Jonsson, Thesis, Lund Univ., LUNFD6/(MFFL-7152)1998.

[20] A. Håkansson, DELPHI 93-49 PHYS 279 (1993).

[21] S. Almehed *et al.*, DELPHI 95-150 LEDI 2 (1995).

[22] H. Carling *et al. The VSAT bunch train scheme* 1995 unpublished.

[23] I. Kronkvist, Thesis, Lund Univ., LUNFD6/(NFFL-7128)1996.

[24] G.A. Schuler and T.Sjöstrand, CERN-TH/96-119.

[25] A.Finch, Mod. Phys. Lett. **A35**(1993)3303-3315.

[26] TASSO Collaboration, M.Althoff *et al.*, Z.Phys. **C31**(1986) 527
      CELLO Collaboration, H:J.Behrend *et al.*,Z.Phys.**C51**(1991) 365.
      DELPHI Collaboration ,P.Abreu et al,Phys.Lett.**B342**(1995) 402

[27] A. Nygren, DELPHI 2001-002 Talk 021 (2001).

[28] T. Alderwereld *et al. Event Generators for* $\gamma\gamma$ *physics*, CERN OPEN-2000-141.

[29] V.M. Budnev *et al.*, Phys Rep **15** (1975) 181.

[30] G.A. Schuler, CERN-TH/96-297 (1996).

[31] I.G. Knowles *et al. QCD Event Generators*, hep-ph/9601212
      G.Cooorcella *et al.*,hep-ph/9912396.

[32] R. Engel *Hadronic interactions of photons at high energies.*
      PhD thesis Universität Siegen 1997.

[33] T. Sjöstrand, Computer Phys. Commun **82** (1994) 74.

[34] S. Nova *et al.*, DELPHI 90-35(1990).

[35] DELPHI collaboration, DELPHI 89-67 PROG 142(1989).

[36] J.Cuevas *et al.* DELPHI 87-26 PROG 71 (1987).
      I. Kronkvist, LUNFD6/(NFFL-7061)1990.
      P. Jonsson,LUNFD6/(NFFL-7075)1993.

[37] G. Jarlskog *et al.*, DELPHI 2001-005 CAL 145 (2001).

[38] OPAL Coll., K. Ackerstaff *et al.* Eur Phys J. **C14** (2000) 199.

[39] L3 Coll., M. Acciarri *et al.*, CERN-EP/2001-012 (2001).

[40] P.D.B. Collins, "Introduction to Regge theory", Cambridge University Press,1977.

[41] Review of Particle Physics,Eur. Phys. J C3 (1998) 205.

Appendix A

Exact position of VSAT modules and LEP beam parameters measurments in 1998-2000.

Exact position of VSAT modules and LEP beam parameters measurements in 1998-2000.

A. Nygren, P. Tyapkin, N. Zimin, G. Jarlskog
Elementary Particle Physics Department
Lund University

Abstract

This report presents detailed information of how the beam-pipe upgrade in 1998 has affected the geometry of the VSAT detector. The shift between DELPHI and VSAT coordinate systems has been determined and presented here along with a beam-parameter analysis with help of the VSAT detector. Finally methods are presented to correct for some errors occurring in the VSAT data base as well as a general shifts of the VSAT modules between 1998 and 2000.

1 Introduction

The VSAT (Very Small Angle Tagger) detector is one of three DELPHI sub-detectors which are able to provide beam related information. The position of VSAT is quite far away (7.7 meters) from the interaction point and its main purpose is to count Bhabhas events with a θ angle around 4-7 mrad. The detector is placed very close to the beam and therefore measurements are affected by the background and beams distortions, which makes the beam related information quite inaccurate. Good results can however be accomplished by using statistically significant amount of data (several thousands of events at least).

The VSAT detector consists of four identical modules, each with a 3x5 cm^2 active detector area. The distance from the LEP beam line to the VSAT modules is since the beam pipe upgrade at the end of 1997 to about 5.7-5.9 cm. The idea was to bring detector modules as close to the beamline as possible, in order to increase electron/positron acceptance for gamma-gamma physics.
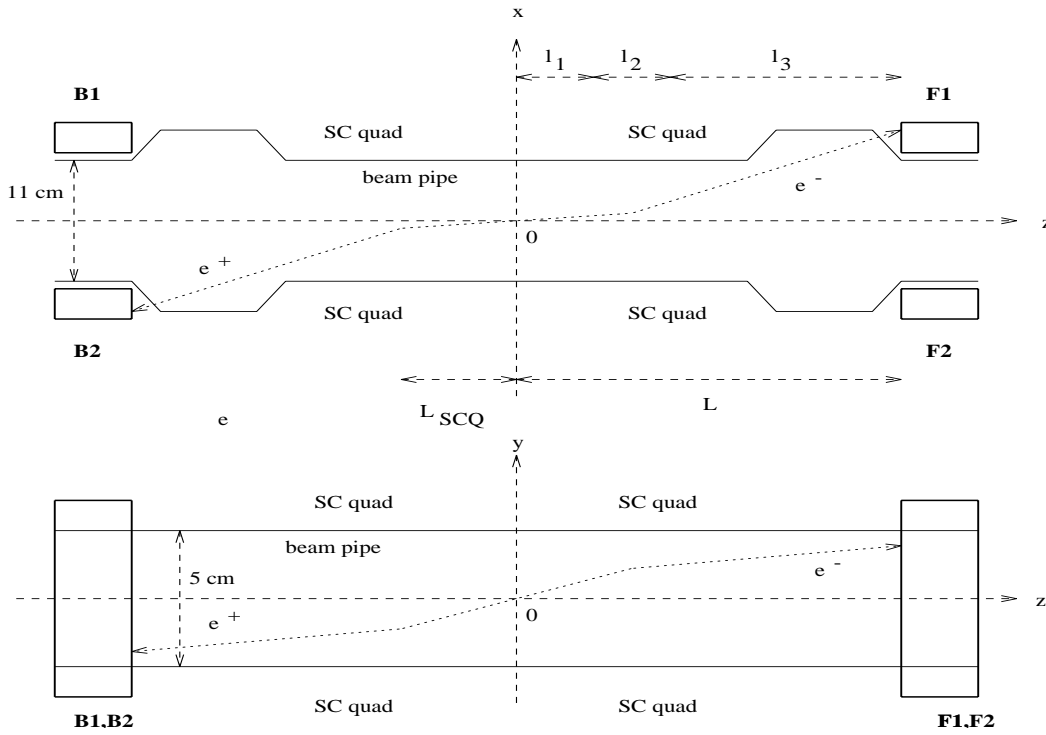

Figure 1: Transverse view of VSAT modules positions in horizontal (up) and vertical (down) planes. The distances given: L=7.7 m, L_{SCQ}=3.7 (from IP to the quadrupole center), l_2=2.0 m - length of quadrupole, l_1=2.7 m, l_3=3.0 m.

Moving the module closer to the beam in X directly increases the VSAT acceptance, as the outer edge of the detector is shadowed by a flange. Events that hit any of the edge strips of the VSAT detector can not be reconstructed and are cut away, reducing the acceptance with about 0.5 mm from the edges.

1

2 VSAT parameter fix in X

The VSAT has been positioned with precise mechanical measurements in relation to the LEP equipment (section 4), which is however not fixed with respect to DELPHI. The VSAT and DELPHI coordinate systems are thus not the same and have to be fixed in position before any beam parameter analysis can be performed. In order to get the most correct position of the VSAT modules it is necessary to use the symmetries of the Bhabha events recorded by VSAT. In the X-Z plane there are 3 beam-spot properties that influence the signals measured by VSAT, shown in Fig. 2 and 3.
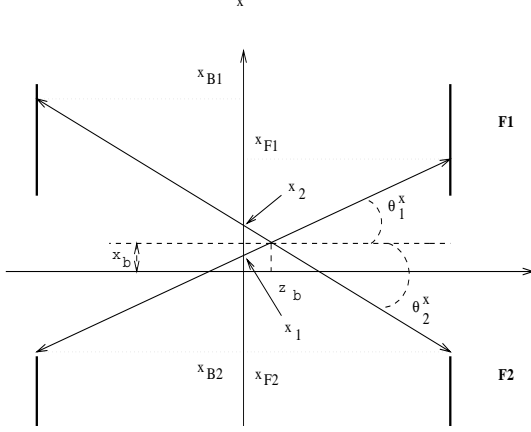

Figure 2: Event with zero tilt, nonzero beam spot displacement in both X and Z position.
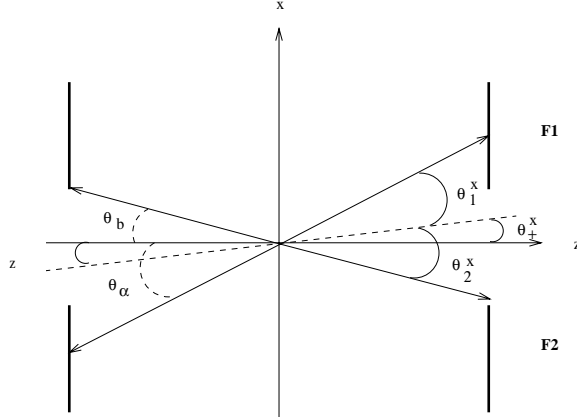
Figure 3: Event with non-zero tilt (acollinearity), zero beamspot displacement in both axes.

As the electrons from an elastic Bhabha event are back to back symmetric, there is a distinct relation between the position measurements in the diagonal modules. The paths of the outgoing leptons are affected by a pair of quadrupoles, which however can be described by a simple focusing/defocusing factor and an effective magnetic length of the VSAT [1]. The relation between the beam-spot position, the relative position of the Bhabha electrons and the beam acollinearity can be expressed as [2]:

$$\Delta X_1 = x_4 + x_1 = 2f_x(x_b - z_b(\theta_1^x + \theta_x)) + \epsilon_x l_x \quad , \tag{1}$$

$$\Delta X_2 = x_3 + x_2 = 2f_x(x_b + z_b(\theta_2^x - \theta_x)) + \epsilon_x l_x \quad . \tag{2}$$

Here x_b is the beam spot position (from the beamline) and ϵ_x is the acollinearity between the beams. The quadrupole focusing factor is described by f_x and its magnetic length by l_x. Finally θ_1^x and θ_x (θ_+^x in Fig. 3) are the angles of the outgoing lepton and of the undisturbed LEP beam. The sum of the x-position of the leptons (ΔX_1 and ΔX_2) are the two VSAT observables for diagonal 1 and 2. If the VSAT coordinate system was fixed totally symmetrically around the beam-spot these would both be equal and have an average around 0.
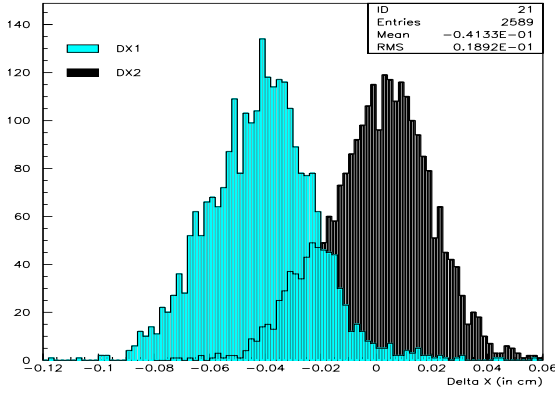
2

Figure 4: The ΔX (cm) distributions for diagonal 1 and 2. The 0.4 mm shift were found to be due to a database error.
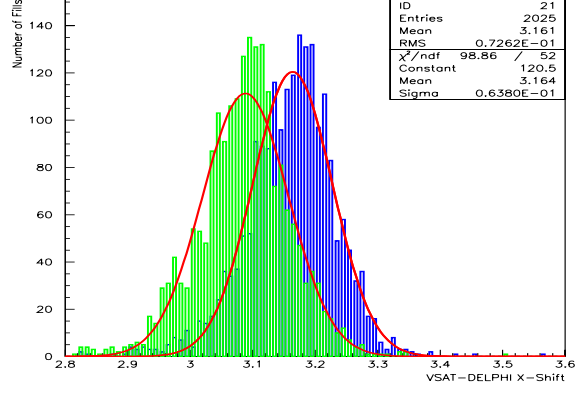
Figure 5: The uncorrected (left) and survey aligned X-shifts (right) between the DELPHI and VSAT coordinate system (in mm).

From Fig.4 it is clear that ΔX_2 is nicely centered around 0, whereas ΔX_1 has an average shift around -0.4 mm. There are two possible sources for this discrepancy, a general shift in the z beam-spot position (z_b) or an asymmetry in the position measurement of any of the modules. It is quite hard to separate the two effects, but they both have the same impact on the calculation of the DELPHI-VSAT X-coordinate system shift (Fig. 5). The f_x and l_x parameters were fixed by consistant fitting the VSAT data to the LEP acollinearity and the DELPHI beam-spot variations (Fig. 6 and 7).
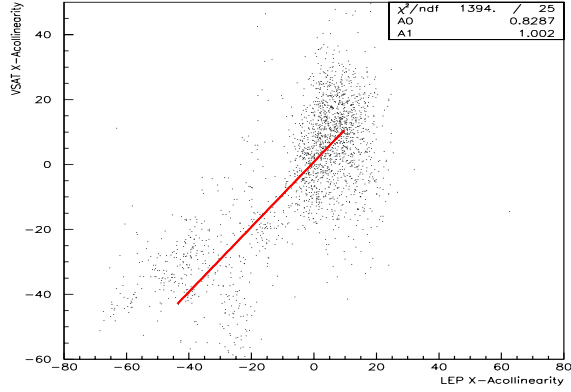

Figure 6: Fitting the l_x parameter to the LEP acollinearity (in μrad) using the VD beamspot data.
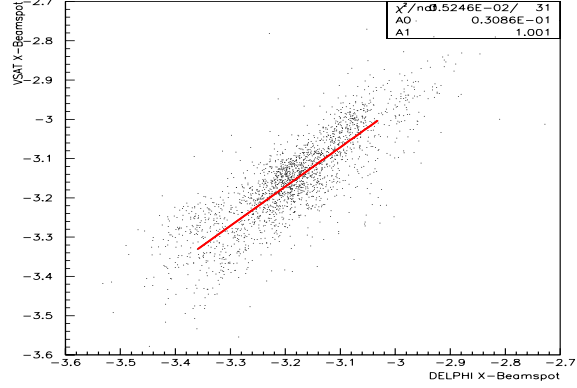
Figure 7: Fitting the f_x parameter to the DELPHI beam-spot (in mm) using the LEP x-acollinearity (ϵ_x).

From equations (1) and (2) it is clear that the fits of f_x and l_x are not independent and a number of iterations were done to converge to the correct values. The final values of f_x and l_x for the LEP II data (1998-2000) were found to be 1.50 and 17.0 respectively. The f_x parameter slightly depends on the beam divergence and the width of the ΔX distribution [3], so f_x=1.5 should be considered as an average. The DELPHI beam-spot shift with respect to the VSAT is then easily extracted from equation (1). This was done in the left hand fit in Fig. 5, resulting in a shift of 3.09 mm.

3

3 VSAT parameter fix in Y

The transport equation in Y looks very similar to the one in X (equation (1) and (2)). There are however two important differences: first the quadrupoles are focusing in Y and secondly the angles in Y are centered around 0 (makes the z_b term neglectable). As the quadrupoles are focusing in Y (f_y is in the order of 0.3) VSAT is not very sensitive to Y-position changes of the beam.

$$\Delta Y_1 = y_4 + y_1 = 2 \cdot f_y \cdot y_b + \epsilon_y l_y \quad , \tag{3}$$

$$\Delta Y_2 = y_2 + y_3 = 2 \cdot f_y \cdot y_b + \epsilon_y l_y \quad . \tag{4}$$

The VSAT data were fitted (Figs. 8 and 9) to the LEP y-acollinearity data and DELPHI beamspot data, according to the equations above. This fit was done in a similar fashion as for x and the resulting l_y and f_y value was 3.40 and 0.25 respectively. It should be mentioned that this fit could only be made for 1999 and 2000, as the acollinearity files for ϵ_y data were unavailable for 1998.
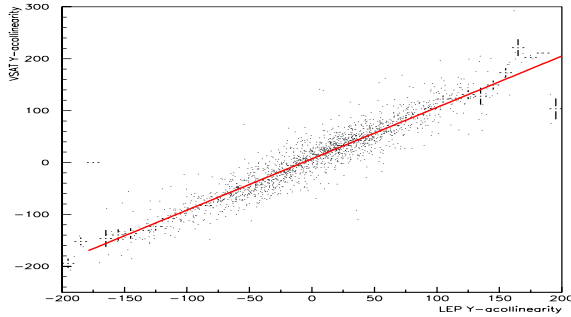

Figure 8: Fitting the l_y parameter to the LEP Y-acollinearity (μrad).
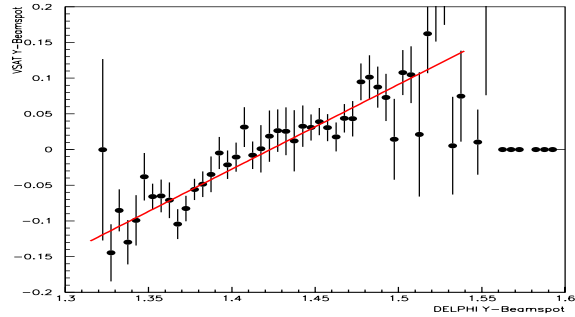
Figure 9: Fitting the f_y parameter to the DELPHI Y-beamspot (mm).

The two differences $\Delta Y_1 - \epsilon_y \cdot l_y$ and $\Delta Y_2 - \epsilon_y \cdot l_y$ should both be centered around zero, but from Fig. 10 it is clear that there is a large shift in both diagonals in opposite direction from the zero-point. This means that, not only the beamline is not in the center of the VSAT detector, but there is also a relative shift between the position measurement of the modules. Taking the difference between dy_1 and dy_2 over the LEP 2 period it is clear that this shift also changes from year to year (Fig. 11).
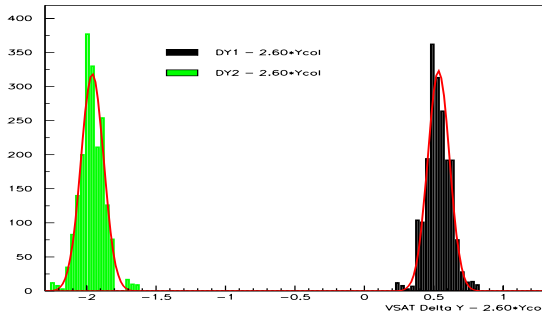

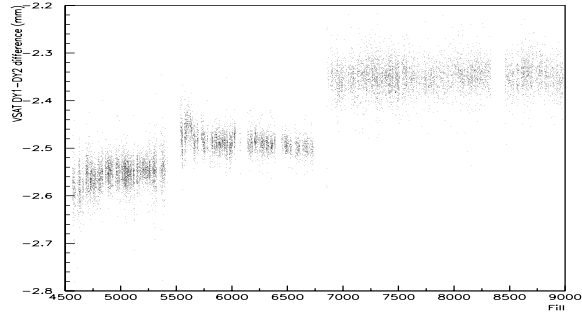Figure 10: The ΔY-shift (in mm) of the two VSAT diagonals (1999).

Figure 11: The difference of the ΔY-shift (mm) over LEP 2.

4

The relative shift from the ΔY measurement is quite accurate, but do not fix the system on its own. The off-energy electron background can however provide a second fix, as hits on the same side of DELPHI (backward or forward) should hit the outer and inner module on the same y-position (if magnetic deflection is neglected). This measurement is less accurate, as the inner modules suffer from a mix of low and high energy background. From Fig. 12 it is however clear that a distinct general shift of the modules can be extracted. These values together with the Bhabha ΔY measurement fix the relative position of the VSAT modules and are presented in the left hand part of Table 1.

$\Delta Module$ (mm)	Measured	Shift	Module	Off e^-	Bhabha	Estimated
$\Delta Y_1(1+4)$	-0.460	0.46	1	0.25	0.86	0.70
$\Delta Y_2(3+2)$	1.928	-1.93	2	-1.26	-0.12	-0.03
Forward (1-2)	-0.8	0.73	3	-2.59	-1.67	-1.90
Backward (3-4)	1.7	-1.66	4	-1.86	-0.13	-0.24

Table 1: The measured relative (Col 2) and absolute (Col 5,6) Y-shift (in mm) of the VSAT modules. From these measurements the module shift were estimated (Col 3,7).

The absolute Y-shift of the modules with respect to the beam-line is quite hard to extract. The general direction and size of any shift of the module position can however be estimated by looking on the peak-position of the Bhabha and off-energy electron distribution for a fill with zero acollinearity. For this purpose fill 6390 was chosen, and the resulting measurements can be found in right hand part of Table 1.

The numbers in Table 1 converge quite nicely (measured value in column 2 with the applied shift in column 3 is approximately 0) and it can be assumed that the absolute measurement of the module positions are more or less correct. If the VSAT coordinate system is corrected with the shifts above it will be centered around the beamline and the shift to the DELPHI beamspot can then be extracted according to equation (3) and (4). As will be shown in section 4 the position of module 3 was 2.87 mm wrong, which will correct most of the discrepancy between ΔY_1 and ΔY_2. The shift between VSAT and DELPHI coordinate system was then found to be 1.77 mm, shown in the left part of Fig. 13. If then the VSAT coordinate system is centered around the beamline and moved up 0.35 mm we finally find the shift to be 1.42 mm (right hand fit in Fig. 13).
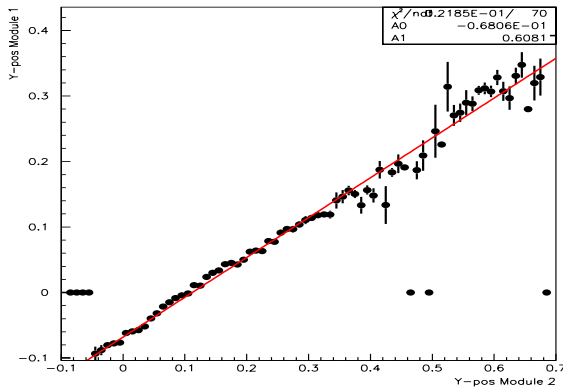

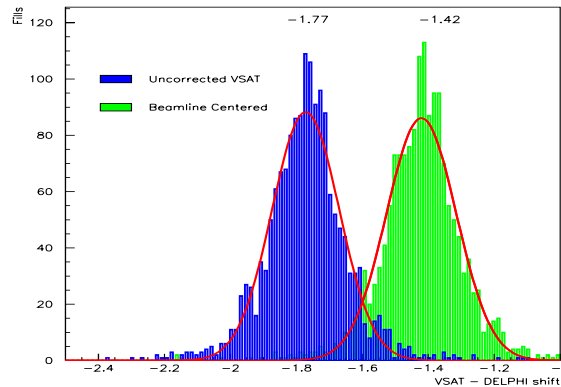Figure 12: The Y-position (cm) in module 1 and 2 for off-energy electrons.

Figure 13: The Y-shift (mm) between the DELPHI and the VSAT coordinate system.

4 VSAT survey measurements

Every time VSAT is put in place or removed, mechanical survey measurements are made. The position of each of the VSAT modules are measured with respect to a bottom plate, which is assumed to be fixed with respect to the beamline. The VSAT was not removed between 1998 and 2000, so the survey measurements at the time of insertion in 1998 should be the same as the measured at the point of VSAT dismantling in year 2000. As clear from the table here below this is however not the case.

Module	1 (B2)	2 (B1)	3 (F2)	4 (F1)
1998 X	-5.728	5.915	-5.915	5.799
1998c X	-5.728	5.915	-5.944	5.799
2000 X	-5.704	5.946	-5.921	5.825
X-Shift	+0.024	+0.031	+0.023	+0.026
1998 Y	-2.399	-2.245	-2.245	-2.377
1998c Y	-2.399	-2.245	-2.532	-2.377
2000 Y	-2.400	-2.247	-2.535	-2.381
Y-Shift	-0.001	-0.002	-0.003	-0.004
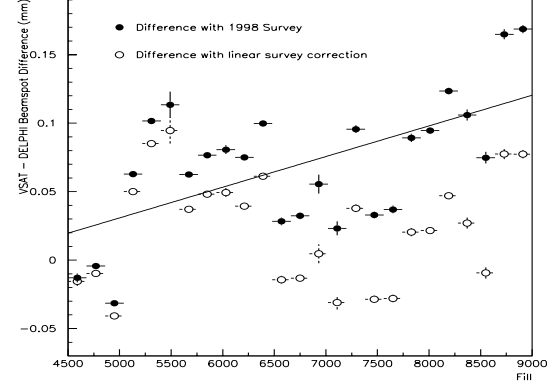
Geometrical surveys for 1998 and 2000, module 3 was miss-edited in database.

Figure 14: VSAT geometry X-shift (mm).

As seen from the table above the x and y measurement in 1998 for module 3 is wrong. By mistake the values for module 2 were inserted for module 3 as well. This error is the main reason for both the ΔX_1-ΔX_2 and ΔY_1-ΔY_2 differences discussed in section 2 and 3. All asymmetries are not solved by the correction of this error, but the situation definitely improves. The second thing to notice is that there is a general shift of about 0.26 mm in x between 1998 and 2000. If the difference between the DELPHI and VSAT beamspot is compared over the years it is clear that there is a small drift (Fig. 14). By linearly compensating for the survey shift, this drift almost fully disappears and the correspondence between VSAT and DELPHI data gets better. The VSAT - DELPHI shift then becomes 3.17 mm instead, as show in Fig. 5.

5 Beam Parameter measurement

The VSAT beam parameters measurements are based on the exactly opposite and equal momentum of the leptons from a Bhabha event in the interaction point. Only true Bhabha events (obtained after various cuts applied during off-line re-processing for the luminosity calculation) was used. One DELPHI cassette number (or file) was used as an elementary sample of data. This assures the number of Bhabha events is high enough to be significant and in the same time the beam parameters can be assumed to be more or less stable. The following quantities from the VSAT Bhabha measurement were used:

6

- Diagonal asymmetry of Bhabha events, $A_D = (N_1 - N_2)/(N_1 + N_2)$ - where N_1 and N_2 are the a number of Bhabha events per diagonal 1 and 2.

- The difference ΔX between modules in the two Bhabha diagonals $\Delta X_1 = x_1 + x_4$ and $\Delta X_2 = x_2 + x_3$ (Module 1 and 3 are the outside modules (w.r.t the LEP ring) and have negative X).

- The difference between the Bhabha Y coordinates (similar to that in X case) $\Delta Y_1 = y_1 + y_4$ and $\Delta Y_2 = y_2 + y_3$.

- Width of ΔX_1 and ΔX_2 distributions - the corresponding value for Y is not useful as the quadrupole field is focusing charged particles in the Y-plane (defocusing in X) resulting in a very narrow delta Y distribution.

Adding equations (1) and (2) as well as equations (3) and (4), results in that the ΔX and ΔY measurements easily can be combined and reduced into two important quantities:

$$\Delta X = \frac{\Delta x_1 + \Delta x_2}{2} = 2 \cdot f_x x_b + \epsilon_x l_x \qquad , \qquad \Delta Y = \frac{\Delta y_1 + \Delta y_2}{2} = 2 \cdot f_y y_b + \epsilon_y l_y$$

The z_b term lost in ΔX disappears as $(\theta_2^x - \theta_1^x - 2\theta_x)$ is very close to zero. If the VSAT data is combined with the beamspot measurement of the vertex detector (x_b), the beam acollinearity (ϵ_x) can be extracted. Naturally the vice versa is also true and both the beamspot position and beam acollinearity is calculated and shown in Figs. 15 and 16.

Figure 15: The beamspot position in X in the DELPHI reference system (in mm).

Figure 16: The X-acollinearity (μrad) of the two LEP beams.

The Y-beamspot measurements are quite insensitive due to the focusing effect of the quadrupoles. As shown in section 3, a dependence is however visible and the same procedure used for x can be performed on Y. This is shown in Figs. 17 and 18, and clearly VSAT parameters follow those extracted from DELPHI and LEP.
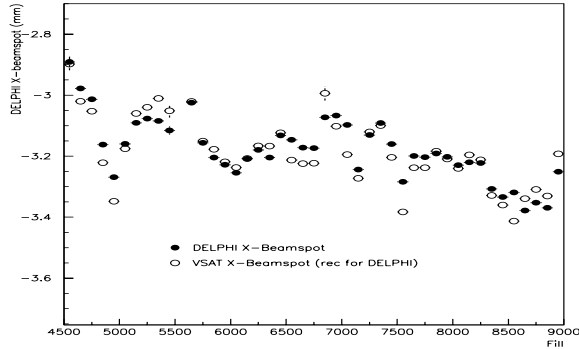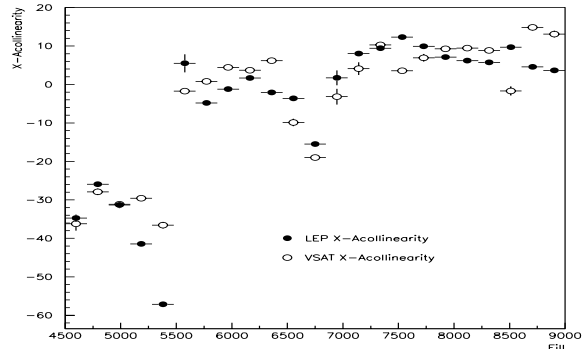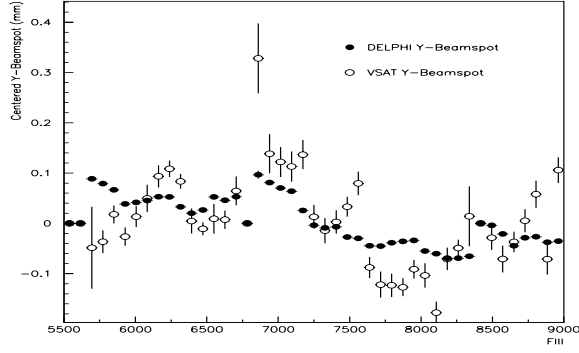
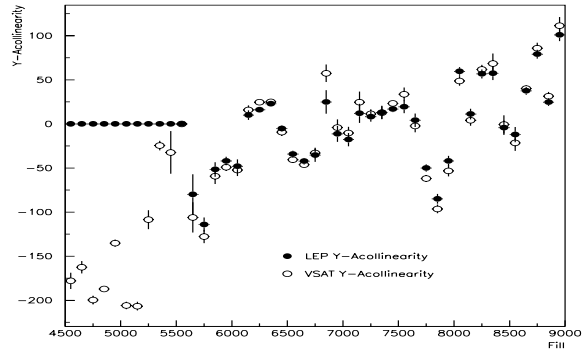Figure 17: The beamspot position in Y in the beamline reference system (in mm).

Figure 18: The Y-acollinearity (μrad) of the two LEP beams.

The Y-acollinearity files were not available for 1998, which is the reason for the zero acollinearity in Fig. 18 and the lack of data in Fig. 17. The average tilt of the LEP beams were also not available for Y, but can however be reconstructed with the help of VSAT data. The average tilts of the LEP beams in x and y can be expressed as:

$$\theta_x = \frac{\theta_+^x + \theta_-^x}{2} \sim 1.75 A_D \quad , \qquad \theta_y = \frac{\theta_+^y + \theta_-^y}{2} \sim \frac{Y_4 + Y_3 - Y_1 - Y_2}{4l_y}$$

Here A_D is the diagonal asymmetry for Bhabhas in diagonal 1 and 2, and $Y_1 - Y_4$ is the Bhabha y-position in module 1 to 4. Both θ_x and θ_y were calculated from the VSAT data over the years 1998-2000 and are shown in Fig. 19 and 20. The horizontal tilt of the beams were available from LEP over that period and the correlation with the VSAT data can be seen in Fig. 19.
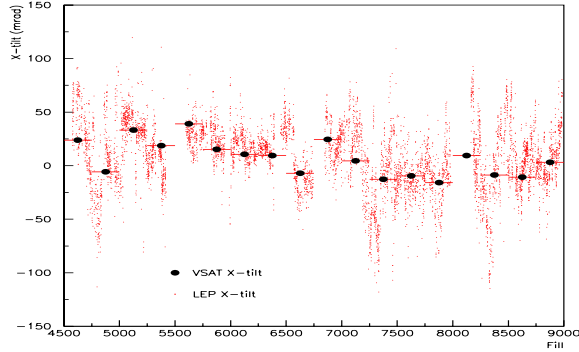
Figure 19: The average tilt (μrad) of the LEP-beams in the horizontal plane.
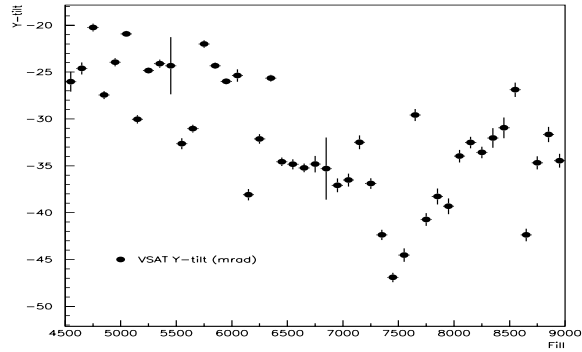
Figure 20: The average tilt (μrad) of the LEP-beams in the vertical plane.

The VSAT data can also be used to spot variations in the Z-beamspot position, but as there were no variations of significance (as seen by DELPHI) during 1998-2000, no information could be extracted. The beam divergence in x and y can be monitored by looking on the width of the ΔX and ΔY distributions. Once again there is however no other data to compare with, so a fix of the parameters is impossible.

6 Conclusion

The geometry of VSAT was changed in 1998 and the increased acceptance gives a bigger $\gamma\gamma$-, Bhabha- and off-energy- electrons flux than before. The data analysis shows good agreement between VD and LEP parameters and those calculated by VSAT. This is a verification that VSAT takes high quality data with high precision in both x and y.

The VSAT geometrical database has had a mistake since the beampipe upgrade in 1998. The VSAT module 3(F2) accidently got the same geometrical value as module 2, which has affected the whole DELANA processing. To correct for this, any analysis should include a subtraction of 0.29 mm from the VSAT X_3 value and 2.87 mm from the Y_3 value. Comparing the geometrical measurements from the surveys 1998 and year 2000, there seem to be a general horizontal shift of about $+0.26$ mm of all the VSAT modules. This corresponds quite nicely with DELPHI-VSAT X-shift change and for a high precision analysis a linear shift over the years should be applied to the data.

The geometrical changes presented here do absolutely not have any impact on the luminosity measurements performed by the VSAT. The online monitoring only depends on the MIG-scalers and do not use the position measurements at all. The offline analysis is always calibrated to the position of the Bhabha peak both in x and y, so any change in geometry will automatically be corrected for.

The general shift between the VSAT and DELPHI beamspot is however important for Monte Carlo generation of $\gamma\gamma$ events. The horizontal shift of the DELPHI beamspot varies from 3.03 to 3.3 mm from 1998 to year 2000. An average of 3.17 mm can be used without any visible impact on the data. The VSAT detector coordinate is slightly off the beamline in Y and needs to be moved up 0.35 mm (when the 2.87 mm shift has been applied in module 3). The DELPHI coordinate system in Y is then 1.42 mm above the VSAT coordinate system (1.77 mm for the uncorrected VSAT).

7 Acknowledgments

References

[1] S. Almehed et al. *Beam parameter monitoring and interaction point measurement in DELPHI with the VSAT*, DELPHI 94-77 PHYS 453

[2] S. Almehed et al., *Measurement of the beam parameter variations in DELPHI with the VSAT*, DELPHI 95-150 LEDI 2

[3] Ch. Jarlskog, *Interaction point estimation and beam parameter variation in DELPHI with the VSAT*, LUNF D6/(NFFL-7110)/1995, Lund University

Appendix B

Proceedings from QFTHEP 2000 in Tver, Russia.

Photon Structure Function Measurements at LEP II

Andreas Nygren

University of Lund

Abstract

The structure of the photon is studied in virtual photon-photon collisions by the four experiments at LEP. The hadronic component of the photon structure function F_2^γ becomes increasingly important at low values of the Bjorken variable. Recent results from LEP II have probed F_2^γ to the lowest values yet and are presented here. A lot of efforts have also been devoted to develop new methods to extract the true invariant mass from the visible mass seen in the detectors. The procedure of unfolding was suffering of severe model dependence, but is now getting better under control.

Proceedings from review talk presented at the the XV International Workshop of High Energy Physics and Quantum Field Theory, Tver, September 14-20, 2000.

1 Introduction

The electron is surrounded by a cloud of virtual photons, in a two beam electron collider there is a finite probability that two of these virtual photons will collide into what is called a $\gamma\gamma$ event (Fig. 1 [2]). This is an excellent system to study the virtual content of the photon, e.g. the hadronic part of the photon, which can help to improve our understanding of both perturbative and non-pertubative QCD.
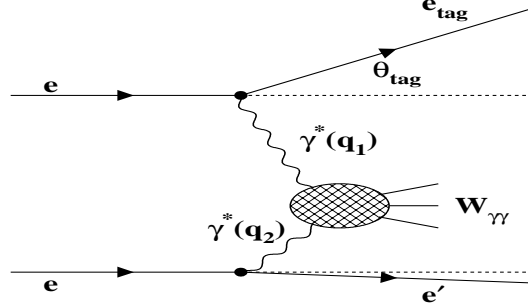

Figure 1: Deep inelastic electron photon scattering. For single tag data the second electron (from the q_2 photon) is anti-tagged and q_2 is approximately equal to 0.

$\gamma\gamma$ events are normally characterized by the invariant mass of the final state ($W_{\gamma\gamma}$) and the squared four momentum of the photons ($Q^2 = -q_1^2$ and $P^2 = -q_2^2$). The Bjorken scaling variable is used to describe the observables and is defined as x $= Q^2/(Q^2 + W_{\gamma\gamma}^2 + P^2)$. The hadronic properties of the photon become increasingly important at low x-values, which can be revealed by precise measurements in this region.

In order to get acceptable precision of the invariant mass it is necessary to detect at least one of scattered electrons. This is possible if one (or both) of the photons has a large enough virtuality $Q^2(P^2)$, and is referred to as a single or double tag event. LEP II has recently accelerated electrons to an energy over 100 GeV and the four experiments have now enough single tag statistics to produce the most accurate measurements yet at the lowest x-value obtained sofar.

2 The Photon Structure Functions

The photon can fluctuate into charged lepton-antilepton or quark-anti quark pairs, were the later for the purpose of calculations can be sub-dived into high and low virtuality fluctuations. The high virtuality part can be calculated by perturbative QCD, whereas the low-virtuality part is described in a non-perturbative phenomenological model involving the summation over vector meson states. The photon wave-function has thus a very complex structure and can be describe by:

$$|\gamma> = c_{bare}|\gamma_{bare}> + \sum_{V=\rho^0,\omega,\phi,J/\psi} v_V|V> + \sum_{q=u,d,s,c,b,t} c_q|q\bar{q}> + \sum_{l=e,\mu,\tau} c_l|l^+l^->$$

,were the last three terms refers to virtual states.

The leptonic part of the wave-function (c_l) is described by QED and will not be discussed here. The partonic content of the photon can be described by two structure functions, F_2^γ and F_L^γ. When one of the photons in the collision is quasi-real with a P^2 around zero the differential cross-section is described as:

$$\frac{d\theta_{e\gamma\to eX}}{dxdQ^2} = \frac{2\pi\alpha^2}{xQ^4}[(1+(1-y)^2 F_2^\gamma(x,Q^2) - y^2 F_L^\gamma(x,Q^2)],$$

$$x = \frac{Q^2}{2q_2 \cdot q_1} \approx \frac{Q^2}{Q^2 + W^2} \qquad , \qquad y = \frac{q_2 \cdot q_1}{kq_2} \approx 1 - \frac{E_{tag}}{E_{beam}}cos^2(\frac{\Theta_{tag}}{2}).$$

y is very small in the region studied, so that the function F_2^γ can be isolated and extracted. As mentioned before special emphasis is put on the low-x behavior of F_2^γ, as it is suspected that the hadronic properties of the photon will result in a rise of F_2^γ in this region. The precision of x mainly depends of the reconstruction from the invariant mass $W_{\gamma\gamma}$, as the Q^2 is determined by the scattered electron. The hadronic system is however not always fully detected and a procedure is needed to reconstruct the true $W_{\gamma\gamma}$ from the visible tracks.

3   Event Tagging and Background

The single tag $\gamma\gamma$ events are tagged with a number of criteria on both the hadronic system and the scattered electrons. The limits of the cuts vary slightly between the four experiments at LEP, but there are four principal tagging criteria that are used:

- The tagged lepton should have an energy greater than E_{min}, which is ranging from 50-70% of the beam energy for the different experiments.

- To assure that the opposite lepton goes in the beam-pipe an anti-tag condition is applied. A lepton with an energy greater than E_{max} (in the order of 20 GeV) is thus not allowed to be seen in the opposite direction of the tagged lepton.

- The visible hadronic mass should be in the range of 3±1 to 50±10 GeV. The limits for the OPAL experiment are shown as two lines in Fig. 2 [1].

- In order to reject leptonic $\gamma\gamma$ events at least 3 charged tracks are required to be registered (marked with a line in Fig. 3[1]).

These trigger conditions isolate the $\gamma\gamma$ signal quite well, however there is still a number of background sources that has to be accounted for. The main background channel is a two-photon process going to a pair of tau's, followed by the Z_0 background. The different background types are presented in Fig. 2 and 3 along with cut criteria for the data.
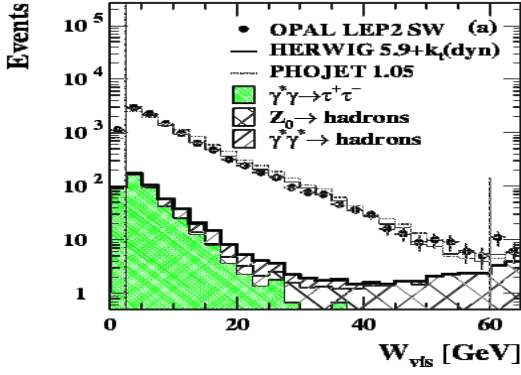
Figure 2: The background processes for $\gamma\gamma$ data. The cut on the visible mass is marked with the two vertical lines.
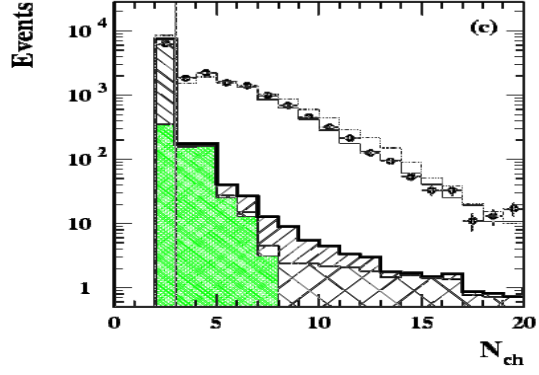

Figure 3: The number of charged tracks for data, background and Monte Carlo. A minimum of 3 tracks are required for hadronic $\gamma\gamma$ events.

4 Unfolding

The energies of the two photons in a $\gamma\gamma$-collision are normally quite different, resulting in a boosted particle system. Therefor a large part of the hadronic system created in a $\gamma\gamma$-collision goes undetected in the beam-pipe and an unfolding procedure is needed to reconstruct the true $W_{\gamma\gamma}$ from the visible. Unfolding is basically a statistical procedure to map one distribution into another. From Monte-Carlo a map is constructed with the generated invariant mass on one axis and the visible on the other (Fig. 4[4]).
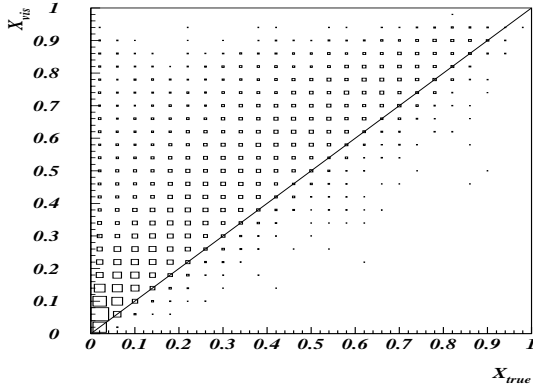
Figure 4: Monte Carlo mapping from x_{vis} onto x_{true}; the data is then unfolded with use of this map.
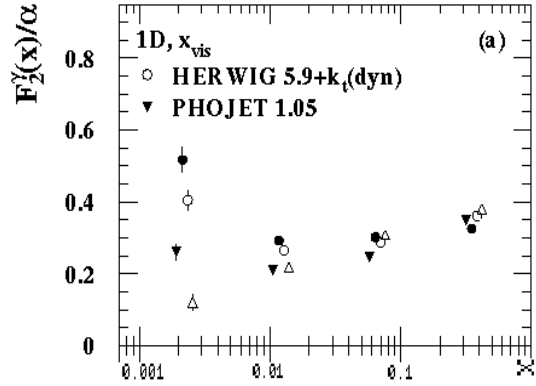
Figure 5: Result of unfolding with different models; the two extreme cases are from two older obsolete models (HERWIG 5.9 and F2GEN).

In mathematical form x is described by $x(i) = \sum_j A_{ij} x_{vis}(j) + b_j$, where A_{ij} is extracted from Monte Carlo and b_j is the expected background distribution. This procedure has the drawback of being quite dependent on which model used in the Monte Carlo generation of A_{ij} (Fig. 5[1]). At lot of effort has recently been made in an attempt to decrease this model dependence.

One approach was to use 2-dimensional unfolding, taking advantage from the fact that W_{vis} becomes more similar to W_{true} when the hadronic shower has high transverse momentum. The energy deposition in the forward direction was used as the second variable for the two dimensional unfolding. In Fig. 6[4] and 7[4] x_{vis} versus x_{true} has been plotted for two different values of E_{17} (the energy deposition below 17 degrees, used by ALEPH), and clearly the value of E_{17} has a large impact on the unfolding matrix.

Figure 6: X_{vis} versus X_{true} with the hadronic shower far away from the beam line.
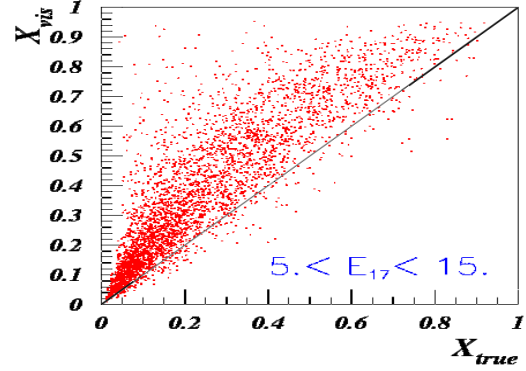
Figure 7: Hadronic shower is closer to the beam-line, and X_{vis} differs more from X_{true}

The visible invariant mass can be improved by including the kinematics of the tagged electron. If we for the hadronic system define $p_{i\pm} = E_i \pm p_{i,z}$ and $p_{i,t} = \sqrt{p_{i,x}^2 + p_{i,y}^2}$, W_{vis} can be expressed as:

$$W_{vis}^2 = (\sum_i p_{i+})(\sum_i p_{i-}) - (\sum_i p_{i,t})^2,$$
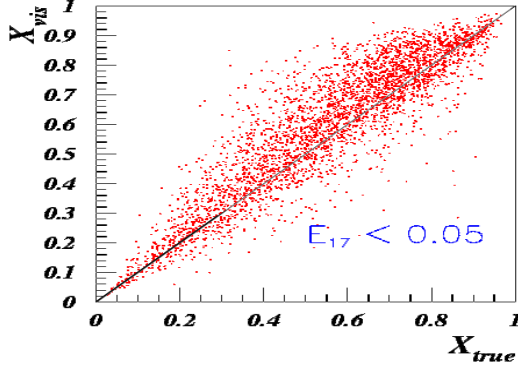
,where i runs over all tracks in the hadronic final state. Assuming that the untagged electron has zero transverse momenta, and using energy and momentum conservations, the sums over p_{i+} and $p_{i,t}$ can be replaced by measurements of the tagged electron (($p_{beam+} - p_{tag+}$) and $p_{tag,t}$):

$$W_{rec} = (p_{beam+} - p_{tag+})(\sum_i p_{i-}) - (p_{tag,t})^2$$

In W_{rec} the hadronic energy only enters in the p_{i-} term, which is a clear improvement as the determination of the electron energy is much better than summing over the hadronic system (Fig. 8[3]). x_{rec} is then extracted from W_{rec} and inserted in the unfolding procedure. The result of the joint combination of 2-dimensional unfolding and replacing W_{vis} with W_{rec} is shown in Fig. 9[1]. From the comparison with the result of simple one-dimensional unfolding presented in Fig. 5, it is clearly seen that the model dependence has been heavily reduced.

The L3 collaboration has also adopted the method of kinematic fitting for high Q^2 data with quite promising result. DELPHI has developed the TWOGAM Monte Carlo generator with the additional resolved photon contribution model, which is less sensitive to the unfolding procedure.

Figure 8: The true, visible and reconstructed invariant mass distribution.

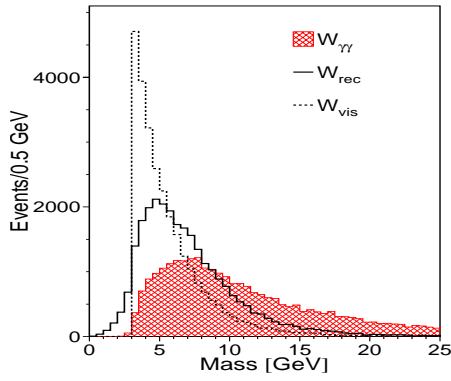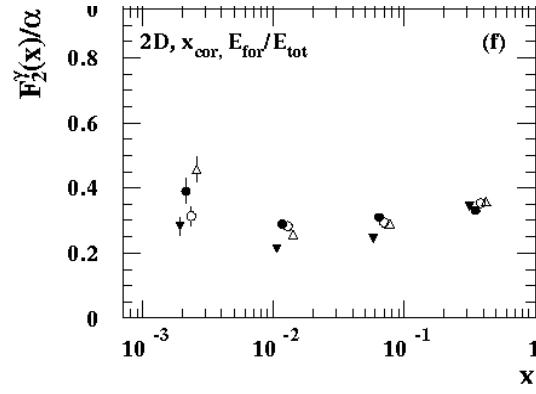Figure 9: The result of 2-dimensional unfolding with reconstructed invariant mass.

5 Monte Carlo Models

A number of different Monte Carlo models have been tried in order to describe the $\gamma\gamma$ physics. More recently general purpose generators such as HERWIG and PYTHIA have also been made available for $\gamma\gamma$ studies. With the new data a number of old models, such as F2GEN, can be rejected, as they do not describe the data satisfactory. There are mainly four models presently used by the LEP experiments:

- **HERWIG 5.9** is a general-purpose QCD Monte Carlo generator to simulate hadron emission reactions with interfering gluons. The old version of HERWIG 5.9 has been replaced with HERWIG 5.9+k_t (dyn) for $\gamma\gamma$ studies. In the new version the quarks inside the photon have a modified transverse momentum distributions (k_t).

- **PHOJET 1.05** is an event generator for pp,γp and $\gamma\gamma$ interactions, described within the Dual Parton Model (DPM). This generator simulates hard interaction by perturbative QCD and uses Regge phenomenology for soft interaction.

- **TWOGAM** is a pure $\gamma\gamma$ event generator that is based on three different processes: the Quark Parton Model (QPM), the Vector Dominance Model (VDM) and the Resolved Photon Contribution (RPC). Each process is generated separately and the RPC model is unique for the TWOGAM generator.

- **PYTHIA** Very recently the general purpose PYTHIA event generator has been made available for $\gamma\gamma$ simulation. Newly obtain results look very promising, but so far no major study has been performed for single tag $\gamma\gamma$ events.

Each of the models have their own advantages and it is hard to favor any before the other. The general purpose generators are dependent on the parameterization of the F_2^γ function. The GRV LO and SaS1D are the most commonly used parameterizations, shown together with two others in Fig. 11[1].

5

6 Results

The LEP data have been studied by all LEP experiments in a wide range of Q^2 intervals, summarized in table here below. From theory the structure function is expected to rise linearly with log Q^2, which is clearly supported by the data of Fig. 10[5]. The additional points from DELPHI[6] and especially L3[2], seem to show a somewhat steeper rise than the other experiments and model predictions (still within error limits though).

Experiment	Q_1^2	Q_2^2	Q_3^2	Q_4^2	Q_5^2	Q_6^2
ALEPH	9.9	13.7	20.7	56.5		284
DELPHI	6.0	13.0	42.0	99	106	400
OPAL	1.9	3.7	8.9	10.7	18.0	135
L3	1.9	5.0	10.8	15.3	23.1	60
L3/OPAL	90	125	225		30	60

The different average Q^2 regions for the F_2^γ studies probed by the four LEP experiments.
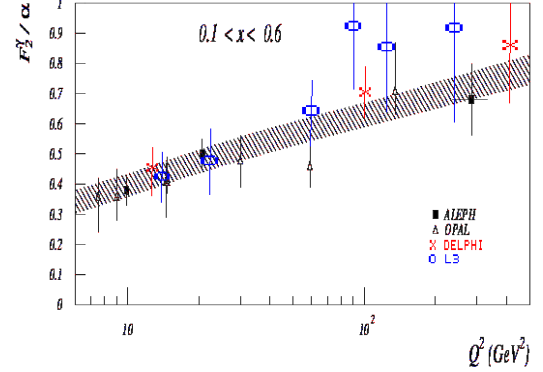
Figure 10: F_2^γ as a function of log Q^2.

The main interest is however focused on the behavior of the structure function at very low x-values. From the theory it is suspected that the hadronic content of the photon should have a rise of F_2^γ in very low x region. To get better accuracy, the x values were unfolded on a logarithmic scale rather than a linear.

The last results from these measurements are presented in Fig. 11[1], where the F_2^γ measurements have been grouped in 4 different Q^2 regions. The lowest obtained x-value comes from the OPAL experiment, which supports the predicted rise from gluons of F_2^γ in all Q^2 regions.
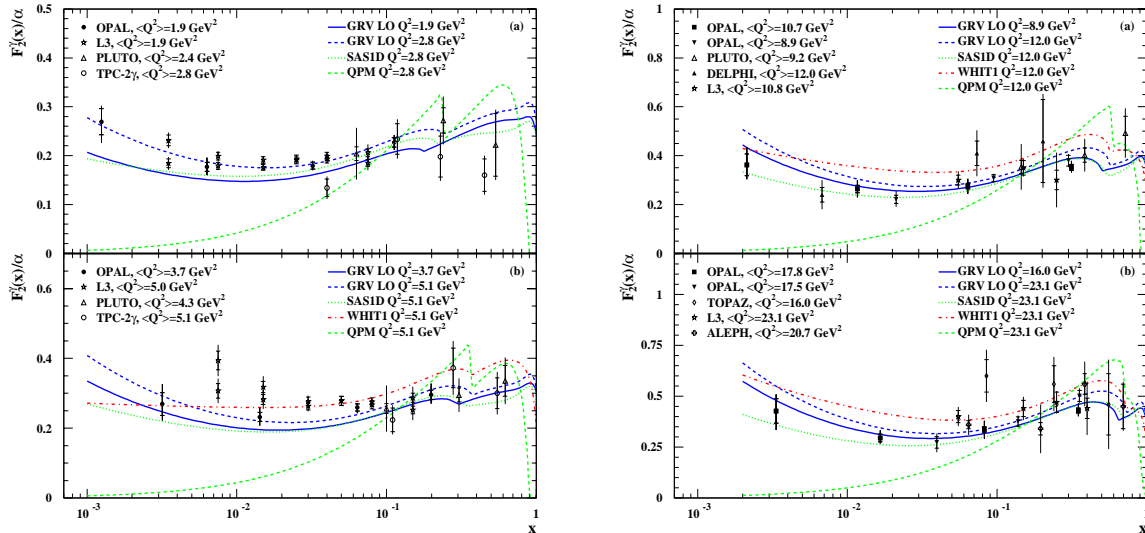
Figure 11: The F_2^γ measurements at low X, for four different Q^2 regions. The double values for each X in the L3 experiment is the result of using different Monte-Carlo models for the unfolding (the upper point is unfolded with TWOGAM the lower with PHOJET).

6

7 Conclusion

Existing $\gamma\gamma$ Monte Carlo generators have been developed further to fit the data better. At the same time some older models can now be excluded and new general purpose generators, such as PYHTIA, have become available for $\gamma\gamma$ simulations. The unfolding procedure has been improved, and the earlier problems of model dependent results have been reduced. This allows for better accuracy in the F_2^γ measurements and has resulted in the best low-x measurements yet. LEP I data can be considered to be more or less exhausted, whereas most of the LEP II results are still to come. With the latest measurements on the LEP II data evidence is already mounting for expected F_2^γ rise at very low-x.

References

[1] The OPAL collaboration, Measurement of the Low-x Behavior of the Photon Structure function F_2^γ, CERN-EP-2000-082, 2000

[2] The L3 collaboration, Measurement of the Photon Structure Function at High Q^2 at LEP, CERN-EP-2000-044, 2000

[3] The L3 collaboration, Study of the Hadronic Photon Structure Function F_2^γ at LEP, CERN-EP-98-98, 1998

[4] The ALEPH Collaboration, A Study of the Photon Structure Function F_2^γ using Two-Dimensional Unfolding,PHOTON99 Conference,Freiburg, 1999

[5] The ALEPH Collaboration, Measurement of the Hadronic Photon Structure function at LEP 1 for $< Q^2 >$ values between 9.9 and 284 GeV^2, CERN-EP-99-053,1999

[6] The DELPHI Collaboration, F.Kapusta et al., Study of the photon structure function F_2^γ in the reaction $e^+e^- \rightarrow e^+e^- + hadrons$ at LEP2, Preliminary,2000

Appendix C

$\gamma\gamma$-Physics background in VSAT

$\gamma\gamma$-Physics Background in VSAT

Sverker Almehed, Andreas Nygren, Nikolai Zimin

University of Lund

Abstract

The VSAT detector at the DELPHI experiment is an important tool to study $\gamma\gamma$ events at very low Q^2. These events are normally boosted along the beam line and detectors at low angles are necessary to achieve good statistics. Since 1998 the VSAT detector has an acceptance region between 4-8 mrad, resulting in a high crossection. Unfortunately the off-energy background is also concentrated at very small angles, which severely disturbs the $\gamma\gamma$ sample. This report will describe the different background processes for $\gamma\gamma$ physics at VSAT, estimate their size and present methods how to reject them most efficiently.

1 Introduction

The Very Small Angle Tagger (VSAT) consists of two pairs of modules placed on each side of the LEP beam pipe $\pm$ 7.7 meters from the DELPHI interaction point (Fig.1). Each of the modules consists of 11 full area silicon detectors(interspaced with tungsten layers) for energy measurement (Fig.2). In order to measure the incident coordinates of the electrons, each module is also equipped with three strip layers for X and Y positioning at shower maximum (see more details in [1]).
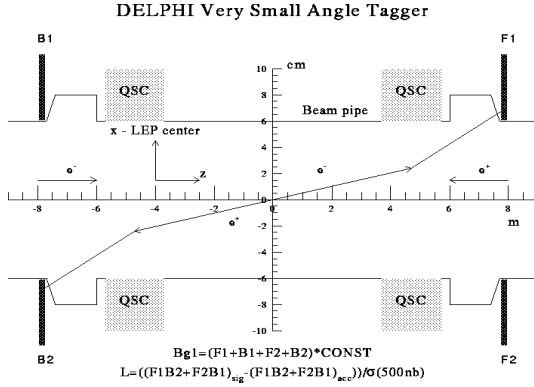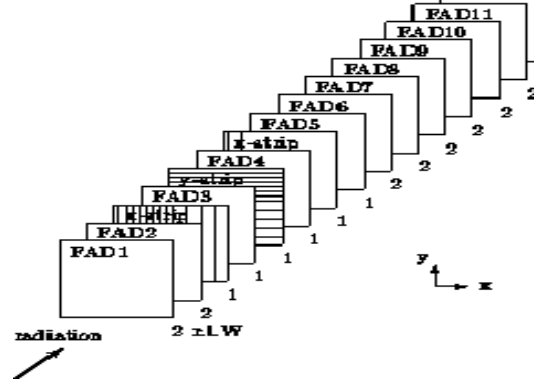

Figure 1: The position of the VSAT modules in DELPHI.

Figure 2: The FAD and strip plane layout of a VSAT module

The beam pipe radius at the detector region was decreased with about 5 mm during the winter shutdown 97/98 in order to allow higher acceptance for $\gamma\gamma$ physics. The detector modules are now located about 5.7 cm from the beam, resulting in an inner detection angle of 4 mrad. The small angle measurements is possible due to a defocusing quadropole in front of the VSAT detector. This is important for $\gamma\gamma$ studies, as the parent electrons normally stay very close to the beam line. A flange in front of the VSAT modules shadows the active detector area and restrict the outer angle to 8 mrad.

One or both (so-called single and double tag) of the scattered electrons associated with a $\gamma\gamma$ collision can be tagged by the VSAT detector. For double tag the kinematics of the event can be obtained with the best knowledge. Unfortunately the VSAT is also over-flooded by off-energy electron background that will dominate over the $\gamma\gamma$ signal. This report will describe how to make the best background rejection and signal extraction for the 1998 and 1999 data taking.

2 Background Types

When $\gamma\gamma$ events are studied in single tag mode, only one electron is measured. The only background source to that process is the coincidence between an off-energy electron from the LEP beam and a no-tag $\gamma\gamma$ event. For the double tag case the scattered electrons from a $\gamma\gamma$ collision hit the VSAT modules on the opposite side of the interaction point(resulting in 4 possible modules combinations). Depending on the source of the scattered electrons, different background processes hit different modules of the VSAT in coincidence with other particles measured by the DELPHI detector:

1

- A Bhabha event and a no-tag $\gamma\gamma$ event,

- Bhabhas that hits the flange and a no-tag $\gamma\gamma$ event,

- Two off-energy electrons hit the VSAT and a no-tag $\gamma\gamma$ event,

- One off-energy electron and a single tag $\gamma\gamma$ event.

Bhabhas and flange bhabhas can only appear in diagonal hits, whereas the off-energy background is mainly concentrated in the outer modules. The flange bhabhas can be removed by requiring that the electron hit the VSAT below 8cm. The bulk of off-energy electrons at low energy can be removed by rejecting events below 30 GeV. A VSAT tag will thus be defined as an energy above 30 GeV and a x-position less than 8cm.

On top of this all events that are close to any of the edges of the VSAT detector will be removed, as a good energy reconstruction is impossible for such events. Unfortunately the main part of the off-energy background will still remain and it is therefor necessary to measure the estimated background level in order to make any assumption on the efficiency of any imposed cuts.

3   Off-energy electrons

The background from off-energy electrons can not be completely eliminated and the remaining background has to be subtracted afterwards. To get this subtraction correct, it is necessary to know how much background we expected to begin with and how much of the background and the signal that were cut away (the later will be discussed in section 6). A number of different methods were used to estimate the total expected off-energy background.

The most natural and simplest way is to measure the probability to have an off-energy electron in any of the VSAT modules [2]. To achieve good statistics the chance coincidence of an off-energy electron and a Bhabha event were used for this purpose. Bhabha events are mainly measured by STIC and VSAT in the DELPHI experiment, both detectors were used to obtain two individual measurements of the off-energy electron probability (Table 1).

Energy	Module 1		Module 2		Module 3		Module 4	
	Off	Gam	Off	Gam	Off	Gam	Off	Gam
189	1.035	0.639	0.180	0.573	1.020	0.590	0.260	0.610
192	1.339	0.672	0.440	0.604	1.498	0.622	0.445	0.639
196	1.404	0.702	0.335	0.626	1.373	0.646	0.340	0.668
200	1.102	0.723	0.220	0.646	1.109	0.671	0.225	0.687
202	0.921	0.735	0.083	0.656	0.787	0.680	0.115	0.703

Table 1: The probability (in %) of an Off-energy electron (off) or a Single tag $\gamma\gamma$ event.

4   Single Tag $\gamma\gamma$ events

The number of expected off-energy electron hits is obtained by multiplying the probability (from Table 1) with the number of no-tag events measured. The number of single tag $\gamma\gamma$ events is then extracted as the remaining part of the data. There is a small probability that an off-energy and a single tag $\gamma\gamma$ electron hit a module at the same time. Less events are therefor seen in the real data, than to be expected from the estimated probability. This is also taken into account when estimating the number of single tag events.

To cross-check these results, the number of expected single tag $\gamma\gamma$ events were also extracted by a second method. This was done by introducing cuts (see section 6) of various sizes on the real data, the Monte Carlo $\gamma\gamma$ sample and the pure off-energy electron data. The number of estimated single tag $\gamma\gamma$ events can then easily be extracted by comparing the number of events in the different distributions before and after the cuts.

$$Gam = \frac{Data_{full} \cdot Off_{rat} - Data_{cut}}{Off_{rat} - Gam_{rat}}, \qquad Off_{rat} = \frac{Off_{cut}}{Off_{full}}, \qquad Gam_{rat} = \frac{Gam_{cut}}{Gam_{full}}$$

Here 'full' is the sample before any cuts, and 'cut' is the number of events after the cuts and 'rat' is the ratio between them. Cuts of different sizes all resulted in the same number of expected single tag $\gamma\gamma$ events, with a standard deviation less than 2% from the statistical average (will be shown in section 6). The number of single tag $\gamma\gamma$ events obtained by this method agrees with the probability calculations within 3%, as seen from the ratio column in Table 2.

| Energy | Outer Modules | | Inner Modules | | Gam(Prop. Calc) | | |
	Off	Gam	Off	Gam	Outer	Inner	Ratio
189	11898	7407	2701	6885	7252	6979	1.004
192	2495	1161	738	1149	1150	1105	1.024
196	7447	3533	1833	3417	3605	3459	0.984
200	5876	3951	1134	3732	3815	3650	1.029
202	2249	1862	249	1813	1870	1796	1.002

Table 2: The number of Off-energy electrons and single tag $\gamma\gamma$ events from cut- and probability calculations.

The final numbers of off-energy electrons and $\gamma\gamma$ electrons in the single tagged data sample for 1998 and 1999 are shown in Table 3. The number of measured single tag $\gamma\gamma$'s was also compared with the integrated luminosity for each energy to get an additional cross-check. Variations less than 1% between the relative numbers of events and the relative luminosities were found.

	Module 1		Module 2		Module 3		Module 4	
Energy	Off	Gam	Off	Gam	Off	Gam	Off	Gam
189	6107	3772	1062	3382	6018	3480	1534	3597
192	1191	597	391	537	1331	553	391	568
196	3754	1889	896	1674	3670	1728	909	1785
200	3018	1979	602	1770	3036	1836	616	1880
202	1217	971	106	871	1040	899	156	925

Table 3: The number of off-energy electrons(Off) and single tag $\gamma\gamma$ events.

5 Bhabhas

For the double tag analysis the Bhabha events also contribute to the background sample in the diagonal hits. The Bhabha process is very well known and a huge statistics is collected by the VSAT detector. The Bhabha background is very well confined in energy and position and can easily be isolated by the following quantities [3]:

$$\Delta X = \frac{|x_1| - |x_2| - \overline{\Delta x}}{\delta \Delta x}, \qquad \Delta Y = \frac{y_1 + y_2 - \overline{\Delta y}}{\delta \Delta y}, \qquad \Delta E = \sqrt{(e_1 - e_b)^2 + (e_2 - e_b)^2}$$

Here x_1, y_1 and x_2, y_2 are the x- and y-positions in the two diagonal modules. The average mean values and widths of the distributions ($\overline{\Delta x}, \delta \Delta x, \overline{\Delta y}$ and $\delta \Delta y$) were defined previously for each DELPHI run, e_1 and e_2 are the reconstructed energies and e_b is the beam energy. A spherical cut in the 3-dimensional space of these quantities is then used to reject the Bhabha events. As it can be completely ($> 99\%$) removed by this cut without any noticeable loss of the $\gamma\gamma$ signal, the Bhabha background do not present any problem in the analysis.

In front of the VSAT there is a flange, which shadows on the outer edge of the detector. When particles interact with the flange they loose energy and Bhabha events disturbed by this fact can not be contained as well. The cut on 8 cm in x-direction of the detector will remove the most of such "flange Bhabhas". The remaining sample is removed by the following criteria, which have almost no impact on the $\gamma\gamma$ signal:

$$(\ |x_1| + |x_2| > 15.0 \ .\text{AND.} \ |y_1 + y_2 - \overline{\Delta y}|/\delta \Delta y < 2.5 \ )$$

6 Cuts-Maps

Off-energy electrons can only be confined in Y-position and in energy resulting in a two-dimensional cut, in comparison with the three dimensional cut for Bhabhas. A typical off-energy electron distribution in the Y and E plane is shown in figure 3, and clearly any trivial mathematical expression cannot be used to define the region of rejection.
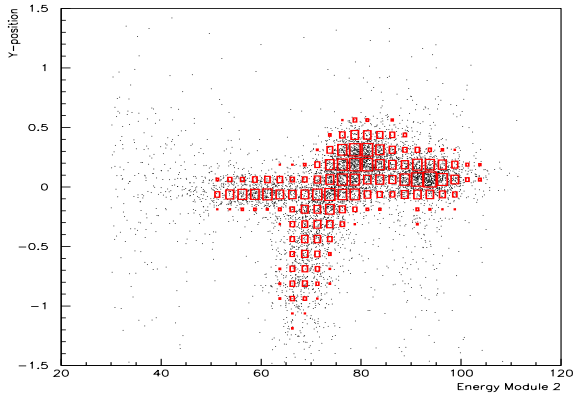
Figure 3: The off-energy background distribution in Y and E. The intensified box area represents the imposed cut.
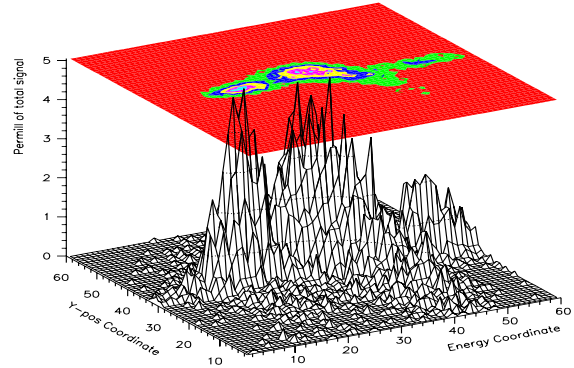

Figure 4: The cut map for off-energy electrons. The height of the bins represent the probability to get a signal.

To deal with this situation a set of two-dimensional cut-maps were defined by using the off-energy electron background recorded by the local VSAT triggers (to get high statistics). As the background changes both in size and shape during the LEP run, cut-maps were constructed for each module and LEP energy data set. The cut-maps used were defined by the following quantities for X and Y:

$$Y_{map} = (Y_{pos} - \overline{Y_{off}} + 1.5) * 20 + 1, \qquad X_{map} = E_{beam} - E + 11$$

Here $\overline{Y_{off}}$ is the average Y-position for the off-energy background for each DELPHI run number. Y_{pos} and E is the Y-position and energy of the event and E_{beam} is the beam energy. The cut-maps are constructed with a grid of 60x60 bins, which is the origin of the other numbers in the expressions. If X_{map} or Y_{map} (x and y in Fig.4) comes outside the map (<1 or >60) the event is accepted.

The height of each bin in the map is defined as the probability(in permill) to get a signal in that bin (Z-value in Fig.4). An event is accepted if its position in the cut-map has a lower z-value than some preset cut-limit. The level of remaining background can then easily be changed by lowering or raising the cut-limit. Different cut-limits were tested (see Table 4) to get the best $\gamma\gamma$ purity in the signal, without loosing to much of it.

Cut-limit	Events after cut	Remaining signal in %			Remaining Background	Purity (in %)
		O + O	O + G	G + G		
0.15	39	0.69	5.17	43.46	6.8	82.44
0.25	51	1.53	8.92	56.1	12.1	76.29
0.30	53	1.79	9.59	57.83	13.1	75.26
0.50	65	3.58	14.62	68.15	20.7	68.20
0.20	209	1.26	8.86	48.12	38.8	78.86
0.30	242	2.32	12.96	57.25	55.0	76.15

Table 4: Impact of adjusting the topological cut-limit on double tag data (in conjunction with the Bhabha cuts). Here O stands for an Off energy electron and G for a single tag $\gamma\gamma$, so O+G is one of each etc.

5

The values in the two last lines (in Table 4) have been applied for all energies, the others only for the 196 GeV data. For double tag analysis a cut-limit on 0.3 per-mill of total signal was used. This keeps almost 60% of the signal and results in a $\gamma\gamma$ purity of 76% in the final sample. Applying such cut-limit on each energy, and summing over all module combinations, result in the values presented in Table 5.

Energy	Remaining signal in %			Remaining $\gamma\gamma$	Signal Purity	Total $\gamma\gamma$	Expected $\gamma\gamma$
	O + O	O + G	G + G				
189	3.68	11.5	49.5	69	78.36	140	144
192	2.13	12.1	55.7	14	72.25	25	21
196	1.78	9.55	57.6	41	76.43	70	64
200	1.75	11.9	61.4	40	75.66	67	66
202	2.24	19.8	62.0	23	78.35	38	32

Table 5: The number of "Remaining" double tag $\gamma\gamma$ events after the imposed cuts and background subtraction. The "Total" number of events before the cuts, extracted by dividing with the estimated signal rejection ('G + G'), should be compared with the number "Expected" from the probability calculations.

The most troublesome background is the coincidence of a single tag $\gamma\gamma$ event and an off-energy electron('O + G'). Only 85-90% of this background can be rejected, keeping the $\gamma\gamma$ purity in the cutted data below 80%. The remaining background is subtracted from this sample to get the final number of double tag $\gamma\gamma$ events. From this the total signal before any cuts can be extracted, which should be compared with the number of $\gamma\gamma$ events expected from probability calculations (will be discussed in section 7).

As the derived cut-map only is imposed one electron, the same type of cut can also be used on the single tag sample to separate off-energy background from single tag $\gamma\gamma$ events. The cut-limit was set to 6 different values presented in Table 6.

Cut-lim	O-Out	O-In	Gam	Signal	Purity	Tot Gam	Ratio
0.10	8.7	17.9	63.8	25320	86.3	34238	0.982
0.25	13.6	23.7	74.6	31144	83.3	34756	0.997
0.50	19.0	35.7	83.6	36964	78.9	34871	1.000
0.75	23.5	44.3	87.8	40607	75.8	35040	1.005
1.50	32.4	67.4	94.3	47720	70.3	35573	1.020
3.00	44.0	90.1	98.0	53784	63.4	34773	0.997

Table 6: Impact of 1-dimensional topological cuts. The average number of the total single tag $\gamma\gamma$ events ('Tot gam') for all cut-sizes is equal to 34875 and shall be compared with the 34681 expected from probability calculations (the sum of Table 3).

In the 'Tot Gam' column the estimated number of single tag $\gamma\gamma$ events is shown, calculated from the formula in section 4. This varies less than 2% from the statistical average of all the cut-limits (the ratio column). The number of events shown in table 6 is summed over all modules and energies, the individual numbers have slightly larger errors due to larger statistical uncertainties (still below 5%).

The estimated number of single tag $\gamma\gamma$ events were also averaged over all cut-limits for each energy and module. This was then compared with the expected number of $\gamma\gamma$ events from probability calculations in table 2, and as seen differences less than 3% were obtained.

7   Data and MC

The single tag case is quite straight forward as only two processes are involved, off-energy electrons and single tag $\gamma\gamma$ events. In this report a single tag is defined as a hit an a module regardless of what is seen in the other (Bhabha events is however rejected). Once the expected background has been calculated the number of single tag $\gamma\gamma$ events can then be extracted as the remaining part of the data sample. Figures 5 and 6 show the total signal, expected MC and derived single tag sample for the inner and outer modules.
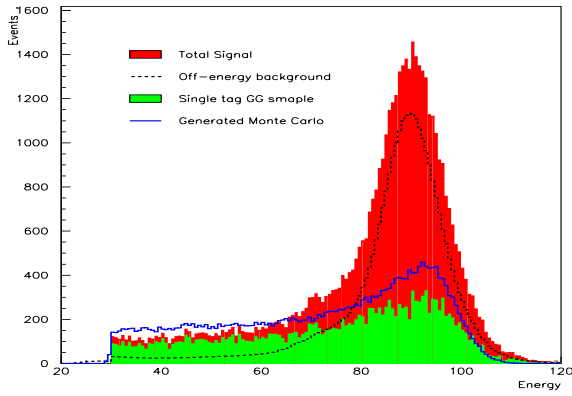

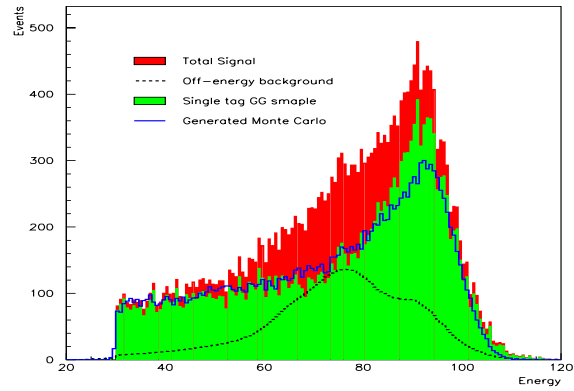Figure 5:   Energy distribution for outer VSAT modules

Figure 6:   Energy distribution for inner VSAT modules

The last version (2.03) of the TWOGAM generator was used to produce the Monte Carlo sample. It has the normal QPM and VDM part plus an additional RPC (Resolved Photon Contribution) part. The RPC part can be varied in size the so called P_t^{min} cut-off parameter. This was fitted to the data in the inner modules, as they suffer less from off-energy electron background. The events generated were then passed through the DELPHI simulation program and the same reconstruction program as for data. An excess of events in Monte Carlo is observed in the outer modules. The origin of this is a shift between the VSAT and DELPHI coordinate system and some acollinearity between the beams, which were both set to zero in the Monte Carlo.

Both the acollinearity of the beams and the beam-spot position was quite stable during the LEP 2. As the VSAT modules have been fixed in position since the start of 1998, we would expect more or less the same event ratio between the modules for all energies. To check the stability of the data each of the modules were compared with the others for all energies. As seen from Table 7, the ratio of single tag $\gamma\gamma$ events between different modules is quite stable. Monte Carlo shows the same result when the modules are on the same side of the beam-spot(1+3 or 2+4), but a fairly large discrepancy in inner/outer modules combinations.

Energy	1 / 2	1 / 3	1 / 4	2 / 3	2 / 4	3 / 4
189	1.115	1.084	1.049	0.972	0.940	0.967
192	1.118	1.081	1.045	0.966	0.935	0.967
196	1.120	1.077	1.043	0.962	0.931	0.968
200	1.118	1.078	1.045	0.964	0.934	0.970
202	1.115	1.081	1.050	0.969	0.941	0.971
MC	1.730	1.093	1.601	0.632	0.926	1.465

Table 7: The ratio of single tag $\gamma\gamma$ events between different modules

The double tag case is harder to deal with, due to low statistics and multiple background processes. The number of double tag $\gamma\gamma$ events is extracted by subtracting the estimated background from the total recorded data. The Bhabha sample is assumed to be eliminated totally by the cuts imposed, so no event reduction due to Bhabhas is needed. The background of two off-energy electrons or one off-energy and one single tag $\gamma\gamma$ is estimated by their probabilities found in Table 1. The double tag statistics after background reduction is very low and a method was developed to decrease the statistical uncertainties somewhat. In this approach the cross-section for a double tag event is expressed in terms a probability for a single tag:

$$P_{double} = P_{single} \cdot P_{single->double} = P_{single} \cdot \frac{N_{double}}{N_{single}}$$

Here $P_{single->double}$ (let us call it P_{sd}) is the probability of seeing the second electron, in a double tag $\gamma\gamma$ event, when the first was already seen. This is slightly bigger than the probability of just seeing a single tag $\gamma\gamma$ event, as part of the kinematic system has been fixed. The reason for this is that the cuts on the hadronic system in the analysis restricts the kinematics of the two electrons somewhat.

The largest error here comes from N_{double} as very few double tag events remain after the background subtraction, which in itself adds an additional uncertainty. To improve this situation the sum of all N_{double} for all energies were taken. The average values of P_{sd} were then scaled back to an individual value for each energy with the use of the single tag sample (P_{single}).

It might not be totally correct to assume exactly the same scaling factor for the P_{single} and P_{sd}, but the systematic error by this operations is much smaller than the statistical error from the double tag sample. To get the final number of expected double tag $\gamma\gamma$ events, the number of single tags in the forward module is multiplied with the P_{sd} factor for the backward module and vice versa:

$$N_{exp,double} = \frac{N_{single,forward} \cdot P_{sd,backward} + N_{single,backward} \cdot P_{sd,forward}}{2}$$

The result of extracting the expected double tag $\gamma\gamma$ sample by this procedure is presented in Table 8. Also shown are the amounts of estimated background from double off-energy electron events (O + O), off-energy + single tag $\gamma\gamma$ events (O + G) and Bhabha (BAB) events. The signal to background ratios is 1:5 for the worst cases, and clearly strong cuts have to be applied to get a pure data sample.

Energy	1 + 4	2 + 3	1 + 3	2 + 4	Total	O + O	O + G	BAB
189	37	34	36	35	141	92	178	123
192	6	5	5	5	21	31	42	17
196	17	15	16	16	64	80	122	81
200	17	16	16	16	65	48	99	73
202	8	8	8	8	32	12	35	21
Tot	85	77	81	80	323	263	476	316

Table 8: The ratios of double tag $\gamma\gamma$ events between different modules

As already shown in Table 5 the correlation between the number of double tag $\gamma\gamma$ events estimated by this procedure corresponds very nicely with the number of double tags expected after the imposed cuts are applied.

8 Conclusion

The background situation for $\gamma\gamma$ physics is quite severe and requires a rather involved analysis in order to get a good understanding of it. The quantitative composition of signal and background in the 1998 and 1999 year data is now fully understood. A number of different and independent methods has been used to extract the expected background and $\gamma\gamma$ event sample in the data. They all produce similar and stable results and this part of the analysis is now fully under control.

The produced Monte Carlo seems to agree well with data, except from an imbalance between inner and outer modules and an overall excess. The origin of the imbalance have now been identified as a shift of the DELPHI and VSAT coordinate system, and this will be fixed in future Monte Carlo samples. The excess of events can be corrected for with adjustment of the P_t^{min} cut-off parameter in the RPC model.

The concept of cut-maps have been introduced to reject the background efficiently. It is now possible to reach a purity of 75-80% in the final $\gamma\gamma$ sample without loosing more than 45% of the signal. In total for 1998 and 1999 about 1400 double tagged events were recorded. Of these around 320 are expected to be genuine $\gamma\gamma$ events. With hard topological cuts a sample of around 250 double tag events has been extracted, with a purity of more than 75%. So even if the background situation at first looked a bit hopeless, the future for the analysis looks quite promising.

References

[1] S.Almehed et al. Beam parameter monitoring and interaction point measurment in DELPHI with the VSAT. Technical Report DELPHI 94-144 PHYS 453, CERN, 1994.

[2] S. Ask et al. LEP machine background and noise in the DELPHI calorimeters. Technical Report DELPHI 99-157 LEDI 12, CERN, 1999.

[3] A.Nygren. VSAT Background and Luminosity 1999. Technical Report DELPHI 2000-054 PHYS 857, CERN, 2000.

Appendix D

LEP machine background and noise in the DELPHI calorimeters.

LEP machine background and noise in the DELPHI calorimeters.

S. Ask [1], **V. Hedberg** [2], **P. Nieżurawski** [3], **A. Nygren** [2], **P. Tiapkine** [2,4],
N. Zimin [2,4]

[1] Summer student, Luleå University of Technology
[2] Dept. of Physics, University of Lund, Sweden
[3] Dept. of Physics, Warsaw University, Poland
[4] JINR, Dubna, Russia

Abstract

The LEP machine background and noise in the DELPHI calorimeters have been
studied in four independent analyses. The main purpose of this work is to estimate
the probability of a shower from these sources in coincidence with a genuine physics
event and to see how best to reject this type of background. Both the 1998 and the
1999 high energy data have been used in this study.

1 Introduction

LEP machine background and noise in the electromagnetic calorimeters can affect many DELPHI analyses. Particularly sensitive are the analyses of two photon interactions [1] and events with a single photon in the final state [2] since these analyses select or trigger on energy in the calorimeters. However, analyses which veto on energy in the calorimeters e.g. STIC also need to take this background into account.

In this note several different studies of calorimeter background have been compiled. At low angles, i.e. in VSAT and STIC, the most troublesome background comes from off-energy electrons caused by bremsstrahlung from beam particles on rest-gas molecules. This background has been simulated in DELPHI [3]. The simulation has given a better understanding of the production and origin of the background but cannot be used for quantitative estimates, since it needs as input the vacuum pressure in LEP, which is not known in detail.

The only way of estimating the off-energy background is to use real data. Any sample of events which is not expected to give electrons in VSAT can be used to estimate the probability of an off-energy electron in VSAT. A few basic questions need to be answered: What is the rate of the background (normalized to luminosity) and how does it vary with time ? What is the probability that an off-energy electron is recorded together with a genuine physics event ? How can the background best be rejected ?

The off-energy background in VSAT has been estimated with three different data samples: VSAT Bhabha events, STIC Bhabha events and muon events. All the analyses were done with 1998 high energy data.

Three different event samples were also used for the study of off-energy electrons in STIC: the STIC single arm events, the STIC Bhabha events and random triggered events. Data from both 1998 and 1999 have been studied.

In the other DELPHI calorimeters such as FEMC, HPC and HAC, there is no off-energy electron background but noise can cause spurious showers. This problem was studied with the 1999 random triggered events.

2 Background in VSAT

At LEP2, VSAT is used mainly to measure the energy and position of the scattered electrons in $\gamma\gamma$ collisions. The main background in this type of analysis comes from the enormous off-energy electron background. The probability of having an off-energy electron faking the scattered electron from a $\gamma\gamma$ event can be calculated with any sample of events which does not give electrons in VSAT. The largest sample available is the VSAT Bhabha sample and it can be used to calculate the probability with a minute statistical error. To estimate the systematic error, other event samples such as muon events and STIC Bhabha events have also been studied.

In the following discussion, the standard DELPHI coordinate system is used with the x axis pointing towards the centre of LEP, the y axis pointing upwards and the z axis pointing in the direction of the electron beam. θ is the polar angle in relation to the z axis and ϕ is the azimuthal angle around the z axis. In this coordinate system, the numbering of the four VSAT modules is as follows:

Module 1	Module 2	Module 3	Module 4
$x < -5$cm, $z < -775$cm	$x > 5$cm, $z < -775$cm	$x < -5$cm, $z > 775$cm	$x > 5$cm, $z > 775$cm

which means that module 1 and 3 are on the outer circumference of the LEP ring and module 1 and 2 are on the DELPHI A-side while 3 and 4 are on the C-side.

2.1 VSAT scalers and Bhabha events

The most direct way to investigate the probability of having an off-energy electron in a VSAT module is to count them and compare the number to the number of bunch crossings during the same period. The VSAT detector is hit by an enormous quantity of off-energy background electrons, so, in order to save disk-space for more interesting processes, only a small fraction of these events are read out.
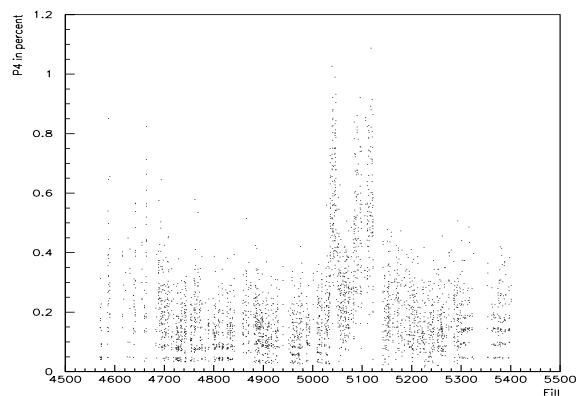
Figure 1: The probability of an off-momentum electron in module 4 for each cassette of 1998 data.
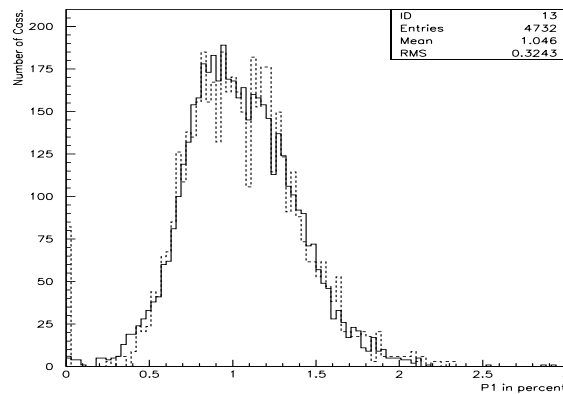
Figure 2: The distribution of the number of cassettes as against the probability of a single electron in module 3, calculated from the scalers (full line) and from the Bhabha events (dotted line).

The VSAT is also equipped with scalers that count the number of hits in each module and the number of Bhabha triggers. The scaler values can be used offline to estimate the probability of background in an individual modules. Since the scalers count all events, the Bhabha scaler value was subtracted to get the true number of single electrons.

The beam and vacuum conditions vary during the year, which alters the VSAT background rate. This is shown in Figure 1, where the probability of a single electron in module 4 have been calculated for each cassette and plotted against the fill number. The increase between fill 5050 and 5100 is due to a LEP vacuum leak.

The full line in Figure 2 shows the probability distribution of single electrons in module 3, as calculated from the scalers on each cassette of 1998 data and Table 1 gives the probability of an off-energy electron in VSAT averaged over all the 1998 data.

Off-energy electrons coinciding with Bhabha events can be used to measure both the probability and the energy and position distributions of this background. The dotted line in Figure 2 shows the probability of each cassette having an electron in module 3 at the same time as a pair of Bhabha electrons in module 1 and 4.

$\mathcal{P}_1[\%]$	$\mathcal{P}_2[\%]$	$\mathcal{P}_3[\%]$	$\mathcal{P}_4[\%]$
1.105±0.00002	0.167±0.00001	1.046±0.00002	0.234± 0.00001

Table 1: The probability of an off-energy electron in the four different VSAT modules. The VSAT scalers were used in this study and the minimum energy required in the trigger was ~15 GeV.
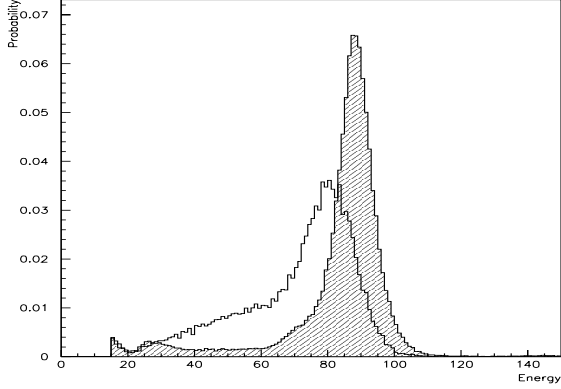

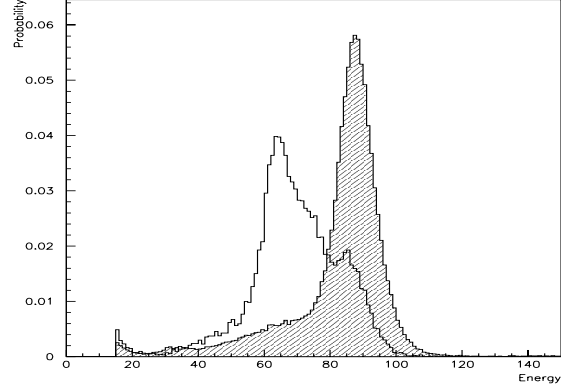Figure 3: Off-momentum background energy distribution for module 1 (shaded) and module 4.

Figure 4: Off-momentum background energy distribution for module 3 (shaded) and module 2.

In this study an energy cut of 15 GeV on the electron in module 3 was made, since this corresponds to the cut in the trigger used by the scalers. The cassettes were required to contain at least 3000 Bhabha events, which reduced the number of cassettes from 4700 to 1600. The distribution in Figure 1 from Bhabha events has therefore been rescaled so that it can be compared to the distribution from the scalers. The two methods seems to be in perfect agreement, with the probability of an off-energy electron in Module 3 varying between 0.2-2.3% .

E_{min} [GeV]	$\mathcal{P}_1[\%]$	$\mathcal{P}_2[\%]$	$\mathcal{P}_3[\%]$	$\mathcal{P}_4[\%]$
15	1.017±0.002	0.1601±0.0008	1.053±0.002	0.2076±0.0009
20	1.005±0.002	0.1580±0.0008	1.044±0.002	0.2049±0.0009
50	0.949±0.002	0.1482±0.0008	0.999±0.002	0.1769±0.0008
70	0.901±0.002	0.0740±0.0006	0.896±0.002	0.1309±0.0007
80	0.803±0.002	0.0354±0.0004	0.784±0.002	0.0744±0.0005

Table 2: The probability of an off-energy electron with energy larger than E_{min} in the four different VSAT modules. The measurement was done with VSAT Bhabha events.

From the energy distributions of the off-energy electrons (Figure 3 and Figure 4) the probability of an off-energy electron in VSAT as a function of an energy-cut can be calculated. The energy is not properly calibrated in the XSDST data and the data used here are taken from the VSAT offline processing with all the corrections applied. The background in the outer modules (1 and 3) has a higher energy as it is produced in a region further away from DELPHI [3]. The probabilities of an off-energy electron in the

3

four VSAT modules are given in Table 2 and are calculated from a sample consisting of $47.5 \cdot 10^6$ Bhabha events, of which 578782 events had an additional off-energy electron in VSAT with energies higher than 15 GeV.
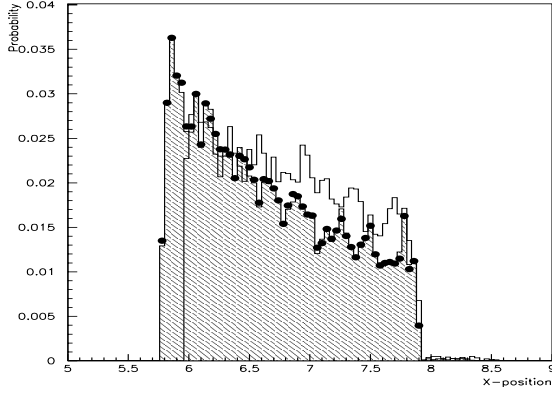

Figure 5: The X distribution of VSAT single electrons in module 1 (shaded) and 2. Comparison is made with a full readout single electron sample in module 1 (dots).
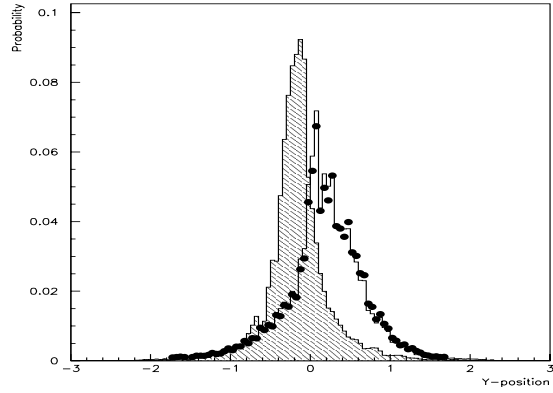
Figure 6: The Y distribution of VSAT single electrons in module 1 (shaded) and 2. Comparison is made with a full readout single electron sample in module 2 (dots).

The best way of removing the background is by a cut on the position of the showers, since the background is concentrated in the horizontal plane. The x and y distributions of the single electrons are shown for both inner and outer modules in Figure 5 and 6. In the outer modules the y-distribution has a sharp peak since it is produced closer to DELPHI. A comparison was made of the position distributions with the single electrons NOT in coincidence with a Bhabha event. This sample contains more events although it has been downscaled. These distributions are shown as dots in Figure 5 and 6 and are in a good agreement with those obtained from the Bhabha events.

E_{min} [GeV]	N_{VSAT}	$\mathcal{P}$ [%]	$\mathcal{P}_1[\%]$	$\mathcal{P}_3[\%]$	$\mathcal{P}_4[\%]$
15	13	4 ± 1	1.6 ± 0.7	1.4 ± 0.6	0.5 ± 0.4
50	12	3 ± 1	1.6 ± 0.7	1.4 ± 0.6	0.3 ± 0.3
60	10	2.7 ± 0.9	1.4 ± 0.6	1.1 ± 0.5	0.3 ± 0.3
70	8	2.2 ± 0.8	1.4 ± 0.6	0.8 ± 0.5	-
80	8	2.2 ± 0.8	1.4 ± 0.6	0.8 ± 0.5	-

Table 3: The probability of an off-energy electron with energy higher than E_{min} in the four different VSAT modules. The measurement was done with dimuon events. N_{VSAT} is the number of events with energy in the VSAT greater than corresponding E_{min}. $\mathcal{P}_i$ means the probability for module $i = 1, 2, 3, 4$. There was no events with a signal in module 2.

4

2.2 Dimuon events

A sample of $e^+e^- \rightarrow Z^0(n\gamma)$, $Z^0 \rightarrow \mu^+\mu^-$ events was also selected to study the probability of having off-energy electrons in VSAT. In this study the 1998 data[2] was used and the selection criteria was optimised with the help of a KORALZ4.2 [4] Monte Carlo sample[3].

To suppress the background, which was mainly due to cosmic muons, it was required that:

1. Two muons were found, one positive and one negative, with no other particles in the event. The muons should be identified as "very loose" or better.
2. The energy of each muon should be $10 < E_{\mu^\pm} < 125$ GeV.
3. The azimuthal angles were required to fulfil $||\phi_{\mu^+} - \phi_{\mu^-}| - 180^0| < 3^0$.
4. Both muons should come from the primary vertex (Q(LPV+4)=0).
5. The transverse momentum of the muons should have $p_{gt}^T > 35$ GeV/c , where $p_{gt}^T \equiv \max(p_{\mu^+}^T, p_{\mu^-}^T)$.
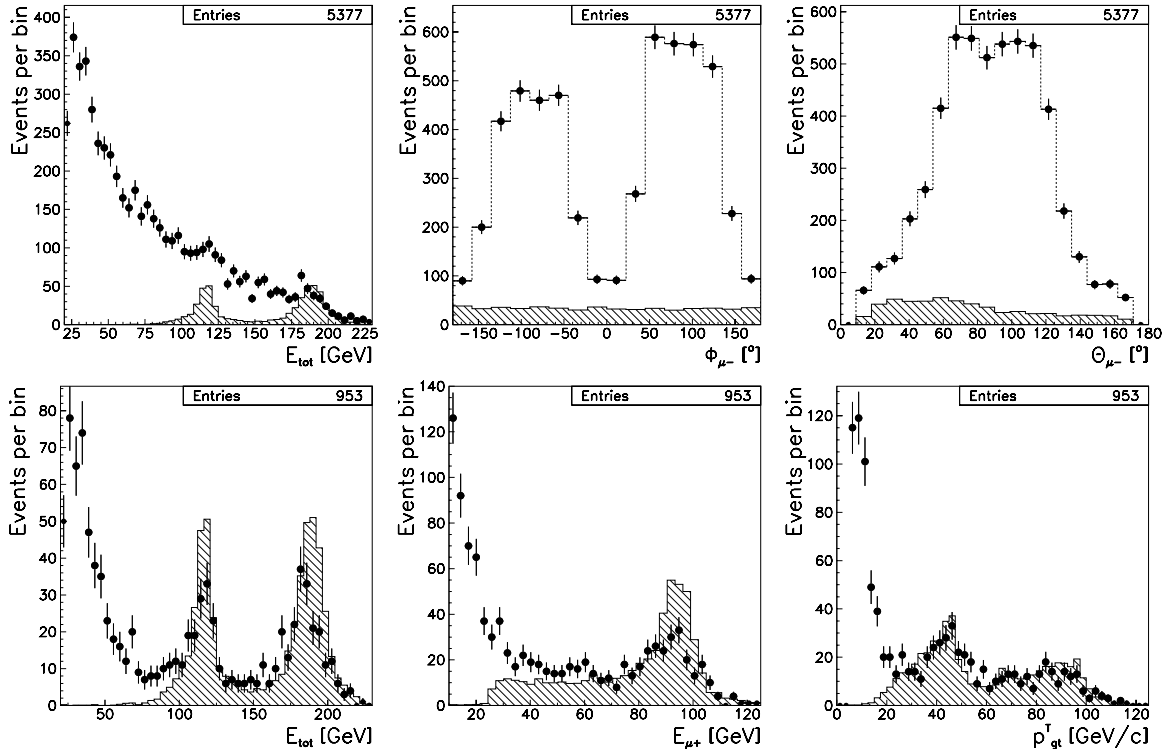
Figure 7: Distributions of E_{tot}, θ_{μ^-} and ϕ_{μ^-} . Points represent data and the hatched histograms represent MC. The top row of plots shows events which fulfil conditions 1, 2 and 3 and the bottom row those fulfilling conditions 4 as well.

The upper three plots in Figure 7 show the distributions of E_{tot}, θ_{μ^-} and ϕ_{μ^-} after conditions 1, 2 and 3 were satisfied. At this stage 4741 events remained, with 495 expected.

5

The angular distributions had broad peaks at $\theta \approx 90^0$ and around $\phi = \pm 90^0$ which were not predicted by Monte Carlo. The reason is of course the large contamination of cosmic muons. Many of the cosmic events can be rejected by the requirement on the primary vertex (condition 4). The bottom three plots in Figure 7 depict the distributions of E_{tot}, E_{μ^+} and p_{gt}^T after the vertex cut. 800 events remained in the data with an unchanged number of expected events.

The last cut on p_{gt}^T removes softer muons coming from $e^+e^- \rightarrow \gamma^*(n\gamma), \gamma^* \rightarrow \mu^+\mu^-$, $\gamma\gamma$ collisions or $Z^0 \rightarrow \tau^+\tau^-$ events. After this cut 369 ± 19 events remained in the data, with $408 \pm 7 \pm 3$ expected from the Monte Carlo study (the second error is due to the uncertainty in the cross section). Good agreement between data and predictions was obtained, as can be seen in Figure 8, which shows different angular distributions such as the polar angle of each muon ($\theta_{\mu^\pm}$), the sum of polar angles ($\theta_{\mu^+} + \theta_{\mu^-}$) and the difference in azimuthal angles ($|\phi_{\mu^+} - \phi_{\mu^-}|$). The total energy ($E_{tot} = E_{\mu^+} + E_{\mu^-}$) and invariant mass of the muons ($W = \sqrt{E_{tot}^2 - (\vec{p}_{\mu^+} + \vec{p}_{\mu^-})^2}$) are also presented in Figure 8. The overall impression from the data-Monte Carlo comparison is that the efficiency is somewhat too high in the simulation and that the energies are slightly high.
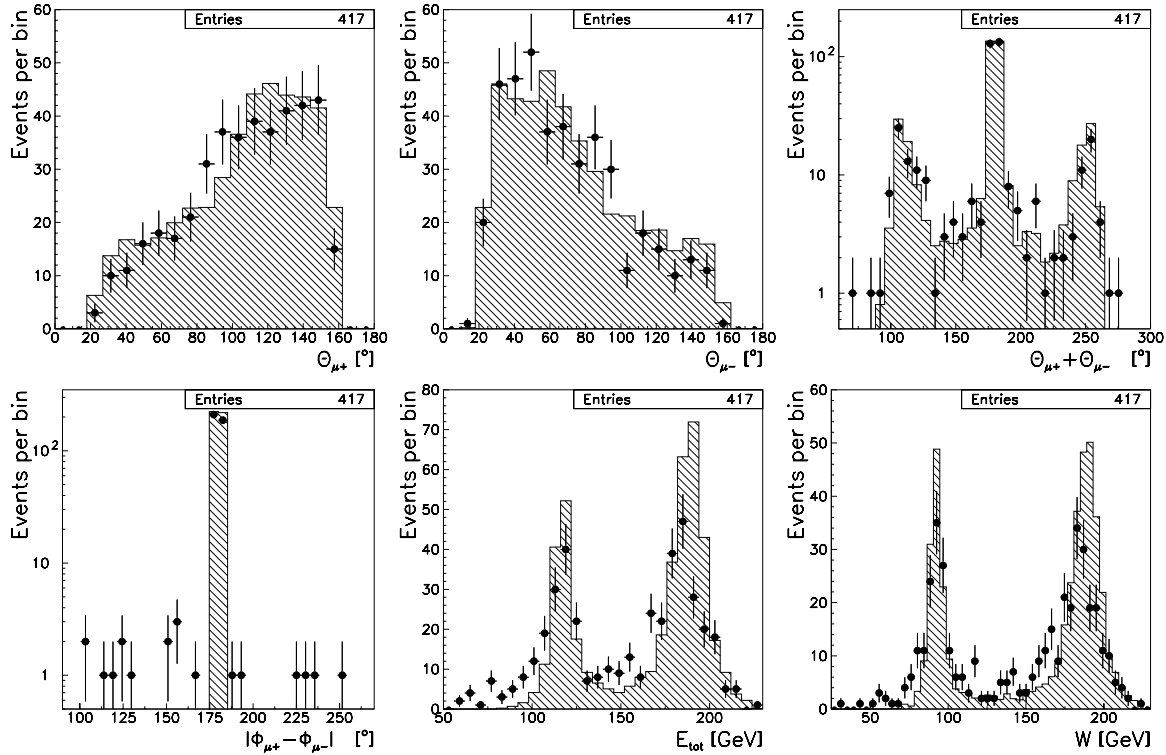

Figure 8: Distributions of polar angle (θ_{μ^+} and θ_{μ^-}), the sum of polar angles ($\theta_{\mu^+} + \theta_{\mu^-}$), the difference of azimuthal angles ($|\phi_{\mu^+} - \phi_{\mu^-}|$), and the total energy of the muons (E_{tot}) and their invariant mass (W).

Out of the 417 selected events, only 18 had an electron in the VSAT. In all of these events, only one module scored a hit. The energy measured by VSAT was corrected using the offline VSAT programs. The total probability and probabilities for each module derived from this sample are shown in Table 3.
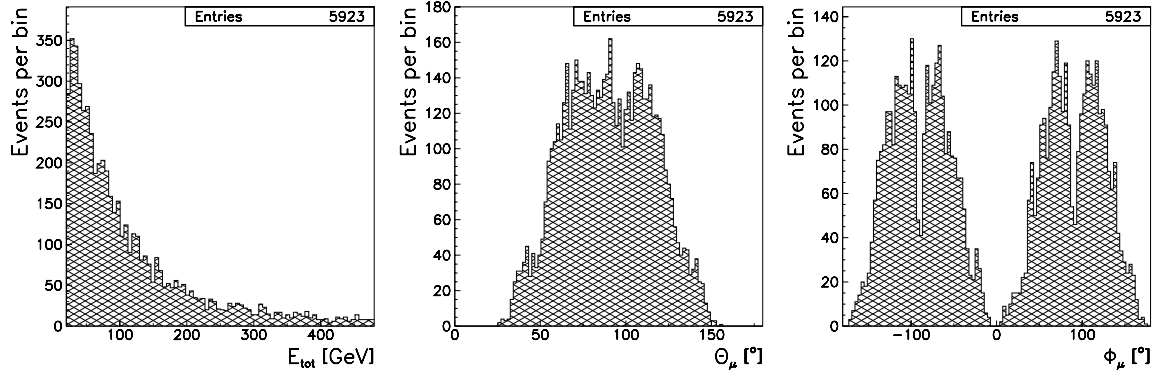
Figure 9: Distributions of E_{tot}, θ_μ and ϕ_μ for events fulfilling conditions 1–4.

E_{min} [GeV]	N_{VSAT}	$\mathcal{P}$ [%]	$\mathcal{P}_1[\%]$	$\mathcal{P}_2[\%]$	$\mathcal{P}_3[\%]$	$\mathcal{P}_4[\%]$
15	113	2.1 ± 0.2	0.9 ± 0.1	0.15 ± 0.05	0.9 ± 0.1	0.11 ± 0.05
50	94	1.7 ± 0.2	0.7 ± 0.1	0.09 ± 0.04	0.8 ± 0.1	0.11 ± 0.05
60	84	1.6 ± 0.2	0.7 ± 0.1	0.04 ± 0.03	0.8 ± 0.1	0.09 ± 0.04
70	75	1.4 ± 0.2	0.6 ± 0.1	0.04 ± 0.03	0.7 ± 0.1	0.08 ± 0.04
80	31	0.6 ± 0.1	0.19 ± 0.06	-	0.35 ± 0.08	0.04 ± 0.03

Table 4: The probability of an off-energy electron with energy greater than E_{min} in the four different VSAT modules. The measurement was done with cosmic muon events.

2.3 Cosmic muon events

The cosmic muon events, rejected in the previous analysis, can also be used to look for off-energy electrons in VSAT. The following cuts were made to select the events:

1. Two muons had to be found, with no other particles in the event. The muons should be identified as "very loose" or better.
2. The energy of each muon had to fulfil $E_\mu > 10$ GeV.
3. Neither of the two muons should come from the primary vertex (Q(LPV+4)$\neq$0).
4. It was required that $|\theta_n + \theta_m - 180^0| < 1^0$ and $||\phi_n - \phi_m| - 180^0| < 1^0$ where n and m can be a positive μ^+ or a negative μ^- .

After this selection, 5396 events were found, 337 $\mu^+\mu^+$ pairs, 336 $\mu^-\mu^-$ and 4723 $\mu^+\mu^-$ events. Distributions of the total energy of the muon pair (E_{tot}) and of the azimuthal angle (ϕ_μ) and polar angle (ϕ_μ) of the individual muons are shown in Figure 9.

Of the 5396 events, there was one VSAT off-energy electron in 136 events and two off-energy electrons in 5 events. The probability of an electron in VSAT computed from these events is presented in Table 4.

2.4 VSAT background in STIC Bhabha events

A sample of back-to-back Bhabha events in STIC was selected by requiring a single shower in each calorimeter with $2.5^\circ < \theta < 8^\circ$ and $0.97 < E_e/E_{beam} < 1.05$. The angle between
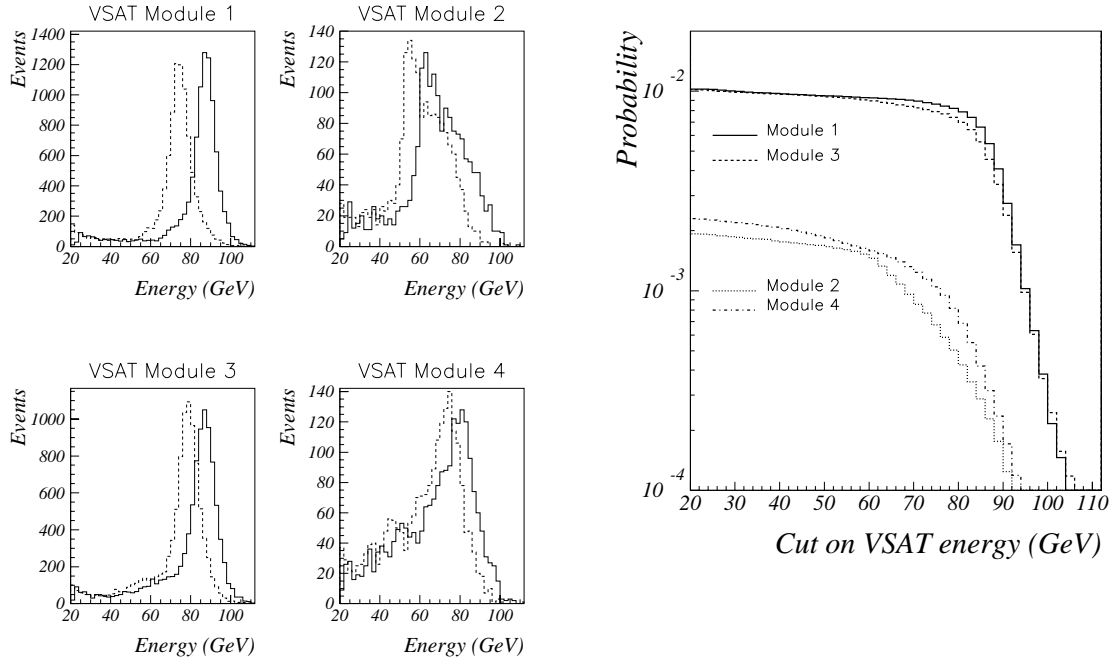
Figure 10: Left: Energy distribution of the showers in the four VSAT modules. The dotted line shows the uncorrected and the full line the corrected spectrum. Right: The probability that an off-energy electron shower will be found in VSAT, as a function of an energy cut.

the two showers was required to be larger than $179.85°$. In all, 925445 events from the 1998 data satisfied these requirements, 22433 of them having at least one shower in VSAT with an energy larger than 20 GeV. Most of the events (22072) had a shower in only one module, while a small fraction had a hit in two (359) or three (2) modules.

E_{min} [GeV]	$\mathcal{P}_1[\%]$	$\mathcal{P}_2[\%]$	$\mathcal{P}_3[\%]$	$\mathcal{P}_4[\%]$
20	1.025 ± 0.011	0.193 ± 0.005	1.017 ± 0.010	0.230 ± 0.005
50	0.947 ± 0.010	0.166 ± 0.004	0.936 ± 0.010	0.184 ± 0.004
70	0.890 ± 0.010	0.085 ± 0.003	0.824 ± 0.009	0.124 ± 0.004
80	0.788 ± 0.009	0.042 ± 0.002	0.699 ± 0.009	0.069 ± 0.003

Table 5: The probability of an off-energy electron with energy greater than E_{min} in the four different VSAT modules. The measurement was done with STIC Bhabha events.

Figure 10 shows the energy distribution of the showers seen in the four VSAT modules. The energy spectrum is shown both directly from the XSDST and after offline corrections. The VSAT modules at the outer circumference of the LEP ring (module 1 and 3) shows 5 times as much background as those on the inner circumference and the energy of the off-energy electron peaks close to the beam energy. In the inner modules the energy distribution is also peaked but broader. Since the energy of the background peaks at high energy, this background cannot be rejected with an energy cut. That is shown in Figure 10 and Table 5 which give the probability of having an off-energy electron in the different
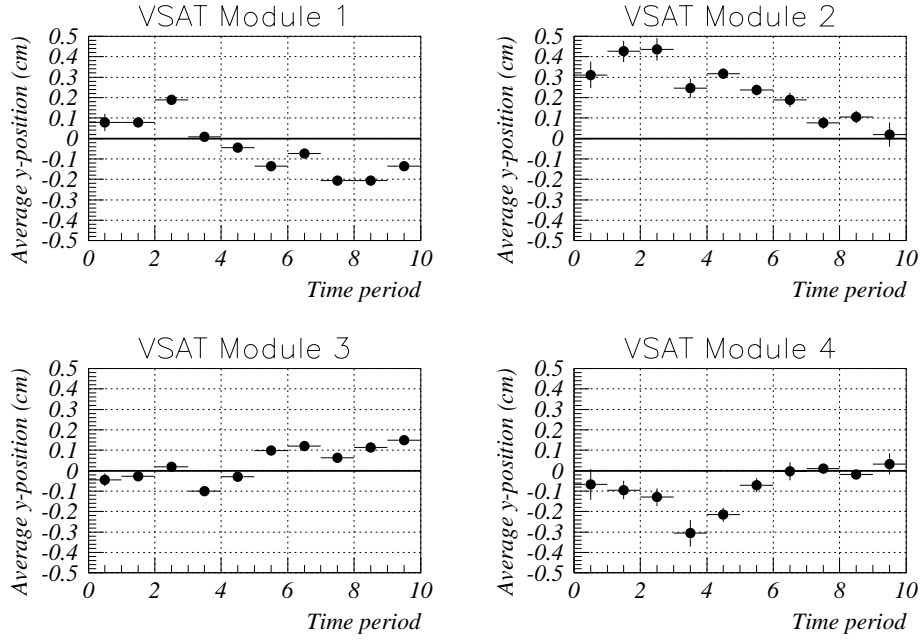
Figure 11: The average y-position in VSAT of the off-energy electron background during different time periods.

VSAT modules as a function of a cut on energy. Both for the inner and outer modules, the cut has to be made at very high energies in order to achieve a sizable reduction in background.

Period	Fills	$\mathcal{Y}_1[mm]$	$\mathcal{Y}_2[mm]$	$\mathcal{Y}_3[mm]$	$\mathcal{Y}_4[mm]$
0	4550-4600	0.78 ± 0.42	3.10 ± 0.65	-0.45 ± 0.30	-0.67 ± 0.76
1	4601-4675	0.78 ± 0.21	4.26 ± 0.52	-0.27 ± 0.13	-0.95 ± 0.45
2	4676-4725	1.88 ± 0.14	4.35 ± 0.55	0.20 ± 0.09	-1.30 ± 0.43
3	4726-4750	0.09 ± 0.10	2.47 ± 0.46	-0.99 ± 0.11	-3.05 ± 0.65
4	4751-4875	-0.45 ± 0.09	3.16 ± 0.27	-0.29 ± 0.07	-2.16 ± 0.33
5	4876-4950	-1.36 ± 0.08	2.38 ± 0.28	0.98 ± 0.07	-0.70 ± 0.34
6	4951-5000	-0.73 ± 0.12	1.89 ± 0.35	1.21 ± 0.08	-0.03 ± 0.44
7	5001-5120	-2.06 ± 0.08	0.77 ± 0.31	0.64 ± 0.07	0.09 ± 0.21
8	5121-5330	-2.05 ± 0.09	1.05 ± 0.31	1.15 ± 0.06	-0.18 ± 0.24
9	5331-5500	-1.35 ± 0.17	0.18 ± 0.60	1.49 ± 0.13	0.33 ± 0.51

Table 6: The average y-position of the off-energy electrons during 10 time periods.

Since the off-energy background is concentrated in the horizontal plane, the best way to reject it is by a cut on y (i.e. the vertical coordinate). However, differences in the magnetic fields in LEP during different time periods mean that the background peak in y moves during a LEP run. To study this, the 1998 data was divided up into 10 time periods as indicated by Table 6 and the average y-position was plotted (Figure 11). Variations of up to 5 mm of the average y-position were observed during the year, considering that each VSAT module has an active area which is only 5x5 cm, this is a significant effect.
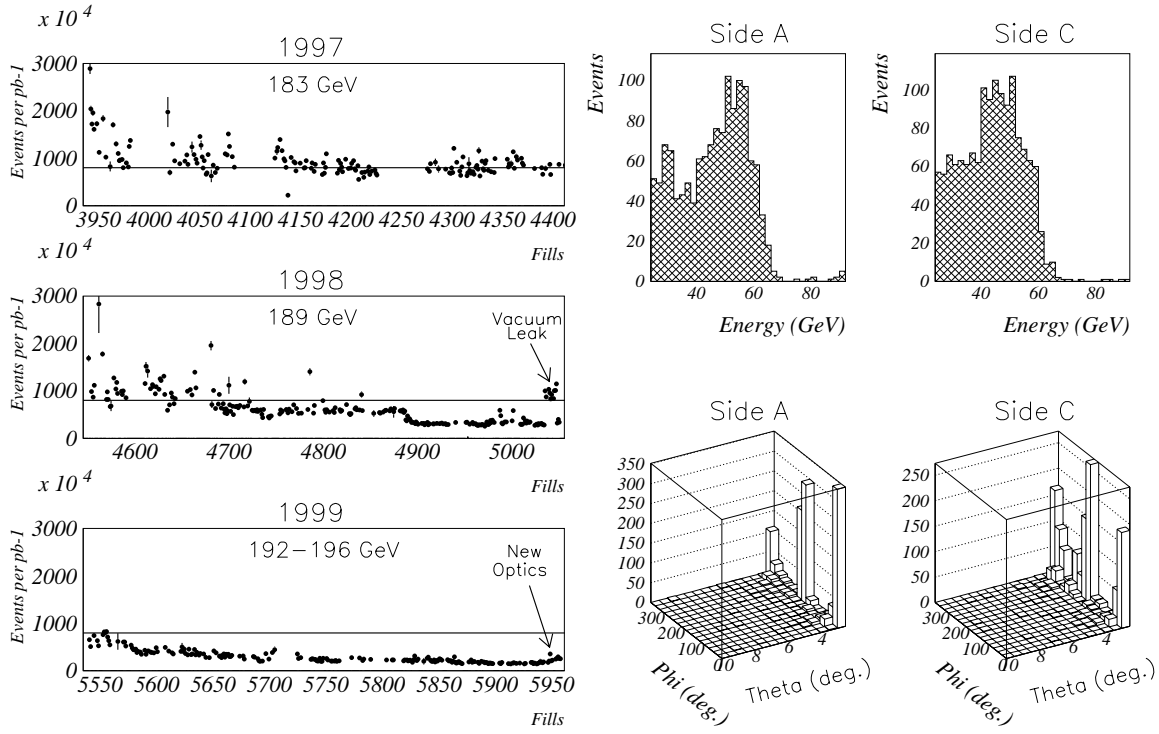
9

Figure 12: Left: The number of off-energy electrons in STIC per pb^{-1}. Only the first 400-500 high energy fills during each year are shown. Right: The energy and theta-phi distributions of events recorded by the STIC single arm trigger. Data from fill 5941 were used.

3   Background in STIC

3.1   STIC single arm triggers

The STIC single arm triggered events can be used to measure the rate of off-energy electrons in STIC [5]. This trigger requires a shower with an energy greater than $\sim$ $0.25 \cdot E_{beam}$ in one of the two calorimeters. The trigger is dynamically downscaled to a constant trigger rate, and this has to be taken into account in the estimation of the rate. Figure 12 shows the rate of off-energy electrons in STIC normalized to luminosity. In 1997 the typical rate of off-energy electrons in STIC was $8 \cdot 10^6$ per pb $^{-1}$. The rate has decreased each year and it is now $< 2 \cdot 10^6$ per pb $^{-1}$.

The energy and angular distributions of the off-energy electrons in STIC are shown in Figure 12 for 1999B data from fill 5941. Most of the background has a large energy and is in the horizontal plane, which results in peaks in the theta-phi distribution. This horizontal background component can, however, be removed by a cut on the polar angle since it does not extend much above 3°.

3.2   STIC Bhabha events

To calculate the probability that an off-energy electron is recorded together with a physics event, the same basic selection of events as in the VSAT study was used, i.e., the events had
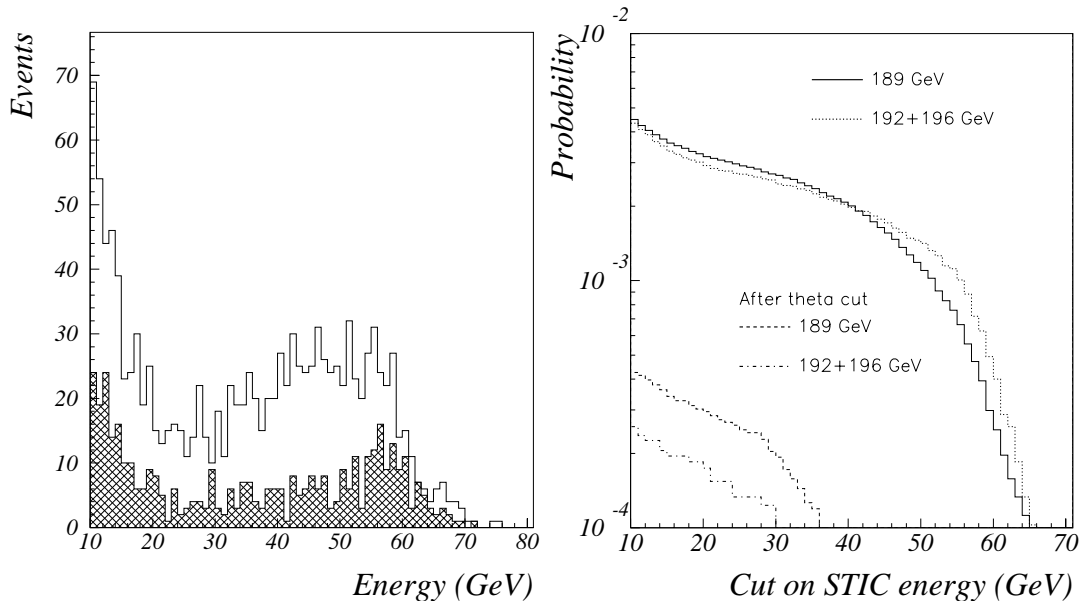
Figure 13: Left: Energy distribution of the third shower in the selected STIC events. The unshaded histogram is 1998 data and the shaded histogram 1999 data. Right: The probability that an off-energy electron shower will be found in STIC as a function of an energy cut.

to have one shower in each calorimeter with $2.5° < \theta < 8°$ and $0.97 < E_e/E_{beam} < 1.05$. The angle between the two showers had to be larger than $179.85°$. A third shower was required in the event and this shower has to be separated by at least $45°$ in azimuth from the closest shower. The angular requirements meant that radiative Bhabha events with a photon energy of at most ~ 8 GeV could survive the selection; the final sample of Bhahbas + an off-energy electron was selected by requiring the third shower to have an energy larger than 10 GeV.

The energy distribution of the third shower in the selected events are shown in Figure 13 for both 1998 and 1999 high energy data. The probability of an off-energy electron in STIC as a function of an energy-cut is also shown in Figure 13. The probabilities in 1998 and 1999 are very similar.

The most effective way of removing showers from off-energy electrons is not by an energy-cut but by a cut on the polar angle. By requiring $\theta > 3°$, most of the background in the horizontal plane is rejected. The probability of having an electron after this θ-cut is given in Table 7 and Figure 13 and it can be seen that the cut reduces the background by at least one order of magnitude.

One surprising observation is that more than a third of the events (36% in 1998D and 43% in 1999B) are accompanied by charged tracks. This is in contrast to Bhabha events without off-energy electrons, where less than 1% of the events are accompanied by charged tracks. Most of the tracks in the off-energy electron sample survive the standard cuts on impact parameters and momentum error and are not concentrated in the forward region. They are, however, short (average length = 27 cm) and have a low momentum (average p = 0.4 GeV). A study of the detectors used in the reconstruction of the tracks (Figure 14) showed that most of the tracks are seen in the VD only.

11

E_{min} [GeV]	189 GeV		192-196 GeV	
	$\mathcal{P}[\%]$	$\mathcal{P}_{\theta>3^\circ}[\%]$	$\mathcal{P}[\%]$	$\mathcal{P}_{\theta>3^\circ}[\%]$
10	0.449±0.013	0.0425±0.0039	0.434±0.021	0.0257±0.0051
15	0.360±0.011	0.0341±0.0035	0.334±0.019	0.0195±0.0045
20	0.318±0.011	0.0295±0.0032	0.292±0.017	0.0174±0.0042
25	0.292±0.010	0.0249±0.0030	0.270±0.017	0.0133±0.0037
30	0.267±0.010	0.0193±0.0026	0.246±0.016	0.0092±0.0031
40	0.201±0.008	0.0081±0.0017	0.198±0.014	0.0072±0.0027
50	0.110±0.006	0.0025±0.0009	0.142±0.012	0.0021±0.0015
60	0.025±0.003	–	0.040±0.006	–

Table 7: The probability of an off-energy electron with energy higher than E_{min} in STIC. The measurement was done with STIC Bhabha events.
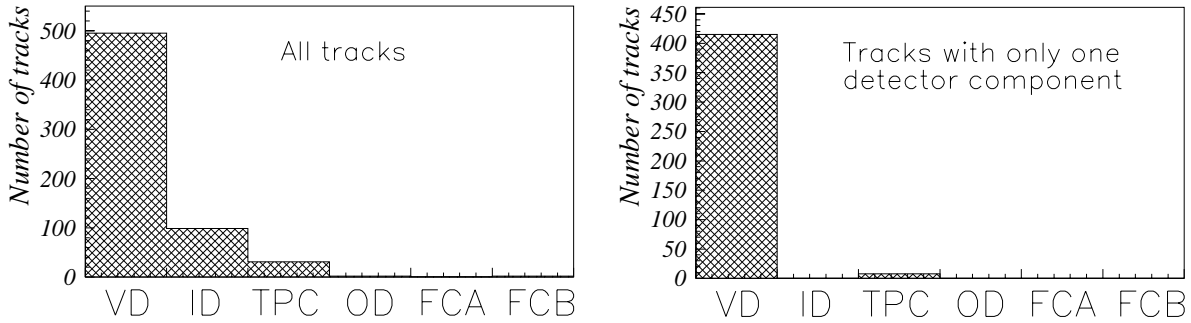
Figure 14: The different detectors used in track reconstruction for all tracks (left) and tracks with only one detector used in the reconstruction (right). 1999B data was used in this study.

3.3   Random triggers

The random trigger in DELPHI is caused by a signal from a scintillator placed close to a radioactive source. It is used to select an unbiased sample of events when no real interaction has occurred. The events taken with the random trigger during the first part of the 1999 LEP run ($\sim$40pb^{-1}) has been studied. Both the A- and the B-processing has been used.

The advantage of using random triggers compared to Bhabha events is that it makes it possible to go down to lower energies. The disadvantage is a smaller event sample. There is also the possibility that the off-energy electrons background is correlated in time to interactions and that the random sample therefore underestimates the off-energy background.

The probability of a STIC shower in a random triggered event as a function of a cut on the STIC energy is depicted in Figure 15. The probability has been calculated for all events with a shower in STIC and for the subsamples when the veto scintillator counters identify the incoming particle as an electron [6] and when the shower has a polar angle of more than 3 degrees.

The most effective way of removing the off-energy background is, as stated previously, by a cut on the polar angle. This is illustrated in the right plot in Figure 16 which shows the theta-phi distribution of the off-energy electrons in the random triggered sample.
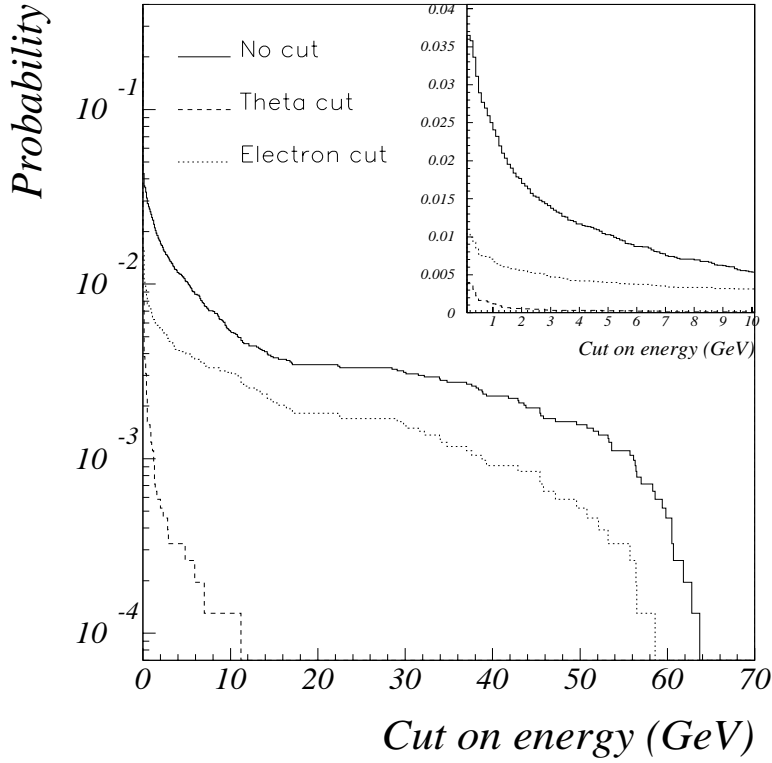

Figure 15: The probability of a STIC shower in a random triggered event as a function of a cut on the STIC energy. The probability has been calculated for all events with a shower in STIC and for the sub-samples when the veto scintillator counters identify the incoming particle as an electron and when the shower has a polar angle larger than 3 degrees.

By requiring a confirmation of the electron from a signal in the veto-counters a sizeable part of the background may be rejected. The reason is that many of the off-energy electrons enter STIC from behind or below the tungsten shield. In principle, the reason could also be that the STIC showers are caused by noise and not by off-energy electrons. That this is not the case can be seen in the left plot of Figure 16, which shows the energy of the showers versus the number of towers used in the shower reconstruction. A shower caused by noise has only one tower in the reconstruction and no showers like this were found with an energy larger than 0.5 GeV.

Table 8 gives the probability for an off-energy electron in STIC for different cuts on energy. An analysis which veto events with more than 0.5 GeV in STIC will lose 3% of the signal. In a search analysis which ends with 10 candidate events the probability of at least one off-energy electron in the events with more than 2.5 GeV is 15% while the probability of such a shower higher than $\theta > 3°$ in the 10 events is only 0.5%.

The probability of charged tracks in the events is 52%±6%, when the energy in STIC is larger than 10 GeV. The tracks are similar to the ones found in the Bhabha sample.
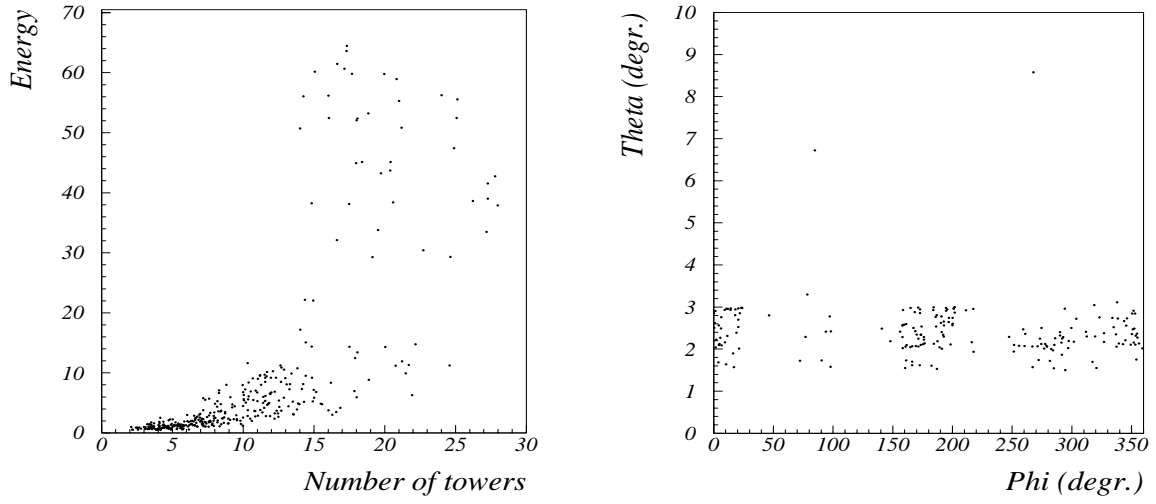
13

Figure 16: Energy versus the number of towers in the shower (left) and the theta versus phi distribution (right). Showers with an energy greater than 0.5 GeV were used in these plots.

E_{min} [GeV]	$\mathcal{P}$ [%]	$\mathcal{P}_{\theta > 3°}$ [%]
0.1	3.65±0.15	0.39±0.05
0.5	2.89±0.14	0.16±0.03
2.5	1.52±0.10	0.05±0.02
5	1.03±0.08	0.03±0.01
10	0.53±0.05	0.01±0.01
15	0.38±0.05	–
20	0.35±0.05	–
25	0.33±0.05	–
30	0.31±0.05	–
40	0.23±0.04	–
50	0.16±0.03	–
60	0.05±0.02	–

Table 8: The probability of a shower with energy larger than E_{min} in STIC. The measurement was done using random triggered events recorded in 1999.

A comparison of the probability obtained at E_{min}=10 GeV with the Bhabha sample ($\mathcal{P} = 0.43 \pm 0.02$) and the random triggered sample ($\mathcal{P} = 0.53 \pm 0.06$) shows a barely significantly higher value for the random sample (contrary to naive expectations). This could be due to the fact the time period studied in the two analyses was not exactly the same.

14

4   Noise in the other calorimeters.

The other DELPHI calorimeters have also been studied by using the random triggered sample. At angles above STIC the calorimeters do not see any of the off-energy electron background. Instead they suffer from noise showers and occasional showers created by cosmic rays. In the 1999A data, a noisy area in HCAL which created high energy showers was observed, but was removed in the 1999B processing (Figure 17). The left plot in Figure 18 and Table 9 gives the probability of a noise-shower in different calorimeters as a function of a cut on the shower energy.
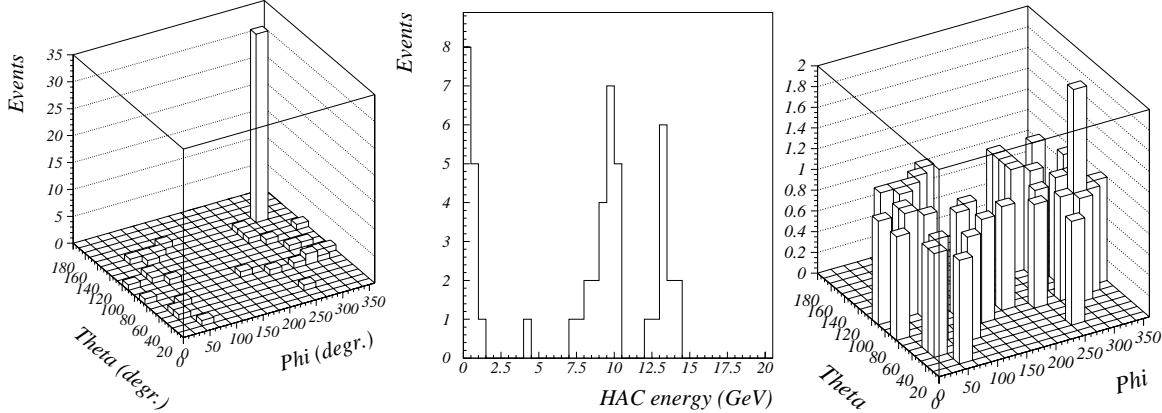
Figure 17: The theta-phi distribution of noise showers in HAC in the 1999A data (left) and the 1999B data (right). The middle plot shows the energy distribution of the peak in the theta-phi distribution.

E_{min} [GeV]	$\mathcal{P}_{HAC}$ [%]	$\mathcal{P}_{FEMC}$ [%]	$\mathcal{P}_{HPC}$ [%]
0.1	5.15±0.18	4.47±0.17	3.12±0.14
0.5	2.21±0.12	4.42±0.17	0.05±0.02
2.5	0.25±0.04	0.05±0.02	0.04±0.02
5.0	0.10±0.03	–	0.03±0.01

Table 9: The probability of a shower with energy higher than E_{min} in HAC, FEMC and the HPC.

The probability plots in Figure 18 are of course only useful for analyses which does not select events based on energy in the calorimeters. If one takes the FEMC as an example, the probability of a noise-shower with energy larger than 2.5 GeV on top of a physics events is completely negligible. If on the other hand single photon events are selected by triggering on energy in FEMC and by not requiring any signals in any other DELPHI detectors (which would confirm the event to be a genuine physics event), events caused by noise in FEMC are selected. In this way one can find hundreds of single photon events in FEMC caused by fake showers. This is illustrated in the left plot of Figure 18 which shows noisy areas in the 1999B FEMC data. In this plot, only noisy areas producing showers larger than 2.5 GeV which survive the Margoni offline noise algorithm are included.
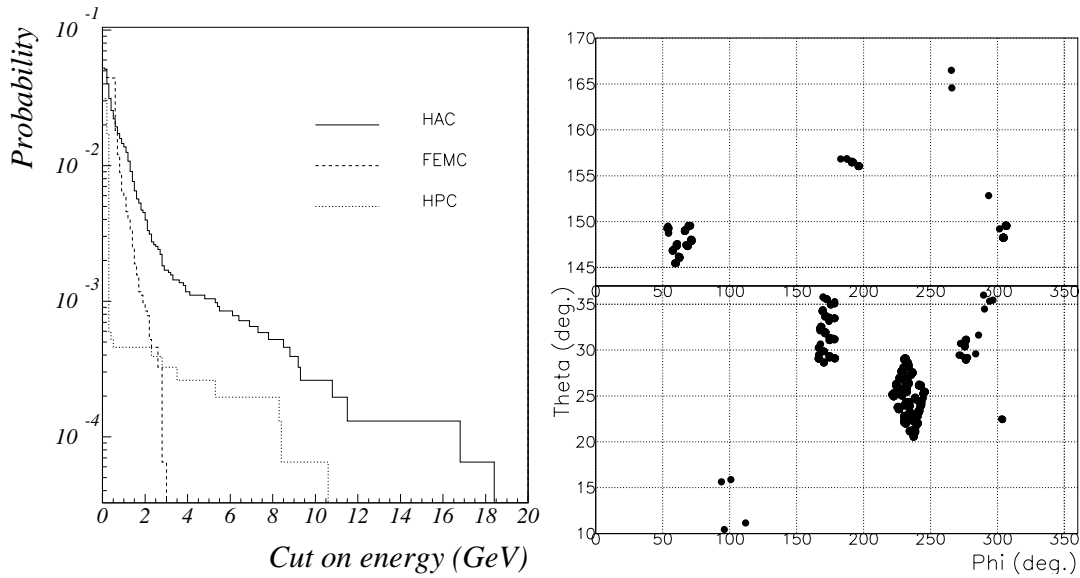
Figure 18: Left: The probability of a shower in different calorimeters as a function of acut on the shower energy. The data used were triggered by the random trigger and come from the 1999 B-processing. Right: Noisy areas in the FEMC calorimeter during the 1999 data taking.

5   Summary and conclusions.

VSAT:

The VSAT Bhabha sample has been used to estimate the probability of an off-energy electron in VSAT on top of a genuine physics events such as an untagged $\gamma\gamma$ event. The statistical precision of this measurement is unbeatable. In an independent analysis a muon sample was selected and the probability to have an off energy electron in VSAT calculated. The result agreed with the VSAT Bhabha measurement within large statistical errors. Finally, a STIC Bhabha sample was used. All features of the background were the same in the STIC and VSAT Bhabha samples. Comparing the probabilities in the four modules by taking the ratio $\mathcal{P}_{VSAT} - \mathcal{P}_{STIC}/\mathcal{P}_{VSAT}$ for E_{min}=20 GeV -0.02±0.01, -0.22±0.03, +0.03±0.01 and -0.12±0.02 are obtained, i.e. a significant difference in the measurement of probability in the outer modules.

The best way of removing the background is by a cut on the measured y-coordinate since the off-energy electrons are concentrated in the horizontal plane.

STIC:

For STIC, a Bhabha sample has been used to measure the background of off-energy electrons. It is limited to electrons with an energy larger than 10 GeV and has therefore been supplemented by an analysis of random triggered events with which the low-energy off-energy electrons can be studied. At 10 GeV the difference $\mathcal{P}_{Bhabha} - \mathcal{P}_{Random}/\mathcal{P}_{Bhabha}$ is -0.23±0.15 .

The most effective way of removing the background is to discard any STIC showers with a polar angle less than $\sim 3°$.

FEMC:

The probability of a FEMC shower with energy above 0.5 GeV is sizeable (4.6%) but it drops off quickly with energy and for $E_{min} > 2.5$ GeV there is no need to take

16

the detector noise into consideration (except in problematical analyses like single photon analyses which select noise events).

HPC:

The energy spectrum due to noise is very steep and with an energy cut of $E_{min} >$ 0.5 GeV the probability to have a noise shower in an event is at the level of 0.05%.

HAC:

The hadron calorimeter is noisier than the electromagnetic calorimeters and certain noisy areas can produce showers with energies of up to 10-15 GeV. However, by a cut of $E_{min} > 2.5$ GeV the probability of a noise shower is reduced from 5% (without the cut) to 0.3% (with the energy cut).

References

[1] The DELPHI collaboration. Phys. Lett. 342B(1995)402.

[2] E. Falk et al, DELPHI NOTE 98-147 PHYS 791.
    E. Falk et al, DELPHI NOTE 98-76 CONF 144.
    P. Checchia et al, DELPHI NOTE 99-77 CONF 264.

[3] E. Falk, V. Hedberg and G. von Holtey, CERN SL/97-04(EA).

[4] S. Jadach *et al.*, Comp. Phys. Comm. **66** (1991) 276;
    S. Jadach *et al.*, Comp. Phys. Comm. **79** (1994) 503.

[5] S.J. Alvsvaag *et al.*, Nucl. Inst. and Meth. **A425** (1999) 106.

[6] P. Ferrari et al, DELPHI NOTE 98-49 CAL 141.

Appendix E

VSAT Background and Luminosity 1999.

VSAT Background and Luminosity 1999

Andreas Nygren
University of Lund

Abstract

This paper presents an overview of general VSAT data quality during 1999. VSAT had no hardware failure during the data taking and shows very good data quality. Some small percentage of the data are however always missing, this will be presented here together with the VSAT corruption level and energy response. Finally the VSAT luminosity and background conditions for 1999 have been analyzed and a luminosity file for 1999 has been produced.

1 Introduction

Before the VSAT offline luminosity can be calculated a number of corrections and normalisations needs to be applied to the data. In LEP II it has also become very important to have good understanding of the background conditions of the off momentum background. The VSAT false bhabha trigger was removed in 1996 in order to lower our T1 rate, as a result the bhabha background has to be estimated with other methods. A VSAT luminosity file has been produced for 1999 and a comparison with STIC data is presented in this paper.

2 Data quality

No major incidents occurred on the VSAT detector during 1999 and the overall data quality is thus very good. Instabilities and corruption are however always present, which should be dealt with before any luminosity analysis. The whole VSAT detector area can not be used and a number of acceptance cuts are made, which reduce the VSAT crossection somewhat.

2.1 Missing Data

Data in the final output can be missing for a number of reasons, most obvious is that the VSAT was off during data taking. This fortunately happens very rarely and more common is that a data file is missing due to that the corruption level of the VSAT data was too high in DELANA. A data file can also be discarded in our local compression program(COMPACT) if it finds the data file to be unacceptable. There are some data files that passes both these checks but still contain no data of interest, this is normally due to very short runs in DELPHI. In the list below the bad and missing data files for 1999 is listed with fill and run number, and amounts to about 0.4% of the total high energy data.

Bad Files(all are Z0 data)	Missing Files	Missing Files
5471: 101413-01	5634: 102517-02	6568: 107038-04
5471: 101415-01	5724: 102988-03	6568: 107038-05
5471: 101415-02	5903: 103796-06	6568: 107038-06
5478: 101440-12	6030: 104531-09	
5482: 101476-01	6083: 104807-03	
5500: 101566-03	6215: 105529-03	6098: All
5522: 101707-02	6383: 106347-01	6569: All

2.2 Data corruption

VSAT stores the collected events in a local buffer, which is emptied every DELPHI event. Sometimes an event or even the whole buffer gets corrupted due to intermittent readout errors in the hardware. This is kept track of to be able to correct any potential problems in the data stream. In fig 1 the corruption rate and one of its components are shown during the 1999 data taking. The average number of corrupted buffers per cassette is visible in figure 2.
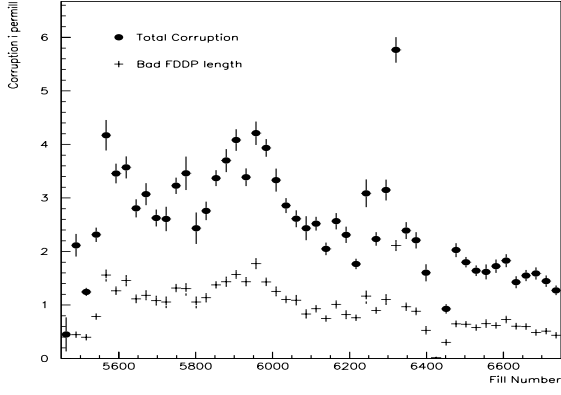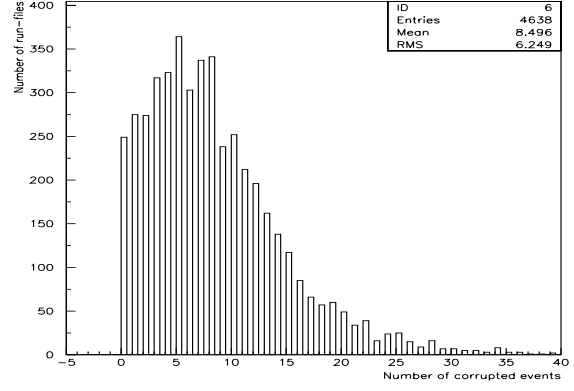
Figure 1: Corruption rate 1999

Figure 2: Corrupted buffers

2.3 Accepted data

The whole detector area of the VSAT can not be used and some acceptance cuts have to be introduced in order to get good quality data. If the detector is hit on the edge there is no telling of how much energy that was absorbed by the detector and an energy reconstruction is impossible, all such events is thus cut away. In front of the VSAT there is a flange that shadows the outer part of the detector. As this flange disturbs both energy and momenta of incoming particles a cut is made on the outer edge in order to remove most of these events.

If the energy of the particle is very low, it will be quite difficult to reconstruct the position properly. If DELANA isn't able to get an accurate position of the particle shower this is marked and these events will also be cut away from the analysis. These types of events only contribute with a small fraction under normal circumstances and are not plotted in figure 3, which only shows the removal rate for the flange and edge cut. The energy distribution of the removed hits are shown if figure 4.
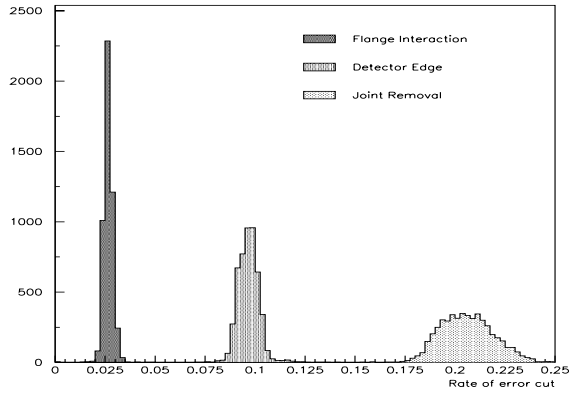
Figure 3: Rejection ratio for 1999 data
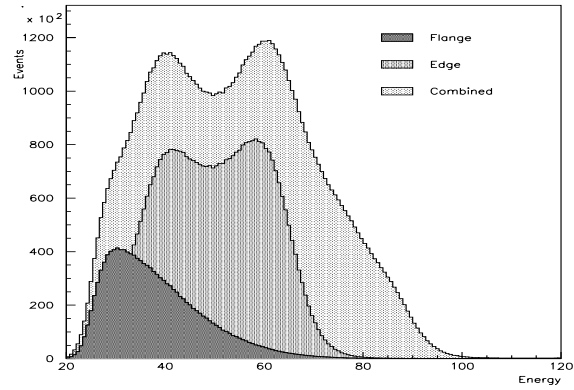
Figure 4: Energy of rejected events

An event is removed if any module register a hit outside the acceptance cuts. This means that the combined acceptance cuts for all 4 modules will remove more events than the individual cuts(figure 3 and 4). It would be possible to check for bhabha triggers and discard any out of acceptance in other modules, this would however only contribute with a few per-mill of statistics to the bhabha sample.

2

2.4 Data stability

The energy response of the VSAT detector varies somewhat over the year, the bhabha-peak energy is however calibrated to beam energy every fill(fig.5). Detector response normally changes during LEP access or during filling time, so this does not have a mayor impact on the data quality within a fill(fig 6). The energy resolution of the detector is more vital to check, as an energy cut is made in order to isolate the bhabha sample. The resolution tends to get worse with time in the outer modules [1], this is natural as the outer modules take most radiation from the off-momentum background.
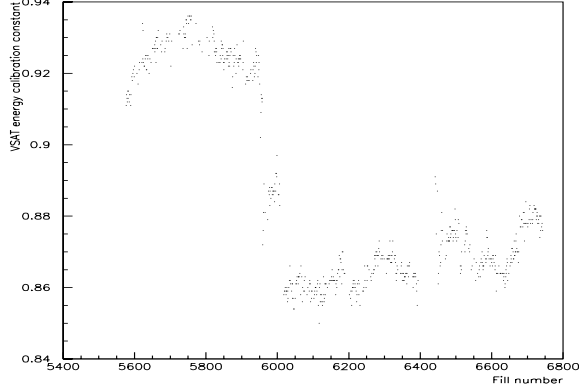
Figure 5: Energy Calibration constant
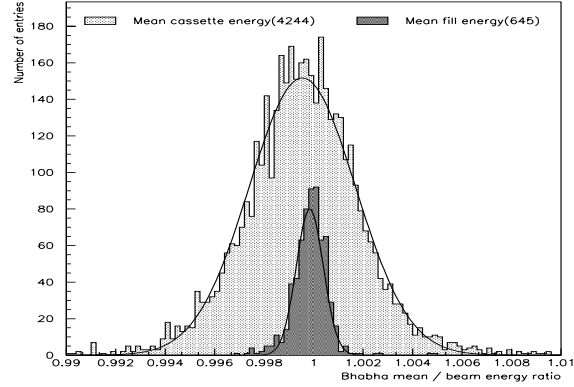
Figure 6: Corrected energy uncertainty

If the VSAT buffer becomes full before there is an DELPHI event, VSAT will trigger the whole Delphi detector. The VSAT buffer length was increased to 25 at the beginning of 1999, as a result we have a T2 trigger rate well below 0.3 Hz at an average T1 rate of 20 Hz. The T1 trigger is activated either by a bhabha or a down scaled single electron trigger. The down scaling system is presently set to balance the inner and outer modules to around 8% of the total trigger sample(fig.7).

3 Background

The vacuum condition in LEP is determined by the static pressure in form of beam gas particles and dynamic pressure from synchrotron radiation. Beam particles can interact with this gas and loose part of their energy, and as the beam travels through quadropoles and bending magnets these particles will leave the beam path. This is called off-momentum background and cause hits in the vsat detector at a rate of about 600 Hz in the outer modules and 140 Hz in the inner.

Naturally there is the possibility that two off-momentum particles hit two diagonal detector modules at the same time. This will then be triggered as a bhabha event, and will contribute to the bhabha sample. The rate of such false bhabhas is proportional to the product of the off-momentum background rates in the diagonal modules. This depends on the vacuum condition in LEP, which is normally worse in the beginning of the year(figure 8).
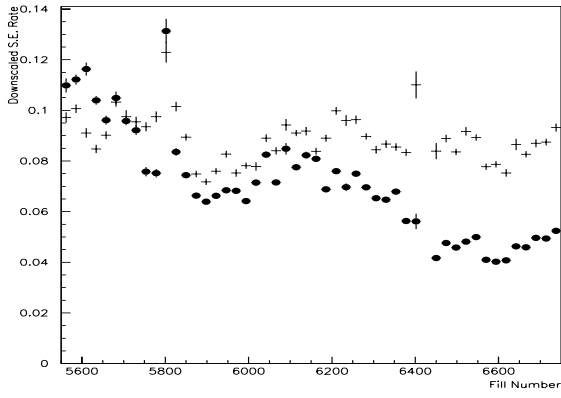
3

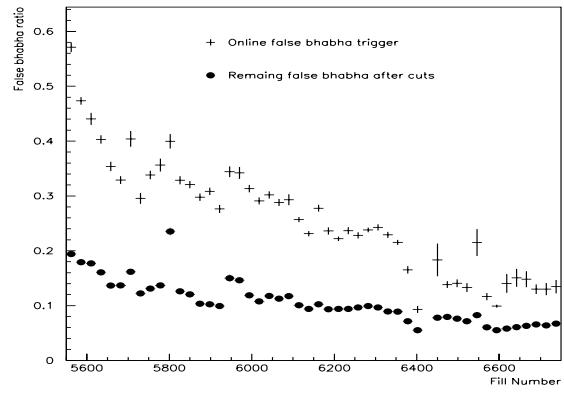Figure 7: The single electron rate in the inner(dots) and outer(crosses) modules.

Figure 8: False bhabha rate from online triggers and after bhabha acceptance cuts.

3.1 Bhabha cuts

To clean up the bhabha sample from background heavy cuts are imposed [2]. A bhabha event is an elastic scattering of e+ and e- from the LEP beam, and the particles should thus have beam energy and opposite momentum. An energy cut is therefore imposed around the energy peak of the two particles(fig 9). As the momentum is directly opposite the difference in x and y position(Δx and Δy) of the two particles should always be constant. A second cut is therefore made around the joint Δx and Δy region(fig 10).
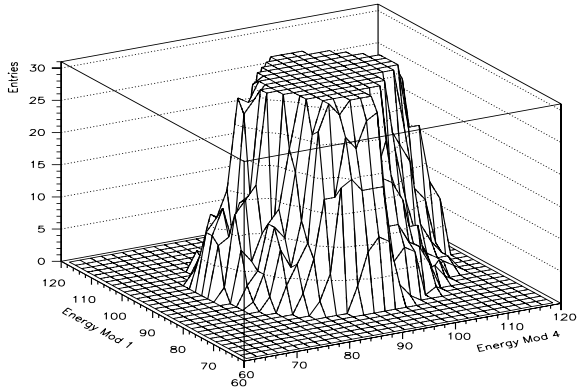
Figure 9: Bhabha Energy Cut
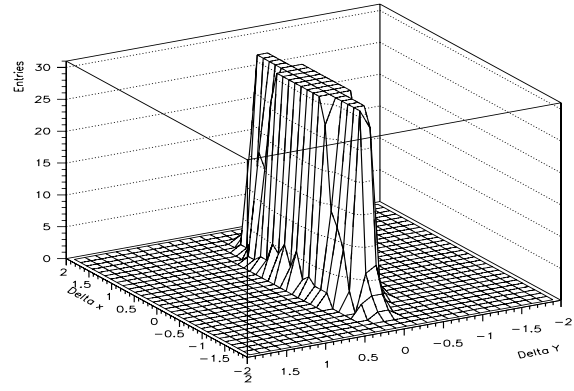
Figure 10: Bhabha Delta xy cut

The efficiency of these cuts heavily depends on the structure of the background particles. The off momentum background is strongly concentrated around the beam position in the y-plane, which varies with the beam conditions. The energy of the background depends on how far away from the Delphi experiment the background was produced, the farther away the higher energy and the stronger the concentration in the y-plane. The cut ratios for the energy and Δxy cut is shown in fig 11. In figure 12 the y-position of the off-momentum background and the bhabha Δy position is shown.
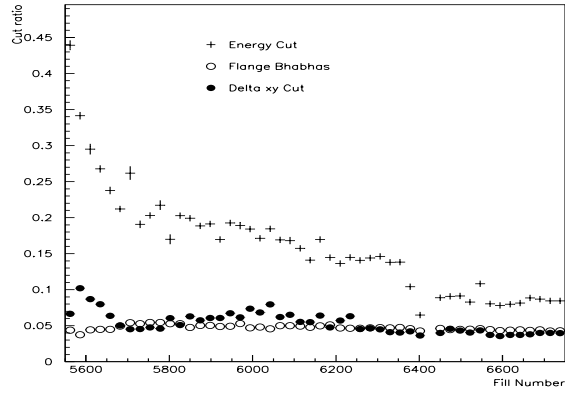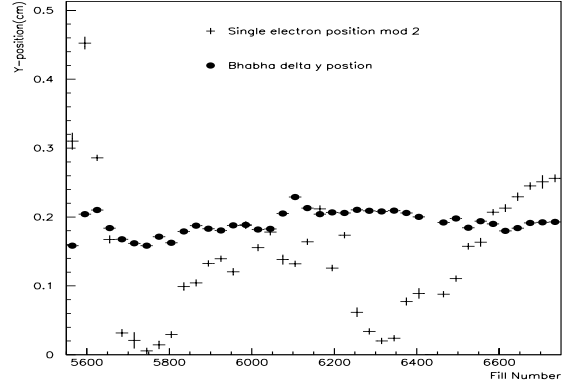
4

Figure 11: The ratio of the bhabha acceptance cuts.

Figure 12: The y-position of the off momentum background and bhabha Δy position

3.2 Remaining background

The background that can not be cut away directly has to be subtracted from the bhabha sample afterwards. Four different methods are used to estimate the remaining false bhabha rate. All these needs to be normalized to the real difference between STIC and VSAT luminosity. The methods are listed below, of which the two last ones seem to provide the best picture of the true background.

- VSAT has an online MIG-scaler that counts the number of delayed bhabhas that hits the detector. A delayed bhabha is a single hit in one module and another hit in the diagonal module 4 bunches later. This counter counts all events with all energies and delta xy values, the false bhabhas removed by the bhabha cuts will thus not be accounted for in this counter. For cases of low statistics it is however a good complement to the other methods.

- The energy cut in conjunction with the single electron rates below and above the energy cut can also be used to get a more absolute measurement of the false bhabha background. The energy cut is unfortunately also contaminated with true bhabhas that have hit a flange in front of the VSAT and lost part of their energy. This disturbs the sample and adds an extra uncertainty to the result.

- About 10% of the VSAT readout data sample consists of single electrons. These can be used to estimate the amount of false bhabhas above the energy cut. The accidental background rate in the bhabha peak can easily be estimated as the product of the single electron samples divided with the run time. The single electron trigger is down scaled so these numbers have to be normalized to the STIC and VSAT luminosity difference.

- The off momentum background is mainly concentrated in the y-position of the beam. This property can be used in order to narrow down the bhabha cuts in this sensitive region. A purer bhabha sample will be obtained with the drawback of the loss of some small sample of bhabhas. The difference between this tighter bhabha cut and the normal bhabha acceptance cut can also be used as a measurement of the background in the bhabha peak.

These 4 different measurements on the VSAT remaining false bhabha background are linearly combined to imitate the VSAT and STIC luminosity difference as good as possible. A breaking point is introduced above a certain statistics limit where the MIG-scaler bhabhas are excluded from the calculations. The normal size of this estimated false bhabha background is about 10% of the bhabha rate after the acceptance cuts in energy and Δxy cut(figure 8).

4 Luminosity measurement

The VSAT detector provides fast online luminosity with small statistical error. The luminosity is produced directly from the bhabha and false bhabha MIG-scalers and adds no extra corrections. The offline luminosity needs much better systematical error, and a lot of corrections and normalisations need to be applied on the data sample.

4.1 STIC Normalization

The exact VSAT geometry in relation to the DELPHI coordinate system is not known to a good precision. In front of the VSAT a flange of the beam pipe also shadows the detector on the outer edge, which also adds uncertainty to the crossection as the exact shape of the flange is difficult to simulate. To achieve a luminosity measurement as good as possible the VSAT detector is therefore normalized to the STIC luminosity, as this has a very small systematical error. Normally the whole VSAT data sample for a year is divided into 2 or 3 groups that are individually fitted to the STIC luminosity.

The VSAT cross section and the final false bhabha rate have to be determined simultaneously as they are directly connected to each other[3]. This is done by scanning the phase space for the smallest total deviation between STIC and VSAT luminosity. The VSAT statistical error is much smaller than STIC's and a comparison needs to be done over as much STIC data as possible. The data is therefore merged together in blocks of 600-1200 STIC bhabhas in order to improve the statistical errors and avoid fitting to statistical fluctuations. A typical fit of the final VSAT false bhabha rate to the VSAT and STIC difference is presented in figure 13.
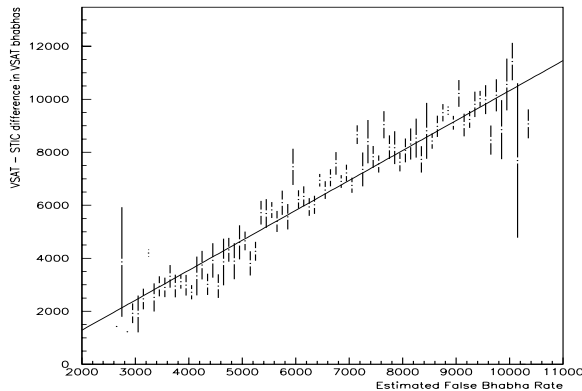

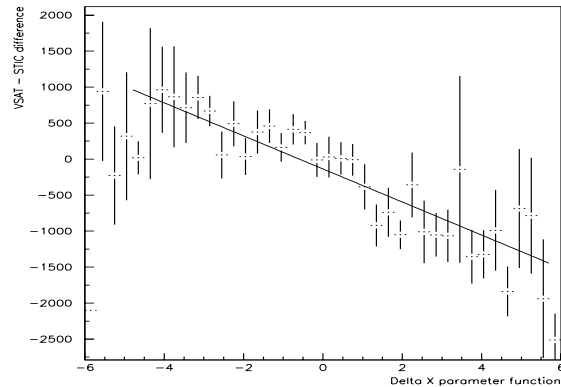Figure 13: VSAT false bhabha rate correction to STIC and VSAT difference

Figure 14: VSAT and STIC luminosity difference as function of delta x parameter.

6

4.2 Beam-parameter Fitting

The VSAT crossection is not constant as it depends on a number of beam parameters [4]. Fortunately VSAT is equipped to handle this as it can measure both x and y position. By checking the differences in x and y of the two incoming bhabha particles it is possible to extract information about the beam conditions that are used to correct the VSAT cross section(fig. 14). The bhabha counting asymmetry between the two bhabha diagonals also provide useful information about the beam that are needed for the correction.

5 Results

When all the corrections have been applied and the VSAT luminosity file has been created, it should be compared to the STIC luminosity. There are mainly two things of interest that should be checked, the VSAT systematical error and big deviations of single cassettes. The systematical error can only be measured if the STIC statistical error is small enough. It is desirable to get the STIC statistical error down to 1-2%, and the data is thus merged in blocks of 3000-10000 STIC bhabhas.
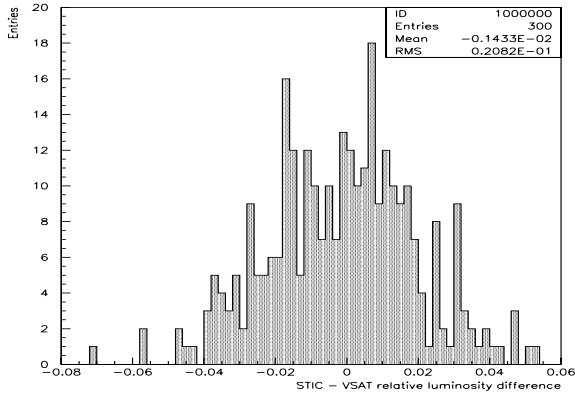
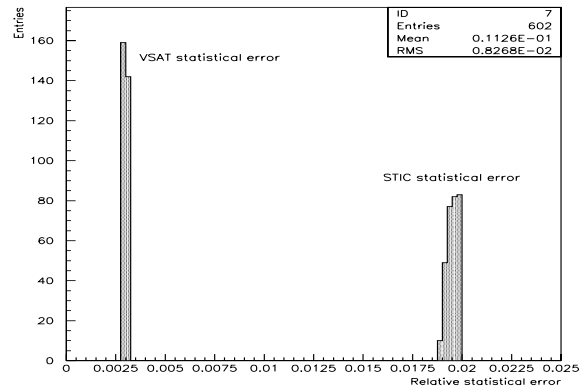Figure 15: Relative difference between STIC and VSAT Luminosity

Figure 16: Relative statistical error for VSAT and STIC Luminosity

The standard deviation of difference of the VSAT and STIC luminosity is then compared to their statistical errors(fig. 15 and 16), and the excess of spread is the joint STIC and VSAT systematical error. The pure VSAT systematical error can only be extracted after that the STIC systematical error has been found. The joint systematical error was found to be about 0.7-0.8% for 1999 year data.

The VSAT luminosity file is primary used to check the stability in the STIC data and search for corrupted DELANA files. The STIC and VSAT luminosities are therefore compared for each common cassette in search for any possible discrepancy. As it can be seen from figure 17 only one cassette showed a big deviation between STIC and VSAT data for 1999. This clearly shows that the STIC and VSAT luminosity for 1999(fig 18) is fully compatible and that the VSAT can produce a good quality luminosity with small statistical error.
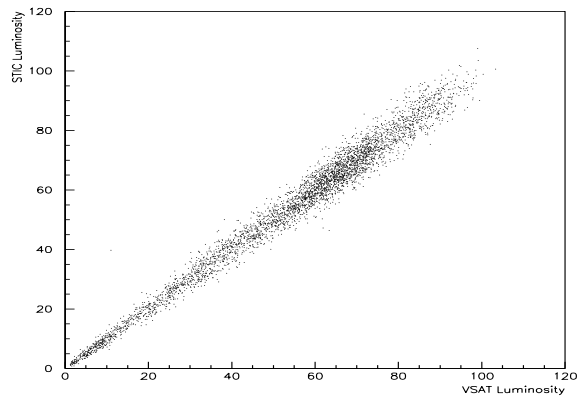
7

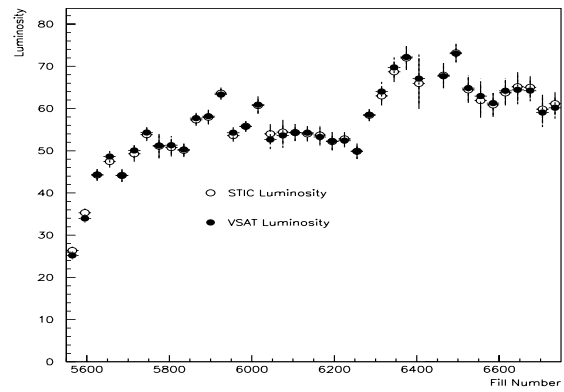Figure 17: STIC vs. VSAT Luminosity

Figure 18: STIC and VSAT Luminosity 1999

References

[1] U.Mjörnmark A.Nygren. VSAT trigger and energy response for LEP 2. Technical Report DELPHI 99-163 CAL 143, CERN, 1999.

[2] Andreas Nygren. New VSAT DST - Physics and Implimentation. Technical Report LUNFD6/(NFFL-7270), Lund University, 1999.

[3] Andreas Nygren. VSAT Analysis Tools. Technical Report LUNFD6/(NFFL-7271), Lund University, 1999.

[4] Per Jonsson. Luminosity Measurments and Two-Photon Physics with the DELPHI VSAT at LEP. Technical Report LUNFD6/(NFFL-7152), Lund University, 1998.

Appendix F

VSAT trigger and energy response for LEP II.

VSAT trigger and energy response for LEP II

Andreas Nygren, Ulf Mjörnmark
University of Lund

Abstract

The combination of higher beam energy, more off-momentum background and more luminosity have had a big impact on the trigger rates and radiation exposure in the small angle region. This report describes this impact on the VSAT detector and what has been done to deal with the situation.

1 Introduction

The Very Small Angle Detector(VSAT) consists of two pairs of modules placed on the beam pipe $\pm$ 7.7 meters from the interaction point(fig 1). The beam pipe radius at the detector region was decreased with about 5 mm during the winter shutdown 97/98 in order to allow higher acceptance for gamma-gamma physics. The detector modules are now located about 5.7 cm from the beam, with an increased trigger rate as a result.

Each of the modules consists of 11 Full Area Silicon detectors(FADS), interspaced with tungsten layers, for energy measurement(fig 2). In order to make leakage correction, Bhabha alignment and beam parameter monitoring, each module is also equipped with three strip layers for X and Y positioning at shower maximum.
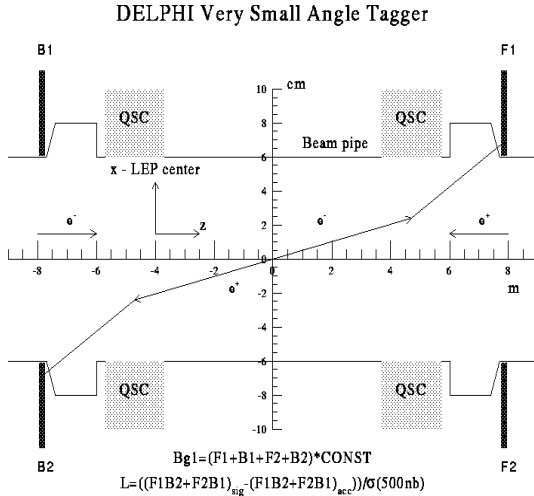

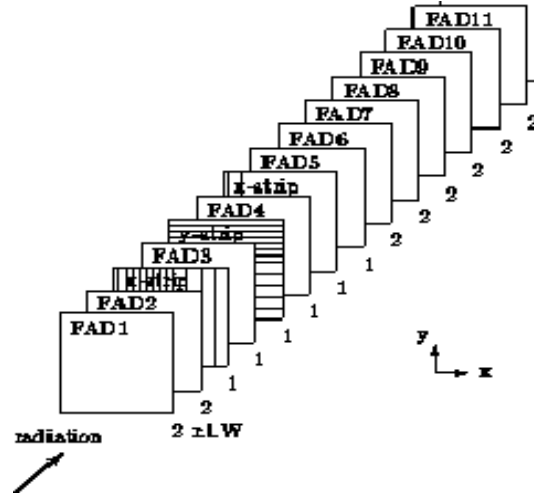Figure 1: The posotion of the VSAT modules.

Figure 2: The FAD and strip plane layout of a VSAT module

VSAT has three types of local triggers - Bhabha, single electron and delayed Bhabha. A Bhabha is a coincidence between two diagonal modules, a single electron is a hit in any module and a delayed Bhabha is an electron in any module and another in the diagonal module 4 bunches later. VSAT has much higher trigger rate than DELPHI and therefore stores its events in a local buffer that is read out every time DELPHI triggers.

If the VSAT buffer becomes full before there is a DELPHI event, VSAT sends a T2 trigger that triggers the whole DELPHI detector. The VSAT T1 trigger nowadays only consists of a downscaled single electrons sample(10% of the triggers) and the Bhabha triggers(the delayed Bhabha trigger was removed in 1996 as it caused the T1 rate to be equal to the single electron rate in the inner modules).

2 Trigger response

The VSAT was built and optimized for precision luminosity measurement at LEP 1. When LEP raised the energy for LEP 2 in 1996 this immediately led to problems with the VSAT FAD plane signal response. The VSAT preamplifiers were manufactured from two batches of which one had a non linear response at high energies.

1

The signal was chopped off on the upper half of the peak(fig 3) as the preamplifiers couldn't drive the signal increase fast enough. In addition some of the electronics became saturated and the signal piled up in the last bin(fig 4). The preamplifiers cannot be exchanged or adjusted during VSAT operation as they are located inside the VSAT modules in the LEP tunnel, so nothing could be done about the situation during 1996 year data taking.

During the winter shutdown 96/97 the slowest preamps were exchanged and calibrated to handle the new signal response. The general amplification was also lowered to avoid the signal piling up in bin 255. This worked fine and a produced nice test results, but when the energy was increased once again for 1997 all the preamplifiers started showing the same problem in the channels with maximum pulse height.
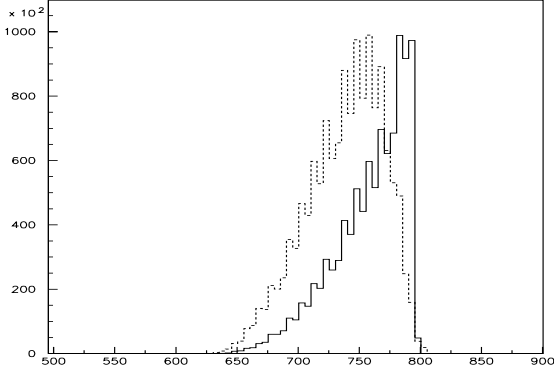

Figure 3: FAD signal shape with old(whole) and new(dashed) timing
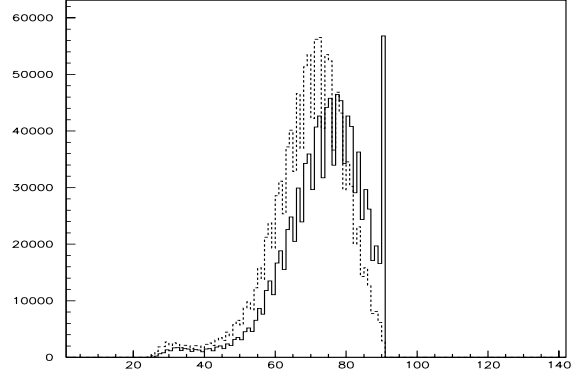
Figure 4: FAD signal shape for saturated (whole) and normal(dashed) FAD plane

When it was clear that there will be no minibunch data at high energy the timing of the signal readout were delayed. This makes minibunch separation impossible with the current electronics. A change in the timing from 5.55 to 5.8 μs was needed to allow the high energy signals to fully propagate(fig 3). The very low energy signals will not be at the signal peak and we get a non linear energy calibration curve. This is however to prefer over a saturated signal as the linearity is important mainly in the high energy region. For 96 and 97 year data a method was developed to partly reconstruct the energy signals with help from the strip planes.

3   Trigger Rates

The movement of the VSAT closer to the beam pipe in combination with higher beam current in LEP led to an increase on the trigger rate on the VSAT modules. The main part of the hits on the detector comes from the off-momentum background. The background is asymmetrical and is highly concentrated in the outer modules(fig 5).

Only a small fraction of the off-momentum electrons are read out as they contain no physics data of interest. The down scaling system can be set individually for inner and outer modules, and is now set up to give about 10% of the total triggers spread equally over the modules. This sample is necessary to obtain in order to estimate the accidental Bhabha rate.

During the high energy running 1996 the VSAT T1 rate started to become too high for DELPHI. To solve this the VSAT delayed Bhabha trigger was removed, which decreased the T1 rate with a factor 10-15. This comes from the fact that the single electron trigger was generating a T1 whenever there was a hit in the inner modules.
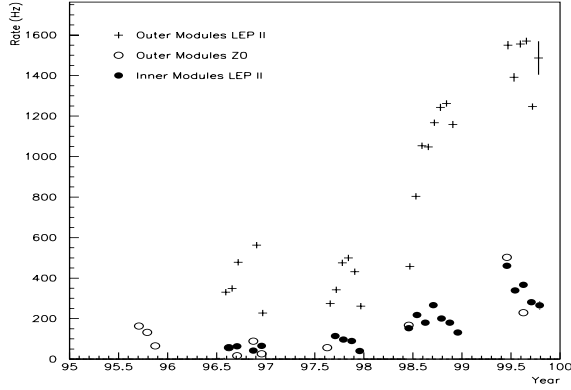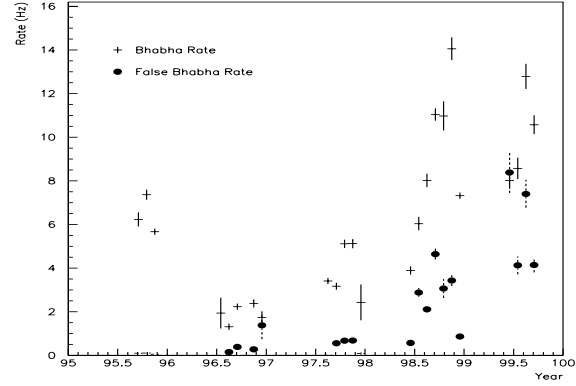

Figure 5: VSAT MIG scaler rate.

Figure 6: VSAT Bhabha trigger rate.

The movement of the VSAT modules increased the accepted VSAT Bhabha cross section. In connection with the strong improvement of LEP luminosity the VSAT Bhabha rate almost tripled. On top of this the Bhabhas from accidental coincidenses from off-momentum background started to make an important contribution to the Bhabha trigger(fig 6), with an average VSAT T1 rate about 15 Hz as a result(fig 8).

The local VSAT buffer started filling up and by the end of 1998 the T2 rate started to become troublesome for Delphi. The VSAT T2 trigger were counting at the rate of 0.5-0.6 Hz in the beginning of the fills, which was almost 10% of the DELPHI triggers. To solve this problem the VSAT buffer length was increased to 20 in 1998 then again to 25 in 1999, giving a reduction of the T2 rate with about a factor 7(fig 7).
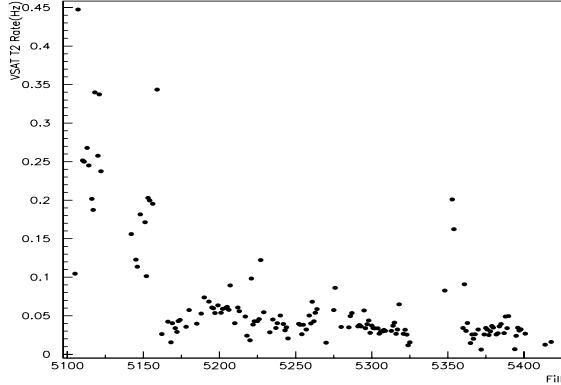

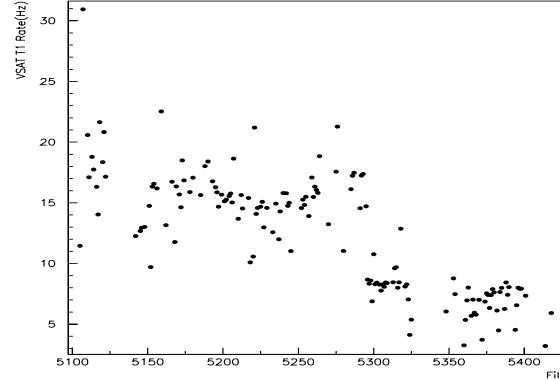Figure 7: VSAT buffer length increase.

Figure 8: VSAT T1 down scaling.

At present the VSAT T1 rate and readout time is also starting to become worrying for DELPHI. The VSAT reads the whole detector at each VSAT T1, while in other detectors just some trigger info is read out. This means that VSAT has a longer readout time than most other detectors and thus produces more dead time for a given T1 rate. The VSAT T1 rate was about 25 Hz in the beginning of the fills during 1999 and if it increases further something might have to be done.

3

Two things could be considered, either to decrease the T1 rate, or to cut the event info and thereby reducing the readout time. The later is not possible as the whole software chain would have to be changed and there is no manpower to do this. At the end of 1998 the T1 trigger was however downscaled by a factor two(fill 5296 in fig. 8) in an attempt to decrease the T2 rate.

A part of the VSAT electronics cannot handle the down scaling and the raw data seen by DELANA from the end of 1998 is corrupted. A method was developed to reconstruct 97% of the corrupted data with the help of other parts of the raw data structure. It is therefore possible to downscale(with some loss of events) the VSAT T1 trigger if a need should arise.

4   Radiation Exposure

There are two ways to investigate if there has been some radiation affecting the VSAT modules. The most direct way is to measure the energy response from the module. If there is a sudden drop in this, it is possible that the VSAT was hit by a large amount of radiation that has degraded the FAD plane energy signal response. The readout signal could however also change for a number of other accidental reasons:

- Change of timing of the hold signal.

- Voltage changes on the drift voltage to the preamplifiers.

- Signal from one or many FAD planes breaks down somewhere in the electronics.

- Pedestal changes of the FAD planes.

A more precise way to see if the FAD planes have been exposed to radiation is to look at the bias current supplied to them. If the planes have taken some damage the bias current will increase. To get an overall picture of the detector behavior both these thing should be correlated to background storms in DELPHI.

4.1   bias currents

With the rates of high energy particles to which the VSAT has been exposed during LEP 2, the FADs have unfortunately taken some radiation damage. As mentioned the damage of a silicon plane can be checked by measuring the bias current. The Delphi Database keeps track of this and it is easy to follow the bias current as long as the database updating program is running.

Figs 10 and 9 show the bias currents for two modules in the VSAT detector, in the backward and forward direction during LEP I and LEP II. The relative behavior is more or less the same for the two other modules in each direction. It is clear the our FAD plane suffer from radiation damage as the bias currents have increased from about 5 to 35 micro amps. The rise in the bias current is a combination of a steady increase of radiation in physics mode and of step functions with heavy radiation.

Two major incidents are visible in the middle of 94 and at the end of 95. After a major radiation incident the modules normally recover somewhat, but the bias does not go down to the same value as before. The modules should however continue to work without any noticeable lack in performance as long as the bias current stay below 100 micro amps.
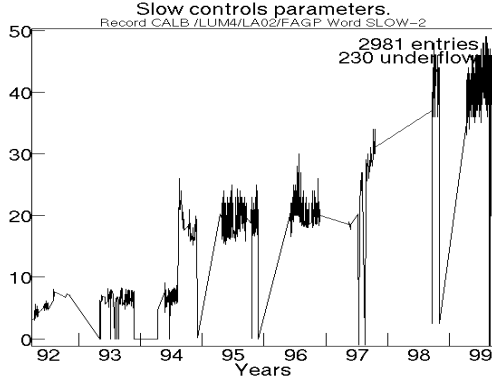

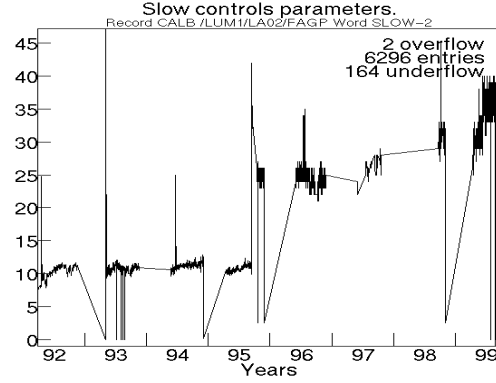Figure 9: Bias current for module 4.

Figure 10: Bias current for module 1.

4.2 Energy response

The energy measurement of the VSAT bhabha peak is normalized with calibration constants to beam energy for every fill, to make sure that the energy readout is correct. If there is a change in the energy response this is directly reflected in these calibration constants. The variations of these constants are shown in fig 11 and distinct step variations are seen. The raw energy signal is pre-calibrated in DELANA and should have a value around one.

When the timing was changed the energy response was lowered and this pre-calibration sunk to about 0.9. The energy scale is also somewhat non-linear in the lower energy regions, which is reflected in that the calibration constants goes up for z0 data. For high energy data the nonlinearity is small and is not visible in any of the calibration constants.
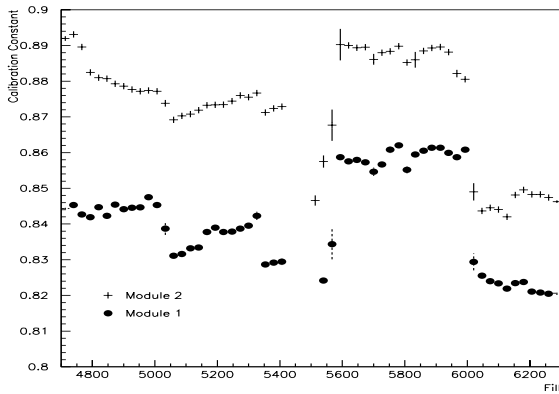

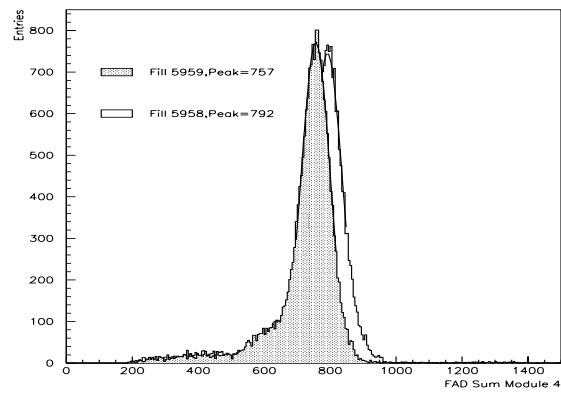Figure 11: Energy calibration constants.

Figure 12: FAD raw energy sum.

As the constants are calculated at the latest stage in the software chain the singal changes were compared and verified with the raw data signal(fig 12). All the step changes seen in fig 11 were cross referenced with the raw data signal changes with a good agreements, certifying that the calibration constants can be used to monitor the FAD-plane response.

All the variation seen above can be related to a stop of the LEP machine for a couple of hours. Small changes in bias currents do not effect the detector performance as almost no correlation could be found between bias current increase and signal response.

4.3   Incidents

The bias current and energy calibration graphs should be correlated to the LEP background conditions and LEP status. VSAT does not take data when we are out of physics, but the VSAT generated background 2 signal is active all the time and is logged in the DELPHI database. The radiation monitors number 2 and 4 for the VD are also sensitive to the VSAT background. Below follows a table listing the major bias and FAD signal changes the VSAT have experienced during the last two years.

Date	Time	Fill	Module	BIAS change(μA)	LEP Events
940809	13.00	2278	4	7-25	BKG spike
950915	11-17	2970	1,2	10-35,12-37	BKG spikes
990608	18-23	5673	1,2	31-38,30-32	BKG spikes at 13,19
990904	07-14	6263	1,2	36-46,31-34	BKG spikes at 10:40
Date	Time	Fill	Module	SIGNAL change	LEP Events
980815	14-17	5035	1-3	-1%	Big long bkg spike
980829	13-17	5112	3,4	+1,+1%	LEP stop
981014	5325	5348	1-4	-1,-.5,-1,+2%	LEP stops + Z0
990520	07-23	5577	1-4	+4,+4,+2,+3.5%	2 LEP stops
990721	10-15	5959	2,4	-1,-4%	LEP stop
990728	6007	6018	1-4	-3,-3,-3,-2%	LEP stops + Z0

Table 1: Signal and bias changes from VSAT FAD-Planes

The upper part of the table shows the jumps of the bias current, on top of this there is a small steady increase with time over the years. The jumps are always correlated to a radiation spike in the VSAT detector. We can however also experience heavy radiation without having a bias current increase.

The lower part of the table shows the FAD signal changes over the last two years. All except the first of these are related to stops in LEP and probably to accesses in the LEP tunnel. As we also have positive changes to the signals, these can not come from radiation damage. An explanation can be that the voltage to the preamplifiers have changed during the stop, which are known to be sensitive to supply voltage changes. This is however difficult to measure directly, as the voltage supplies are located inside the LEP tunnel.

The first incident is related to a long duration radiation peak(see fig 13), which pulled down the FAD plane response. Normal background two rate is around 1-3 during physics, and background storms normally do not last more than 10-40 seconds. In this case VSAT was exposed over 20 minutes with high radiation. The bias currents were not logged at this time(unknown reason), but a big jump from 97 to the end of 98 can be seen(fig 9). Looking at fig 11 this drop of signal response is clearly visible at fill 5035, the signal do however recover after some time.

5   Energy resolution

The changes in the energy response of the detector prevents the VSAT to put the correct energy in the common DELPHI data. On a local level the energy is corrected each fill, so any small changes in the signal response is not a problem. What is more vital for our data is that the resolution of our detector does not deteriorate. The resolution for 98 and 99 can be seen in fig 14 for outer module 3 and inner module 2.
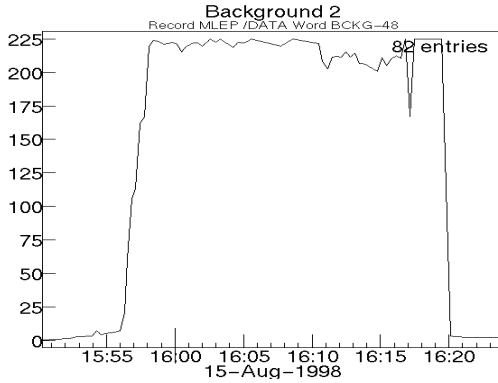

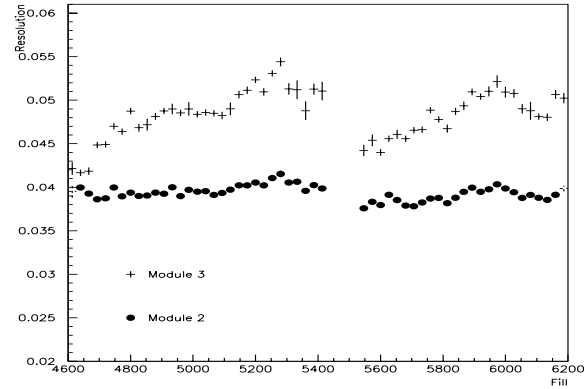Figure 13: Background radiation storm.

Figure 14: VSAT energy resolution.

The off momentum background is much higher in the outer modules and as seen from the figure this leads to a deteriorating resolution during the year. The modules do however seem to re-cooperate during the shutdown and longer stops of LEP. The inner modules are more or less stable on the same level.

From this it is easy to suspect that the resolution of the modules gets worse when they are "hot" from radiation exposure. Beam currents are always higher in the beginning of a fill, so the resolution should improve with the duration of a fill. This is clearly reflected in fig 15, where the resolution for all four modules have been plotted versus cassette number.

In fig 16 the resolution have a been plotted against the trigger rate in the inner and the outer modules. The increase on the resolution with the hit rate in the modules is clearly visible. The resolution is calculated as the width of the Bhabha peak when the off-momentum background has been subtracted. The background energy is shifted about 10% from the Bhabha peak energy and will broaden the peak if present. The resolution has therefore also been plotted against the ratio of false Bhabhas in the same plot. No dependence on the false Bhabha background is visible, so the background has been successfully removed.
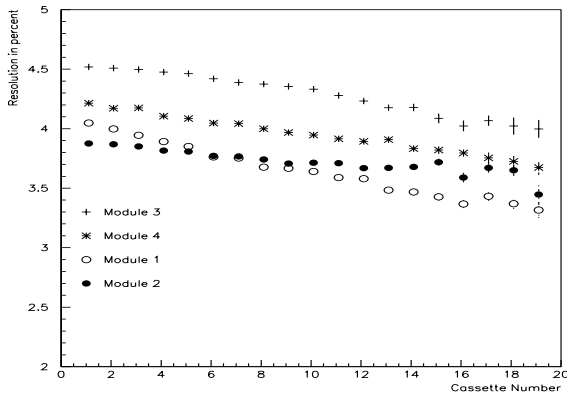
7

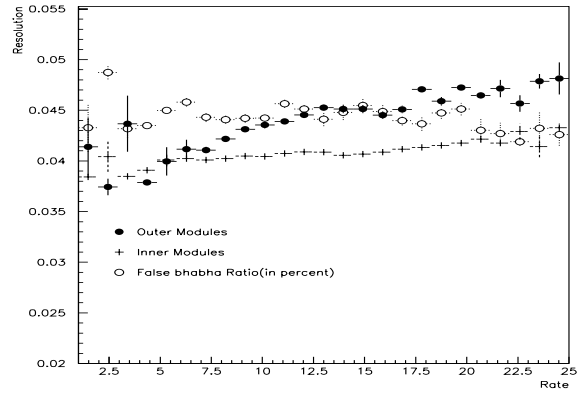Figure 15: Resolution during fill for all four modules.

Figure 16: Resolution as a function of trigger rate and background.

6   Conclusion

The higher energy of LEP II have been a challenge to the VSAT detector. The electronics have been successfully modified and adjusted to cope with the new situation and VSAT is taking good data. For 96 and 97 a software scheme have been developed to reconstruct the energy in the saturated FAD planes. The increase of off momentum background can be handled with good accuracy even though the VSAT false Bhabha trigger has been removed.

The increase of trigger rates facing the VSAT could be kept under control by changing the trigger structure and increasing our buffer length. VSAT does not present any problem to the DELPHI T2 rate and if the T1 rate should rise to unacceptable limits it is now possible to downscale our trigger.

It is clear that VSAT is taking radiation damage from background storms with an increase of bias current as a result. The performance of the detector will however not be affected as long as bias currents stay below 100 micro amps, which should not be reached until the end of 2000. The signal response from the detector changes from time to time in connection with LEP access, but do not affect the resolution of the detector. It is clear that outer modules loose resolution during the LEP running, but recover during the shutdown. Overall there are no worries for the general performance during year 2000, when VSAT will fulfill its lifelong mission.

8

Appendix G

Forthcoming results in two-photon collisions.

Forthcoming results in two-photon collisions at very low Q^2 from LEP2

S. Almehed [1], G. Jarlskog [1], F. Kapusta [2], U. Mjornmark [1], A. Nygren [1], I. Tyapkin [3], N. Zimin [1,3]

[1] Departament of Physics, University of Lund, Sweden

[2] LPNHE, IN2P3-CNRS, Universités Paris VI et VII, France

[3] JINR, Dubna, Russian Federation

Abstract

Experimental results that may soon be obtained in two-photon collisions at very low momentum transfer Q^2 at LEP2 are reviewed. A kinematical range is presented for both the forward and very forward detectors used to measure scattered electrons and positrons. A new acceptance, after this year's upgrade of the beam pipe at the position of the very forward detectors, is evaluated. The corresponding statistics are calculated for an integrated luminosity of 400 pb^{-1}, the total collected by the end of LEP2 operation according to current plans.

Proceeding of the talk presented at Workshop on Photon Interactions and the Photon Structure, Lund, 10-12 September 1998

1 Introduction

Studies of $\gamma\gamma$ collisions at very low momentum transfer Q^2 at LEP2 are attractive for many reasons (see, for example, [1]). First of all, it is worth pointing out that at present both theoretical and experimental knowledge is very poor in this range, and that previous measurements at LEP1 suffered from low statistics[2, 3]. LEP2's increased integrated luminosity can help greatly in improving the information provided.

There are at least three samples of $\gamma\gamma$ events that bring promise of interesting new results if they are studied: viz., depending on tagging conditions, a sample of single tagged events and two different samples for double tagged events. In all LEP experiments there are two ways of tagging the scattered electrons or positrons, either using the very forward calorimeters to detect polar angle of $\theta < 15$ mrad and thereby provide the measurements of very low momentum transfer squared Q^2, or using the forward calorimeters ($\theta > 30$ mrad) to provide measurements of Q^2 in a region of higher transferred momenta.

For the single tag case[2], when only one of the scattered electrons or positrons is measured while the other goes into the beam pipe, higher statistics can help to further distinguish between the various parametrizations used to describe the quark and gluon densities inside the photon[4].

For the double tag case[3], when both the scattered leptons are detected in the very forward calorimeters, reliable measurements of the total $\gamma\gamma$ cross-section in a range of high $\gamma\gamma$ centre-of-mass energies can be provided for the first time.

For the double tag case, when one scattered lepton is detected by the very forward calorimeters, giving the smaller measured momentum transfer P^2, while the second is detected by the forward calorimeter, giving the measured Q^2, the so-called virtual photon structure, *i.e.*, the effect of non zero virtuality of the tagged photon on the photon structure function[1] can then be studied.

Simplified theoretical concepts state that a total cross-section of $\gamma\gamma$ interactions can be described by a sum of three components: a non-perturbative term describing a soft hadronic part by a Vector-meson Dominance Model (VDM), a perturbative term describing a point-like coupling of the photons to a quark-antiquark pair by the Quark Parton Model (QPM) and a term for the hard scattering of the partonic constituents of the photon, the so-called Resolved Photon Contribution (RPC). Either one (the single resolved case) or both photons (the double resolved case) may perturbatively fluctuate into $q\bar{q}$ pairs. In the single resolved case one parton from the photon subsequently interacts with an other bare photon, while in the double resolved case one parton from each photon participates in a hard interaction thereby creating the high-p_T jets. The other partons create the so-called remnant jets which normally travel at low angles from the axis of $\gamma\gamma$ system (mainly into the beam pipe). These are the main ideas of the model, which is more complicated in reality. More detailed considerations can be found in[5]. For the single or double resolved perturbative part the lowest order diagrams are normally calculated with the different parametrizations used to describe parton density functions of the photon. These are available in PDFLIB[4]. There is a single free parameter p_T^{min}, the minimum transverse momentum of the outgoing partons, which has to be specified and used in order to separate the RPC from the non-perturbative contribution. These values of p_T^{min} were found for the parton density functions from the requirement to reproduce the visible experimental two-photon cross-section at the Z^0 peak. Since the RPC was treated using leading order QCD factorization, a hard scattering subprocess gives the dominant scale

p_T^2, taken also as the factorization scale.

Well-known for many years, the VDM and QPM models are widely used to describe the experimental data at any beam energies and any Q^2 range . The relatively new RPC model has being tested at KEK, HERA and LEP1 (see, for example, the last Workshop Photon'97[6]) in the region of low $Q^2(< 2(\mathrm{GeV}/c^2)^2)$, and quite recently it was extended into a higher Q^2 region[7].

It is also important to mention, that depending on the tagging conditions, which in fact simply define the Q^2 region, the relative contributions from different models may vary widely.

Thus it is really important to get an estimate for the statistics for all of the cases mentioned above.

2 Kinematical range and luminosity

During the 1997-1998 year shutdown period all LEP experiments were equipped with a smaller beam pipe at the position of their very forward calorimeters, which are normally used for luminosity measurements as well. Initially the upgrade was proposed by the DELPHI experiment[8] in order to increase acceptance for the Very Small Angle Tagger (VSAT) and thus to improve the statistics available for two-photon studies. The following consideration has therefore been made for the DELPHI setup. The principle of the upgrade was very simple: namely, to decrease the radius of the LEP beam pipe in the horizontal direction. The upgrade was simpler still because the DELPHI VSAT itself had previously been fitted with instruments designed to accommodate the larger acceptance.
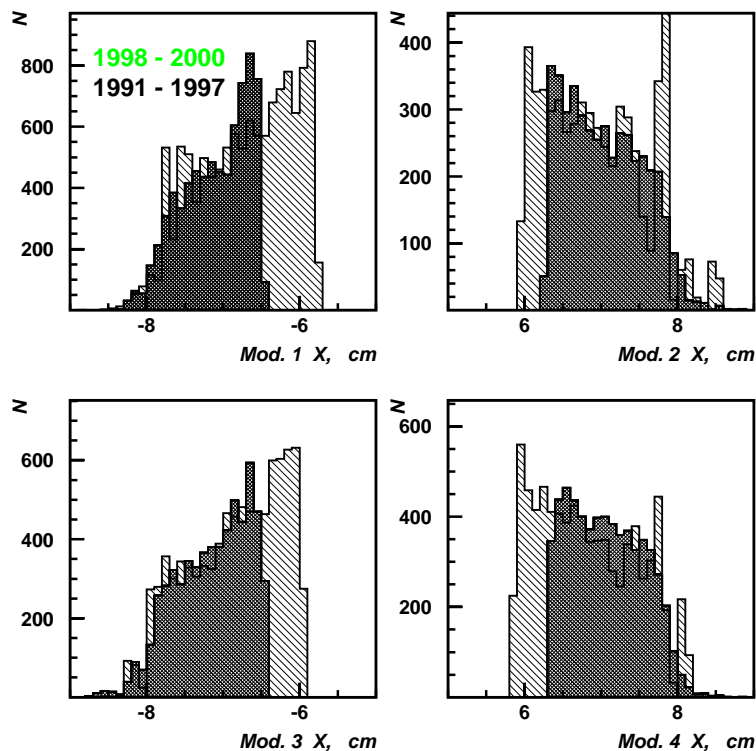

Figure 1: New and old acceptance of all four modules of the DELPHI VSAT detector. An arbitrary vertical scale is used to show only the profit from the active detector area increased in x-coordinate direction.

Four VSAT modules are situated in the horizontal plane at $\simeq 7.7$ m from the interaction point, behind the superconducting quadrupole magnets which produce the final focus. These magnets deflect the scattered electrons and positrons from the direction of the beam pipe, and thus permit measurements at very small polar angles. At the modules there is a small elliptical section of the beam pipe providing a thin window in front of the calorimeters. The instrumented area of the VSAT modules is not large, being only 5 cm high and 3 cm wide for the x-position measurements. The active area used was previously even smaller, $i.e.$, 2 cm in the x-direction, because for the outer range in x of the modules there was a dead zone due to a flange located in the beam pipe about 70 cm in front of the detectors. The upgraded beam pipe is made with a $\simeq 0.5$ cm smaller radius in the x-direction, and the VSAT modules have been moved closer to the beam line. Thus we can benefit greatly from the increase in cross-sections and the active detector area was also enlarged. The upgrade has now been also adopted by all the LEP experiments.

Rates of occupancy of the VSAT modules obtained from this year's preliminary analysis are shown in Fig. 1 together with results from previous years. Here the benefit of the upgrade can clearly be seen. As expected, the tails of the distributions behave similarly at high x, thereby confirming that all (hardware and software) modifications were properly carried out.

As shown in [8], the increase in cross-sections because smaller polar angles can now be detected should increase statistics by a factor $\simeq 2$ for double tagged events and by a factor $\simeq 1.5$ for single tagged events. These factors are used in estimate of the final statistics.
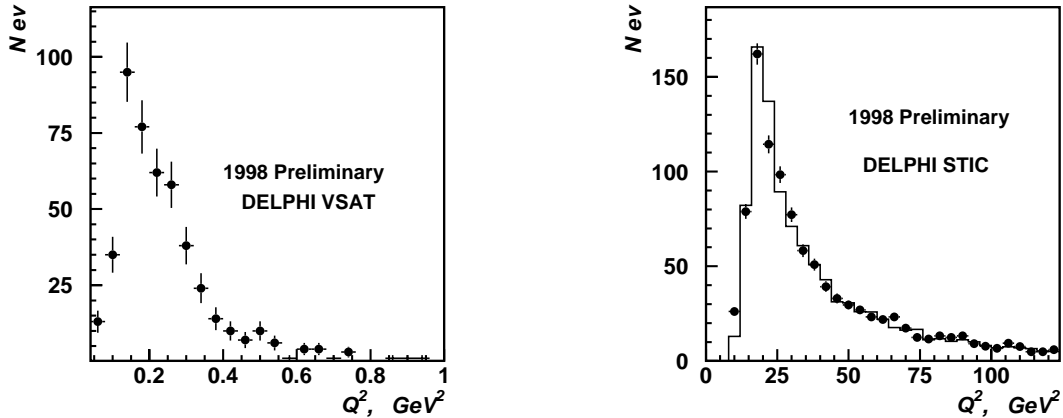

Figure 2: Momentum transfer distributions measured by the DELPHI VSAT and STIC detectors. An arbitrary vertical scale is used to show the relative statistics for different ranges.

The kinematical coverage of the very forward and the forward detectors shown in Fig.2 provides the answer to questions concerning the upper and the lower limits of the Q^2 scale, and also shows how far the measurements can explore the regions of low Bjorken-x, where the main theoretical interest lies. For the very forward detectors (the DELPHI VSAT), the statistics are concentrated below 1 GeV^2 and peak at around 0.2 GeV^2, while for the forward detectors (the DELPHI STIC) they go up to $\simeq 100$ GeV^2. The range of invariant masses W from 5 GeV to 80 GeV can be reasonably measured with high enough statistics, so results can be obtained in the regions

- $10^{-4} < x < 2 \cdot 10^{-2}$ for the VSAT and

- $2 \cdot 10^{-3} < x < 0.8$ for the STIC.

4

1998 was a very successful year for LEP with a record integrated luminosity of $\simeq 200$ pb^{-1}. For next two years, however, the prime stress will be on maximum attainable beam energies. According to current plans, a luminosity of $\simeq 200$ pb^{-1} is expected to be collected by the end of LEP2 running. Thus, a total integrated luminosity of $\simeq 400$ pb^{-1} will have been used for the statistics estimations.

3   Difficulties in the analysis

Though the analysis appears to be well understood, there are several complications. In order to obtain reliable results for all possible Q^2 regions, an accurate reconstruction of the energy and the polar angle of the tagged particle is needed. Therefore, many corrections have to be specified and then applied. The most important ones for energy reconstruction are new calibration constants and in particular, new leakage corrections due to the higher energy in comparison with LEP1.
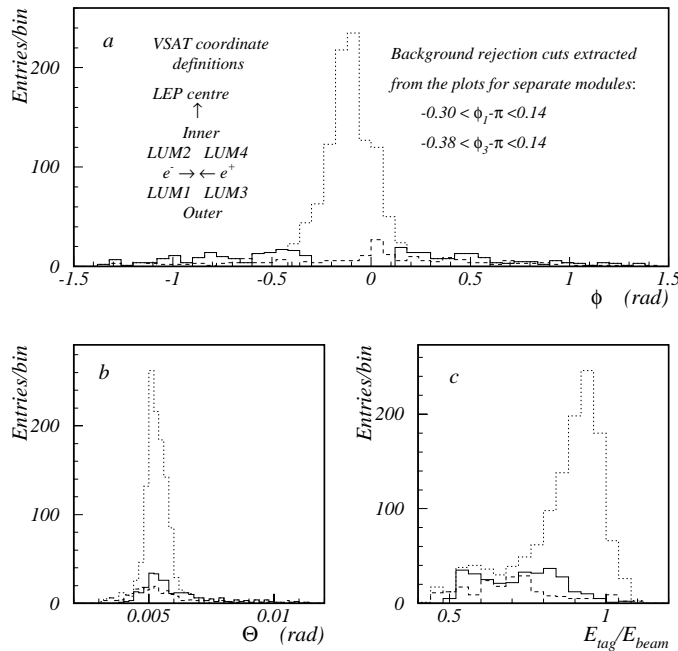

Figure 3: VSAT off-momentum electron background distributions, found from a random coincidence between well measured Z^o events and high energy signals in one of four VSAT modules (denoted LUM1 to LUM4 in the inset) : (a) ϕ and (b) Θ-distributions, (c) E_{tag}/E_{beam}. The dashed lines show the background behaviour in the inner modules 2 and 4, and the dotted lines in the modules 1 and 3 (outside of the LEP ring) before rejection. Solid lines show the remaining background after applying cuts on ϕ to the outer modules as indicated in (a).

On the other hand, the quality of the energy measurements can be checked for each LEP fill, or even for each run, by using Bhabha events. Moreover, the new acceptance means there are more statistics available. The reconstruction of the initial polar angle θ is based on a determination of the energy and the position of the tagged particle, which is traced backwards in an iterative procedure from the detector through the superconducting quadrupole and the solenoid magnetic fields to the interaction point. For the position reconstruction accurate geometrical survey measurements of the position of the VSAT modules in relation to each other at the beginning and the end of the data taking year are essential. Clearly, the angle reconstruction procedure is very sensitive to the LEP beam parameters, which sometimes vary even within a fill. Thus, to define the angle in the event vertex as precisely as possible, the beam spot position, the angles between the beams and the parameters of the superconducting quadrupoles all have to be known and taken into account for each data taking fill or even run. High background is usually a serious problem for the analysis. Surprisingly enough, however, in our case the presence

of abundant background (off-momentum electrons for single tagged events and Bhabha events for double tagged events) helps improve the angular reconstruction. Most of the off-momentum electrons are concentrated in the horizontal plane and enter the two VSAT modules on the outer side of the LEP ring. By studying their sharply peaked impact point distribution, the y-coordinates of the outer modules can be aligned with respect to the beam axis. By using the strict collinearity of the Bhabha events, the y-coordinates of the inner modules can also be aligned. Of course, very careful study of the Bhabha events is needed to do so. In turn, effective rejection of the background also depends on how accurately the θ angle is reconstructed and how well the LEP beam parameters are defined. The results of a simple rejection of background at LEP1 energies[2] are shown in Fig 3. Now, with better understanding of the background, it can be rejected more efficiently, albeit in a more complicated and labour-intensive way.

Nevertheless, it is beyond doubt that the background in the final analysis can be rejected as efficiently as it was for LEP1 double tagged data (Fig.4).
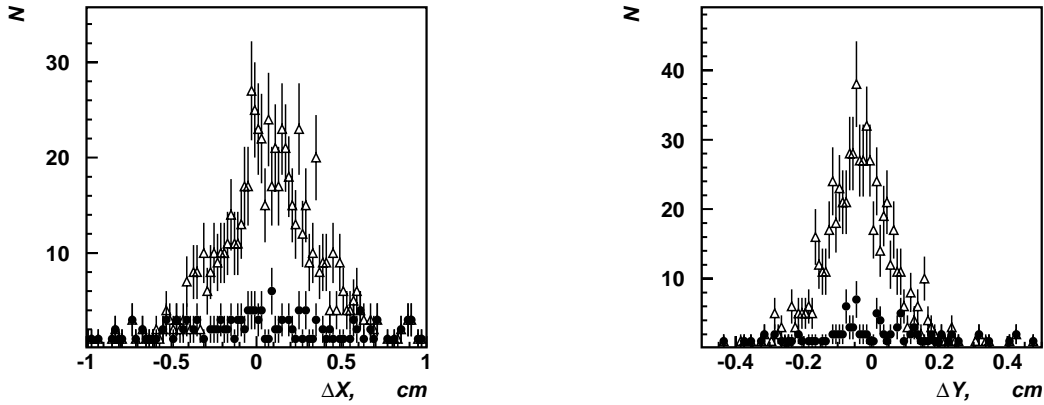

Figure 4: VSAT double tagged events. Triangles are before rejection and points are after rejection of the background from the Bhabha events.

4   Statistics estimates

As mentioned above, the total integrated luminosity collected at LEP2 after the upgrade of the very forward calorimeters is expected to be $\simeq 400$ pb^{-1}. This number is used hereunder to estimate the available statistics for all of the topics.

4.1   VSAT single tagged events

Of particular interest to an analysis of single tagged events is the rather large contribution[2] to the total $\gamma\gamma$ cross-section from RPC. This is indeed the case where there is a hope of finding the best parametrizations of parton density function in the photon. As mentioned above, an extensive compilation of existing parametrizations is available in [4].

By comparing data obtained with higher statistics at LEP2 with the three component model predictions a distinction may possibly be drawn between the Gordon-Storrow (GS), Glück-Reya-Vogt (GRV), Levy-Abramowicz-Charchula (LAC1) and Schuler and Sjöstrand (SAS) parametrizations[9].

6

The published results from DELPHI at LEP1 are used to estimate the statistics. Around 500 events were obtained for an integrated luminosity of $\simeq 30$ pb^{-1}. Taking into account the factor of $\simeq 1.5$ after the VSAT upgrade, $\simeq 10.5$ K events are expected to be available for the final analysis.

4.2   VSAT-VSAT double tagged events

The double tag mode is attractive because both the hadronic invariant mass produced and the absolute momentum transfers squared for both photons can be directly measured, as in small angle approximation the invariant mass is reconstructed from the energy measurements of the tagged particles. This means that there is little need to apply the unfolding procedure to extract the total $\gamma\gamma$ cross-section, which may now be measured in a wide region that was previously inaccessible.

The previous analysis of LEP1 data suffered from very low statistics. Only 43 events survived after all selection criteria had been applied to pick out $\gamma\gamma$ events and reject Bhabha background. To illustrate this both the tagged energy and the invariant mass distribution of the hadronic system are shown in Fig.5, where the level of agreement between data and simulation can bee seen. The limited statistics mean that not much information can be extracted despite good agreement between data and simulation.
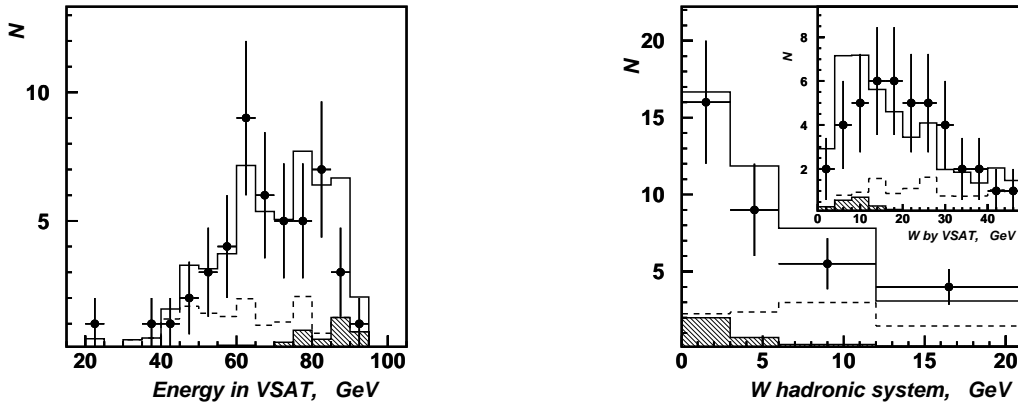

Figure 5: DELPHI LEP1 double tag events. VSAT-tagged energy and invariant mass reconstructed. Points are data, solid lines are the full VDM+QPM+RPC predictions, dotted lines are the QPM+RPC and hatched histogram - QPM part.

At LEP2 energies the accuracy of the invariant mass reconstruction improves. With the factor $\simeq 2$ after the VSAT upgrade taken into account, $\simeq 350$ events available for the final analysis of DELPHI data may be expected. A similar number of events should be recorded by the other LEP experiments.

4.3   VSAT-STIC double tagged events

Since the rate of double tagged events in the main forward calorimeters is very low, because of the relatively high $\theta > 30$ mrad, the double tagged results expected to come from events with one tag in the main forward calorimeter (the STIC for DELPHI) and the other tag in the very forward ones (the VSAT for DELPHI) are more promising. To a certain extent the effects of the target photon non-zero virtuality, $P^2 \neq 0$, on the photon structure function $F_2^\gamma(x, Q^2; P^2)$ can be studied only with this sample. Such studies are attractive mainly

for two reasons: our present state of experimental knowledge is very poor, and because of the rise in the LEP beam energy the non-perturbative hadronic contribution (VDM) is expected to be suppressed with increasing P^2, allowing for a perturbative prediction of the photon structure function. More details can be found in [1]. There are still no results available from the LEP experiments. A two-photon generator TWOGAM, which was successfully tested in previous DELPHI studies, is used to estimate the number of events in this case. Taking into account the factor $\simeq 1.5$ after the VSAT upgrade, $\simeq 200$ events are expected to be available for the analysis. Since the forward and the very forward calorimeters have different acceptances for the other LEP experiments, the number of events can differ by several times from one experiment to the next.

5   Summary

Due to its high energy and increased integrated luminosity, LEP2 provides a unique opportunity to study the topics described above, with good prospects for obtaining new interesting results. Though the analysis technique is very laborious, the procedure is well understood and clear. A fairly large number of events is expected for the single tagged events detected by the very forward calorimeters. Unfortunately however, this is not true for either of the double tagged event samples, for which the statistics available are very limited, so that a combined effort by all the LEP experiments is needed if we want to obtain reliable results.

References

[1] P. Aurenche *et al.*, Physics at LEP2, eds. G. Altarelli, T. Sjöstrand and F. Zwirner, CERN 96-01 (1996) 291.

[2] DELPHI Coll., P. Abreu *et al.*, Phys. Lett. **B342** (1995) 402.

[3] DELPHI Coll., N. Zimin, Proc. Photon '97, Egmond aan Zee, eds. A. Buijs and F. Erne., World Scientific, Singapore, (1997) 74.

[4] H. Plothow-Besch, Comput. Phys. Commun. **75** (1993) 396.

[5] G. Schuler and T. Sjöstrand, Nuclear Physics **B407** (1993) 539.

[6] Proc. Photon '97, Egmond aan Zee, eds. A. Buijs and F. Erne., World Scientific, Singapore, (1997).

[7] DELPHI Coll., I. Tyapkin, Proc. of 28th International Conference on High Energy Physics, Warsaw, Poland, World Scientific, Singapore, (1996), 729.

[8] S. Almehed *et al.*, JINR Rapid Commun., **3[83]-97** (1997) 47.

[9] L. Gordon and J. Storrow, Z. Phys. **C56** (1992) 307.
M. Glück, E. Reya and A. Vogt, Phys. Rev. **D46** (1992) 1973.
H. Abramowicz, K. Charchula and A. Levy, Phys. Lett. **B269** (1991) 458.
G. Schuler and T. Sjöstrand, Phys. **C68** (1995) 607.

Appendix H

1998 runnin review worksop, the VSAT project.

1998 running review workshop, the VSAT project

Goran Jarlskog, Ulf Mjoernmark, Andreas Nygren, Pavel Tyapkin, Nikolai Zimin

Experimental Elementary Particle Physics department of Physics Institute, Lund University

Abstract

This report gives a brief account of the performance of the VSAT hardware and software during 1998. Overall, the detector was very reliable and there are no serious problems of operation.

1 Hardware

1.1 Improvements made in the shutdown 97/98:

A smaller elliptical beam pipe was installed at ± 7.5 m from the collision point (the VSAT group had requested a cylindrical subsection of the beam pipe with a 10 mm reduction in horizontal radius). Compared to the old beam pipe the new one has a 5 mm smaller radius in the horizontal plane while the vertical radius is the same as before [1]. Resulting increase of the geometrical acceptance is shown in the Fig. 1.
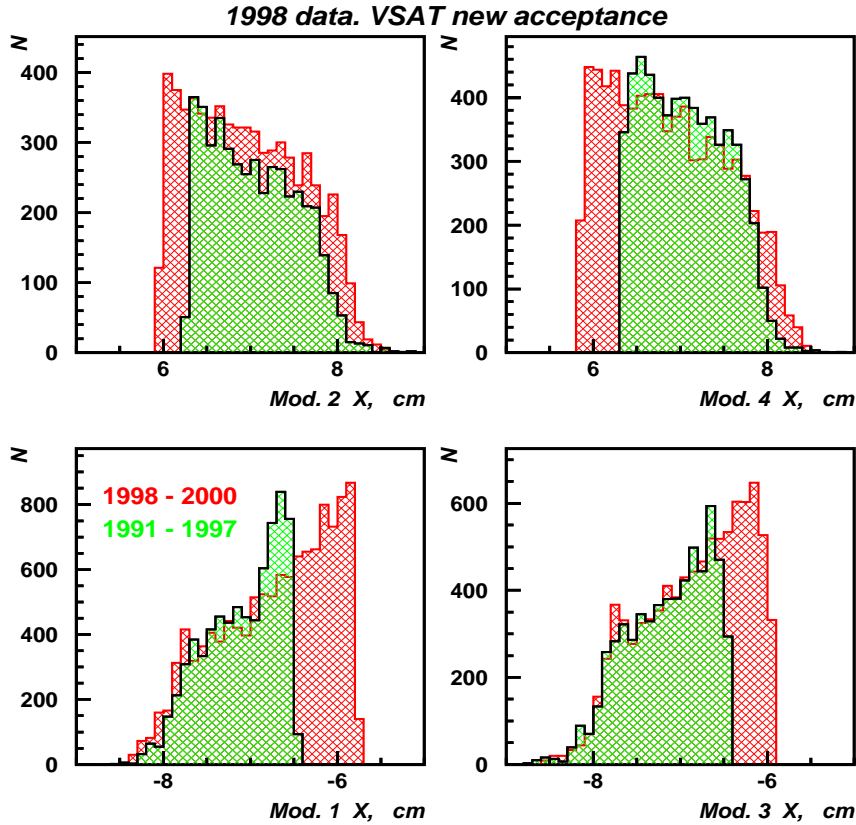

Figure 1: VSAT geometrical acceptance in X plane before (97) and after move (98)

Preliminary results from the current analysis show that the VSAT acceptance is significantly improved after last year upgrade. Unfortunately the new beam pipe pieces were produced with a bit larger x-dimension than specified. The specification was an increase of the acceptance of 5 mm in each module, and as can be seen above this clearly not the case. For this reason the statistics available for double tagged events is increased only by a factor 1.8 instead of 2.

The final number of events depends also from the procedure of background rejection which is now under revision. For single tagged events the increase in statistics is a little less than 1.5. What is important is that the kinematical range in Q^2 (up to 0.6 GeV^2) and invariant mass W (up to 100 GeV) of the gamma-gamma system W (up to 100 GeV) are obtained as predicted and give us an opportunity to get results in this range for the first time.

At high energy some amplifiers of the FADs (full area silicon planes), located at the depth of 6 to 10 radiation length, were saturating at the peak of the shower. This was caused by a limitation in the amplifiers to reproduce the true rise time of the signals. Since the readout is a sample and hold the exact timing of the hold is crucial – a shift of the hold signal to 250 ns later removed the saturation (see Fig. 2 and Fig. 3). This was implementation in June 1998. For data taken before that date the signals from the strip planes, which are also located around shower maximum, can be used for a correction of the energy in the saturated FADs.
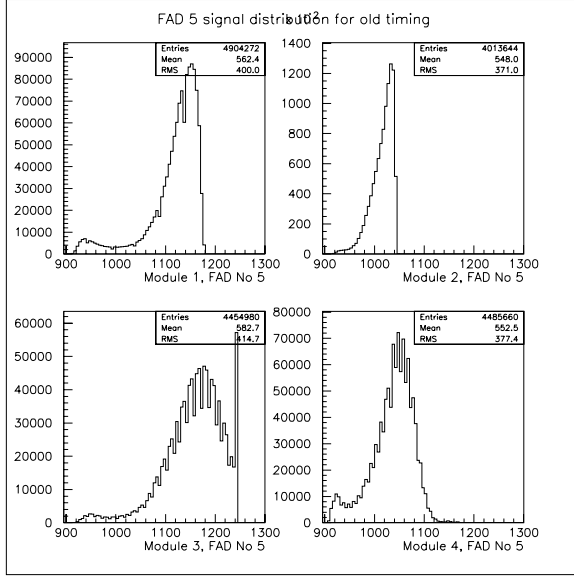
Figure 2: FAD plane Number 5 amplitude distribution for all modules (1,3 - outer modules, 2,4 - inner modules) with old timing - 5.55 μs

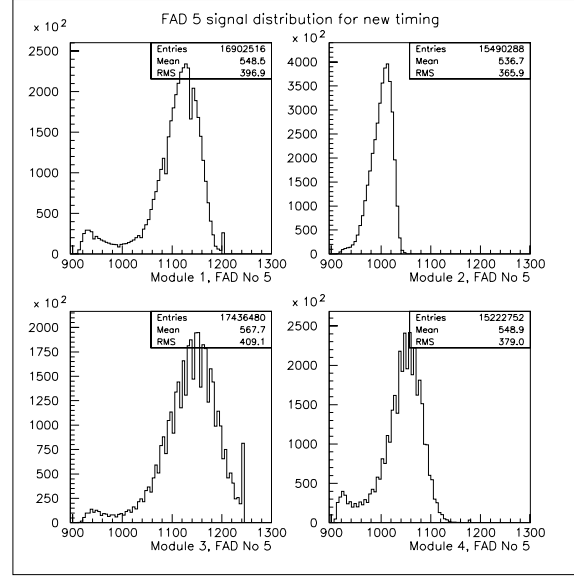Figure 3: FAD plane Number 5 amplitude distribution for all modules (1,3 - outer modules, 2,4 - inner modules) with new timing - 5.80 μs

1.2   Major problems/damages:

In May a FASTBUS card (LURFB) designed to handle the minibunch scheme of LEP burned. For the repair we had to send for the engineers from Sweden who made the card and lost about 5 days of running, mainly at the Z. A bad connector was also found which prevented downloading the programs to a DSP handling minibunches (this was repaired in October 1998). In May also a NIM crate handling the trigger information broke down, about 1 day was lost. None of the problems above affected the central data acquisition of DELPHI.

2

1.3 Backgrounds:

The VSAT is built to measure the off-momentum background in LEP and can cope with various conditions. VSAT have a background rate of about 500 electrons per second in the outer modules and about 100 for the inner. These are down-scaled by a factor 400 and 130 respectively, so that they in total consist about 10% of our readout triggers. The number of accidental Bhabha triggers from the off momentum background increased with the luminosity of LEP (False Bhabha to real Bhabha rate is given on Fig. 4), but did not affect the data-taking adversely.
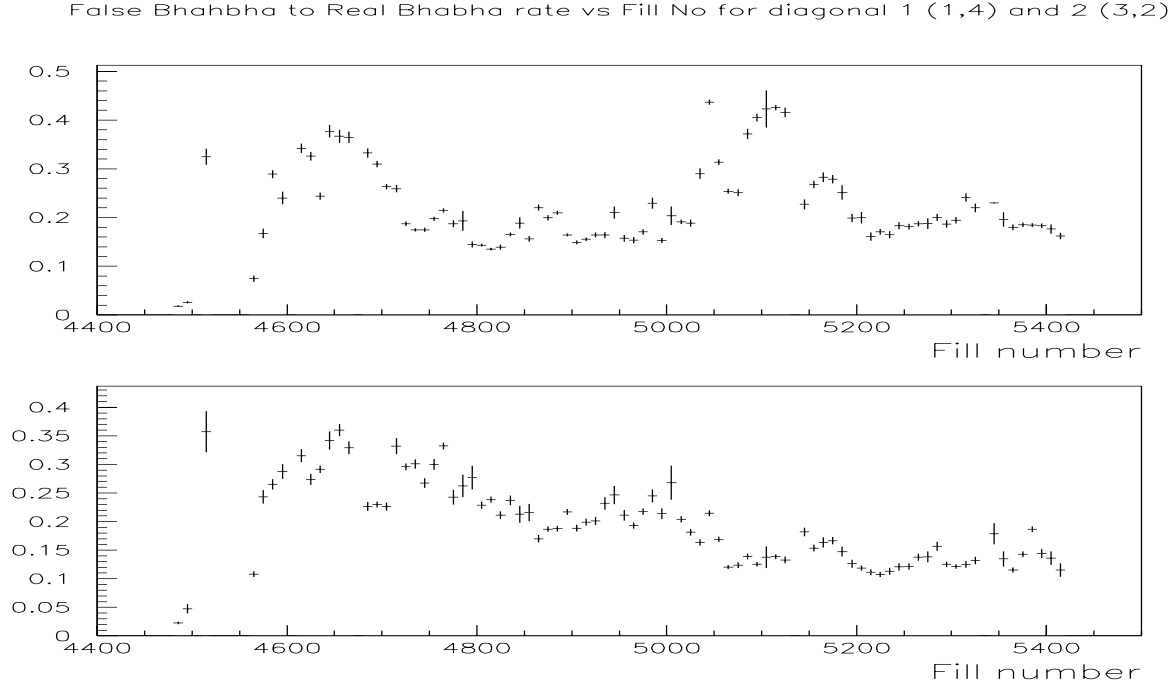
Figure 4: False Bhabha to real Bhabha rate

1.4 Spares:

The VSAT electronics is unique and does not have spares. If faults occur they have to be investigated by our engineer on call (from Sweden). Minor problems can be handled by the physicist in charge of the VSAT at CERN.

1.5 Future:

The LURFB card used now to handle minibunches will get a spare that can be used for the high energy running with only one bunch. A second LURFB for minibunches is built but not yet tested (we are not sure when this will be done since the engineer who designed it has left). We do not plan any changes but cross our fingers that things will keep running as nicely as in 1998 (after May).

3

2 Software

2.1 Improvements made 97/98:

The output from DELANA was modified to include the information from the x- and y-strips of the silicon planes in order to improve determination of the shower position at DST level. All preamplifiers were carefully calibrated (again). The information in the XSDST was extended to be used for two-photon physics analysis.

As the VSAT is shadowed by a flange in the beam pipe, the movement resulted in a pure increase of the active detector area. This new region of the detector was never used and had to be calibrated. The VSAT modules is of limited size and at the edges the energy shower leaks out of the detector. Before the shadow of the flange prevent particles to reach out on the far side in x, and only leakage calibration on the inner edge were done. With the move of the modules it is necessary to correct for leakage on the other side as well(fig 5). Leakage correction were also applied in the Y direction(fig 6), even if very few events reach the edges in y.
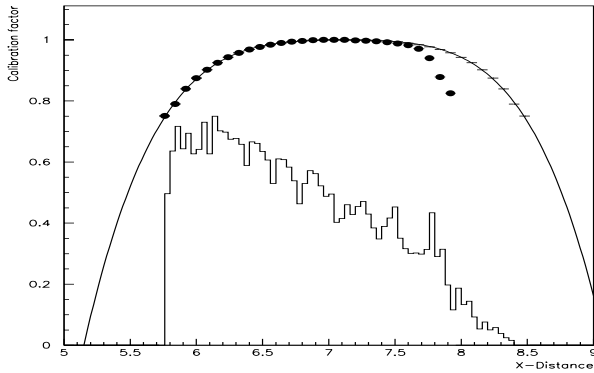
Figure 5: VSAT energy leakage calibration in X (dots=data) and the X-distribution for all events.
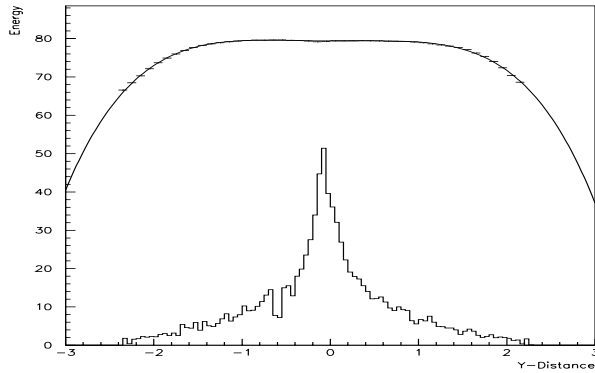
Figure 6: VSAT energy leakage calibration in Y (bars=data) and the Y-distribution for all events.

A four degree polynomial was used as a leakage correction function. The drop of the data on the far side of X is energy losses due to interaction with the flange and have nothing to due with detector leakage.

2.2 Major problems/bugs:

There are no major problems. The disk storage space is critical and must be watched carefully. At high energy there is some longitudinal leakage from the modules that we have not made a correction for so far, this will be investigated. During the data taking for 1998 a resident bug from beginning of LEP was found in DELANA. In the event that all four modules in VSAT get hit at the same time, some of our counters get out of phase and causes some corruption. The likelihood for this was vanishing small up to 1998 and no effect could be seen on the data. With the increase of background an luminosity in LEP and the movement of the detector closer to the beam, this effect became visible in our data sample. A fix has already been implemented and the data should be corrected next time DELANA runs on it in the end of 1999.

4

2.3 Monitoring:

We are quite happy with the (automatic) monitoring system introduced by Andreas Nygren [3]. It is easy to spot problems in the offline data stream. The central online monitor had a mysterious problem throughout the year, with strange spikes appearing in the data now and then. These effects could not be reproduced when the central monitor was run stand alone in playback on the data. A fix to work around the problem was implemented in the central monitor, which now works fine.

3 Performance

Higher background and luminosity in from the LEP beam in addition to the increased crossection due to the movement of the modules, heavily increased the radiation hitting VSAT during 1998 in comparison to previous years. The main part of the radiation comes from the off-momentum background, which is concentrated in the outer modules. We have therefor bigger degradation of the detector silicon planes in these modules, clearly visible in fig 8.

The resolution jump in module two around fill 4640, is due to the fact that we temporarily lost the signal from one of our fad-planes. We lost about 0.6-0.9 % of resolution in the outer modules and about 0.2-0.3% in the inner. With just two more year of running this is acceptable without any intervention to improve the situation. The average resolution for the whole year is shown in fig 7.
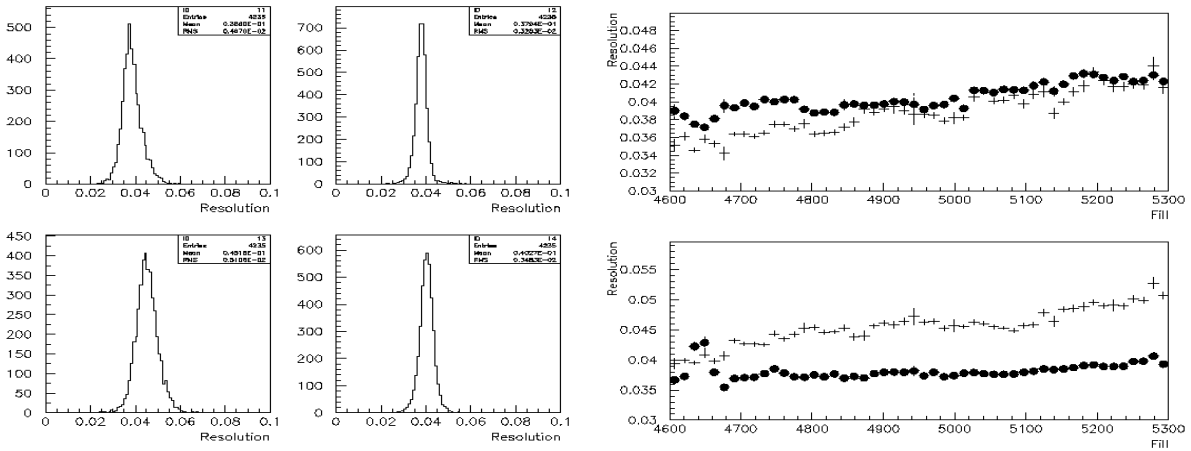

Figure 7: Energy Resolution R=dE/E of each module (Note: 1, 3 - outer modules, 2, 4 - inner modules)

Figure 8: Resolution development during 1998 running, crosses=outer modules and dots=inner

Every year a luminosity analysis is made to check the stability of the STIC detector for shorter periods of time. VSAT can not measure the absolute luminosity, and therefor have to be normalized to STIC data for normally 3 to 5 periods of running. After normalisations and corrections STIC and VSAT luminosity can be compared as shown in Fig 9.

VSAT crossection also have to be calibrated in correspondence to certain beam-parameters that can be measured with the X- and Y-strip planes. For example Fig. 10 shows the center Y-coordinates of the beam as measured in each detector (about usual procedure look at [4]).There has clearly been a gradual shift in Y-position during 1998.
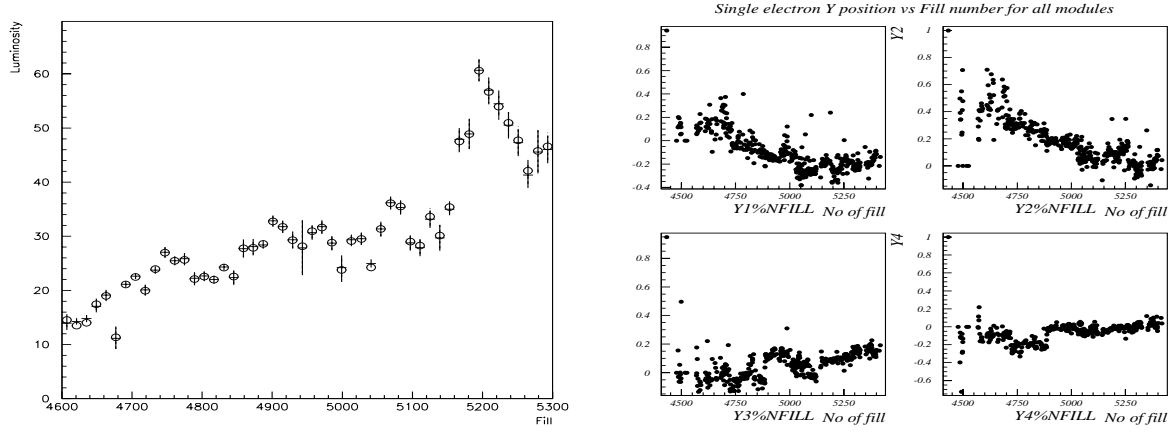

Figure 9: VSAT (circles) and STIC (crosses) luminosities in nb^{-1}

Figure 10: Y position of the beam (cm) in each module

The energy signal from the FAD-planes is calibrated every fill. Changes in these calibration constants is normally an indication of that something have happened with beam energy or VSAT electronics. As the FAD timing was changed, the energy calibration constant was changed also. This can be clearly seen on Fig. 11 - big step from 0.97 to 0.85. Some other correlated steps in the graphs is also clearly visible, probably as a result of a power cut.

After calibration we have a very nice and clean bhabha peak at a very stable energy. The energy variations on the bhabha peak for all the year is shown in fig 12. We have a energy variation of less than one permill, which is very satisfactionary.
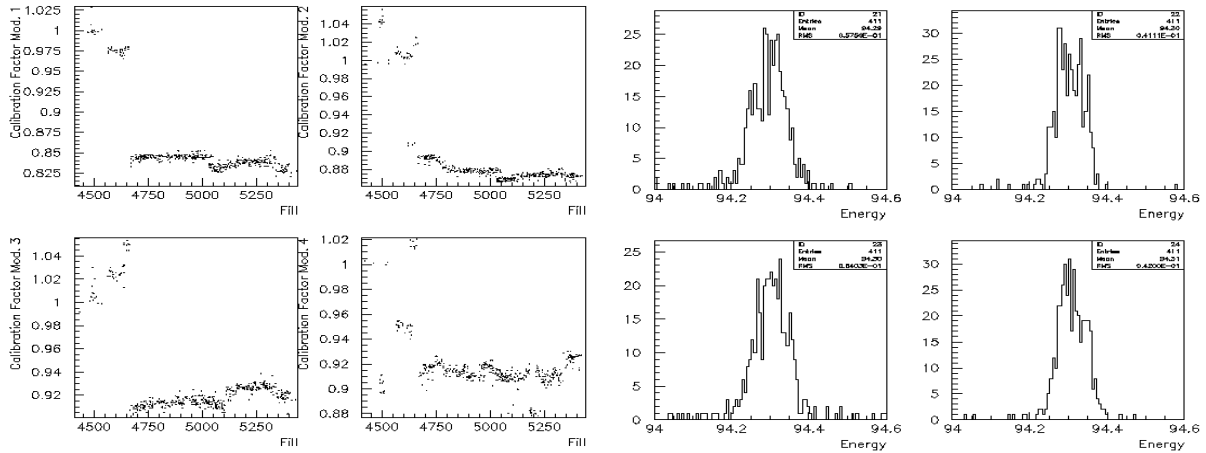

Figure 11: Energy calibration constants during 1998

Figure 12: Bhabha Energy (in GeV) deposited in all modules during 1998

6

4 Manpower

The Lund group has one physicist stationed at CERN in charge of the VSAT (in 1997/98 it was Andreas Nygren, in 1999/00 it will be Pavel Tyapkin). Weekly checks on the raw data quality is done in Lund by Ulf Mjornmark. For each year of running the beam parameters of LEP are determined and the acceptance of the VSAT is recalculated using those inputs. If the range of parameters change too much new simulations [5, 6] are done in order to have the correct coverage in parameter space (by Sverker Almehed). The main VSAT analysis effort is on tagged electrons/positrons for two-photon physics. Nikolai Zimine is coordinating this effort [1]. It is unsatisfactory to have only one person in charge at CERN for the entire remaining period.

5 Trigger rate

The VSAT T1 trigger rate was low during LEP I, which in turn produced a neglectable amount of T2 triggers. In the beginning of LEP II the T1 rate increased mainly due to our delayed Bhabha trigger. This was removed during 1996 and since then we have had a T1 rate of about 10-20 Hz. Due to this removal the false Bhabha background has to be estimated off-line from the single electron rate (about 10% of the VSAT triggers are read out from the single electron off momentum background). This estimated rate of false Bhabhas is normalized (see Fig. 13) to the STIC [7] and VSAT luminosity difference. This works pretty satisfactory as can be seen Fig 14, where the STIC and VSAT luminosity difference before and after false Bhabha subtraction is plotted.
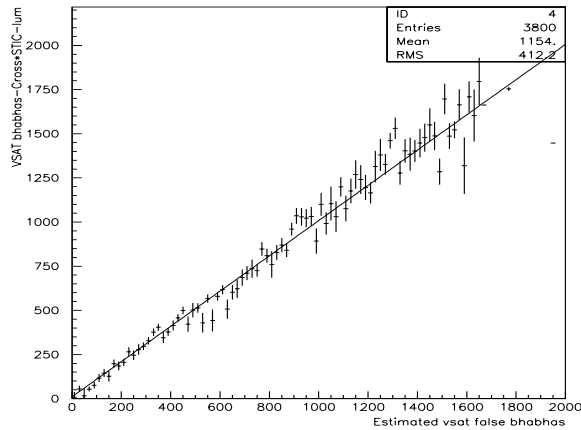

Figure 13: The difference between VSAT and STIC luminosity versus VSAT estimated number of false Bhabhas
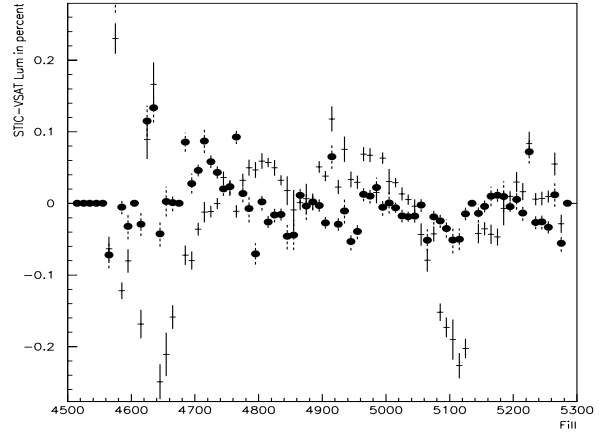
Figure 14: The difference between STIC and VSAT luminosity before (crosses) and after (dots) false Bhabha subtraction

The movement of the detector closer to the beam pipe and the increase of luminosity, background and energy of the beam pushed up both T1 and T2-trigger rate rapidly during 1998. Many long discussions were ignited during several pit-meetings about our trigger system. Two solutions to deal with the problem were pursued by the VSAT group.

VSAT events are recorded in an internal buffer which is read out each DELPHI Event and causes a DELPHI trigger only if it becomes full. The internal event buffer length was increased from 12 to 20 events at the start of fill 5162, which pulled down the T2 rate with a factor 4 in the critical period at beginning of the fills (see Fig. 15 and 16).
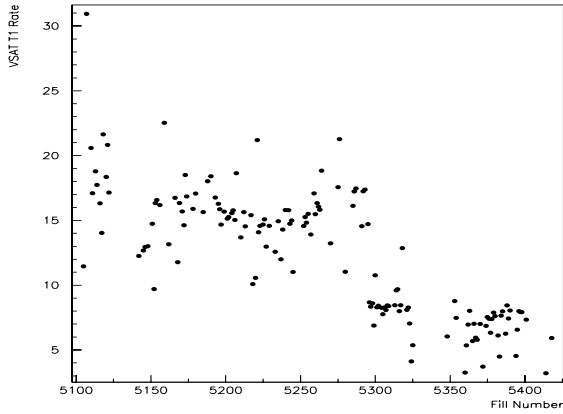

Figure 15: The VSAT T1 trigger rate in Hz versus fill. T1 down-scaling with a factor 2 at fill 5296 can clearly be seen.
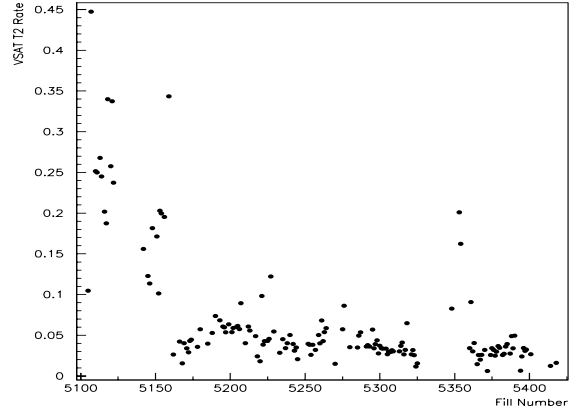
Figure 16: The VSAT T2 trigger rate in Hz versus fill. Buffer length increase at fill 5162 is clearly visible, but no effect from the T1 downscaling.

To improve the situation further the VSAT T1 trigger rate was down scaled by a factor two at fill 5296. This worked fine for our T1 trigger, but the T2 rate continued to be the same(clearly visible around fill 5350 were the buffer length by mistake were set to 12 again). This is due to an error in the logic of the hardware, which in turn also caused some troubles(correctable, but undesirable) in the running of DELANA as well. The people who built the hardware system have left the VSAT group and we will therefore not correct it. Instead we will run with no down scaling and increase our buffer length to 25.

References

[1] S.Almehed, G.Jarlskog, F. Kapusta, U.Mjornmark, A. Nygren I. Tyapkin, N. Zimin,
Forthcoming results in two-photon collisions at very low Q^2 from LEP2
DELPHI 98-175 PHYS 814, 7 December 1998

[2] Ivan Kronkvist,
Data Base and Slow Controls of DELPHI VSAT and Two-Photon Physics using
DELPHI at LEP
ISBN 91-628-2182-2 LUNFD6/(NFFL-7128) 1996

[3] Andreas Nygren,
THOR
LUNFD6/(NFFL-7151), Lund, 1997

[4] Jonas Bjarne,
Two-Photon Physics and On-line Beam Monitoring Using The DELPHI Detector at
LEP
LUNFD6/(NFFL-7089), Lund, 1994

[5] A. Håkansson,
Beam dependent correction applied to the VSAT relative acceptance
DELPHI 93-49 PHYS 279

[6] A. Håkansson,
Luminosity Measurement at LEP using the Very Small Angle Tagger of DELPHI
ISBN 91-628-1091-X LUNFD6/(NFFL-7077), 1993

[7] E. Falk, V. Hedberg, P.Ferrari, C. Matteuzzi,
Photon Analysis with STIC
DELPHI 98-147 PHYS 791, 3 August 1998